ADVANCED ORTHOGONAL FREQUENCY-DIVISION MULTIPLEXING SYSTEMS WITH CYCLIC PREFIX-LESS MULTIPLE-INPUT AND MULTIPLE-OUTPUT DISCRETE FOURIER TRANSFORM SPREADING AND UNMANNED AERIAL VEHICLES-ASSISTED CYCLIC POSTFIXED WINDOWED SCHEMES

A Dissertation
IN
Computer Networking and Communication Systems
and
Computer Science

Presented to the Faculty of the University
of Missouri–Kansas City in partial fulfillment of
the requirements for the degree

DOCTOR OF PHILOSOPHY

by
MD MAINUL ISLAM MAMUN

M. S. University of Missouri-Kansas City, Kansas City, USA, 2019
M. Sc., University of Rajshahi, Rajshahi, Bangladesh, 2006
B. Sc., University of Rajshahi, Rajshahi, Bangladesh, 2005

Kansas City, Missouri
2023

ADVANCED ORTHOGONAL FREQUENCY-DIVISION MULTIPLEXING SYSTEMS WITH CYCLIC PREFIX-LESS MULTIPLE-INPUT AND MULTIPLE-OUTPUT DISCRETE FOURIER TRANSFORM SPREADING AND UNMANNED AERIAL VEHICLES-ASSISTED CYCLIC POSTFIXED WINDOWED SCHEMES

Md Mainul Islam Mamun, Candidate for the Doctor of Philosophy Degree

University of Missouri–Kansas City, 2023

ABSTRACT

In the proper designing of spectrally efficient 5th Generation (5G)/Beyond 5G (B5G) systems, minimization of Peak-to-Average Power Ratio (PAPR) of the time domain Orthogonal Frequency-Division Multiplexing (OFDM)/Cyclic Prefix (CP)-less OFDM signal and reduction of baseband signal Out-of-Band (OOB) spectral power in the vicinity of boundaries of the transmission frequency band is very much essential. In the perspective of considering the non-compatibility of CP-less Single-Input Single-Output (SISO) OFDM technique with Multiple-Input Multiple-Output (MIMO) technology adopted 5G systems, we present the first CP-less MIMO OFDM System. It is based on incorporating Discrete Fourier transform (DFT) spreading, signal discrimination with Walsh-Hadamard

coding, and PAPR reduction with Tukey (tapered cosine) time-domain windowing techniques. This combination of mechanisms provides an effective combination of benefits related to Bit Error Rate (BER), PAPR, Complementary Cumulative Distribution Function (CCDF) of PAPR, and OOB spectral power. The BER performances of our system in its simplified (SISO) form are compared with the CP-less SISO OFDM system. Additionally, the estimated OOB powers are also compared with various future-generation wireless communication systems such as DFT-Spread Windowing and Restructuring Orthogonal Frequency Division Multiplexing (WR-OFDM), Universal Filtered Multi-Carrier (UFMC) and Filter Bank Multi-Carrier (FBMC). Our simulation study shows that the proposed scheme achieves OOB spectral power attenuation of 142 dB with PAPR of 8.56 dB and BER of 10^{-4} under a scenario of Signal-to-Noise Ratio (SNR), $E_b/N_0 = 15$ dB with 16-Quadrature Amplitude Modulation (16-QAM) modulation.

To improve the spectral efficiency and robustness of wireless communication systems, on the other hand, drone-assisted 5G and beyond 5G wireless communication networking capabilities require strong consideration of constrained transmission power, user equipment receiver sensitivity, coverage area, and severe mmWave path loss. We present a Non-terrestrial downlink wireless communication system using a Cyclic Postfixed Windowed Orthogonal Frequency Division Multiplexing (CPW-OFDM) signal format. We demonstrate the impact of combining a Tukey windowing technique with Clipping and Filtering (CF) techniques for the simultaneous reduction of both OOB energy and PAPR.

Block Diagonalization (BD) channel precoding provides Multi- user Interference (MUI) reduction, while $(3, 2)$- Single Parity Check (SPC), Repeat and Accumulate (RA) channel coding, and Zero Forcing (ZF) signal detection schemes improve BER. Numerical results confirm that the proposed Non- terrestrial downlink CPW-OFDM system is suitable for multi-user signaling on mmWave frequencies.

APPROVAL PAGE

The faculty listed below, appointed by the Dean of the School of Computing and Engineering, have examined a dissertation titled "Advanced Orthogonal Frequency-Division Multiplexing Systems with Cyclic Prefix-Less Multiple-Input and Multiple-Output Discrete Fourier Transform Spreading and Unmanned Aerial Vehicles-Assisted Cyclic Postfixed Windowed Schemes," presented by Md Mainul Islam Mamun, candidate for the Doctor of Philosophy degree, and certify that in their opinion it is worthy of acceptance.

Supervisory Committee

Deep Medhi, Ph.D., Committee Chair
Department of Computer Science & Electrical Engineering

Cory Beard, Ph.D.
Department of Computer Science & Electrical Engineering

Praveen Rao, Ph.D.
Department of Computer Science & Electrical Engineering

Md Yusuf Sarwar Uddin, Ph.D.
Department of Computer Science & Electrical Engineering

Preetham Goli, Ph.D.
Department of Computer Science & Electrical Engineering

CONTENTS

ILLUSTRATIONS

TABLES

ACRONYMS

eMBB Enhanced Mobile Broadband

MBFSN Multimedia Broadcast Single Frequency Network

5G NR 5G New Radio

B5G Beyond 5G

DFT-s-OFDM Discrete Fourier transform-spread-OFDM

ITU International Telecommunication Union

VAR Virtual and Augmented Reality

CP-OFDM Cyclic Prefix OFDM

SISO Single-Input Single-Output

OOBE Out-of-Band-Emission

PAPR Peak-to-Average Power Ratio

BER Bit Error Rate

QPSK Quadrature Phase Shift Keying

MIMO Multiple Input Multiple Output

OFDM Orthogonal Frequency Division Multiplexing

QAM Quadrature Amplitude Modulation

LDPC Low-Density Parity-Check

3GPP 3rd Generation Partnership Project

LAPs Low Altitude Platforms

HAPs High Altitude Platforms

UAV Unmanned Aerial Vehicle

LoS Line-of-Sight

NTC Non-terrestrial Communication

D2D Device-to-Device

V2V Vehicle-to-Vehicle

mmWave Millimeter wave

cmWave Centimeter Wave

UFMC Universal Filtered Multicarrier

FBMC Filter Bank Multicarrier

WOLA-OFDM Weighted Overlap and Add based OFDM

CPW-OFDM Cyclic Postfixed Windowed OFDM

SPC Single Parity Check

BD Block Diagonalization

MUI Multiuser Interference

CCDF Complementary Cumulative Distribution Function

WR-OFDM Restructuring Orthogonal Frequency Division Multiplexing

WPRN Wireless Powered Relay Network

RF Radio Frequency

EHU Energy Harvesting Users

BS Base Station

NOMA Non-orthogonal Multiple Access

TS-NOMA Time Sharing Non-orthogonal Multiple Access

URLLC Ultra-reliable and Low-latency

SUs Secondary Users

DF Decode-and-Forward

PS Power Splitting

TA Time Allocation

RSU Roadside Unit

ITS Intelligent Transportation System

SFIM Space-Frequency Index Modulation

CF Clipping and Filtering

DM Digital Modulation

CF Clipping and Filtering

ISI Intersymbol Interference

CDS Channel Delay Spread

FEC Forward Error Correction

SNR Signal to Noise Ratio

PSD Power Spectral Density

FFT Fast Fourier Transform

IFFT Inverse Fast Fourier Transform

CSI Channel State Information

RA Repeat and Accumulate

ICI Inter-carrier Interference

IUI Inter-user Interference

ZF Zero-Forcing

MMSE Minimum Mean Square Error

SC-FDMA Single-carrier Frequency Division Multiple Access

FD-DFE Frequency-domain Decision Feed-back Equalization

LTE Long-Term Evolution

A2G Air-to-Ground (A2G)

ACKNOWLEDGEMENTS

First of all, I would like to express my deepest gratitude to my Ph.D. advisor Dr. Deep Medhi to give me the opportunity to work under him. He trained me in the skills of doing research step by step and writing research papers. He always encouraged me. His strong support helped me to overcome my bad times. He was always at my side in whatever situation I was in throughout this challenging journey of Ph.D. I learned a lot about the scientific way of doing research through his guidance. His great personality influenced me to be positive, dynamic, and passionate about my research. I also would like to thank Dr. Medhi for supporting me to present my research works at different conferences throughout the world.

I also would like to express my deepest gratitude to my Ph.D. supervisory committee member Dr. Cory Beard for his research advice, support, guidance, and valuable feedback on my Ph.D. research.

I also would like to acknowledge the continuous support, guidance, and feedback of my other committee members Dr. Praveen Rao, Dr. Yusuf Sarwar Uddin, and Dr. Preetham Goli for making this possible. Without their support, this dissertation would not have been completed.

I also would like to thank Dr. Masud Chowdhury, Dr. Ghulam Chaudhry, and Dr. Joseph Parisi for their continuous support, guidance, and elite patronization during my whole Ph.D. Journey.

I am thankful to the School of Graduate Studies of the University of Missouri-Kansas City (UMKC) for supporting me through the School of Graduate Studies Research Grant and Preparing Future Faculty (PFF) award. All these have motivated me to give continuous effort toward my research. Special thanks go to my PFF mentor Dr. Candace Schlein.

I like to thank all my labmates at Network Research Lab (NeTReL) for their help, advice, stimulating discussion, and adding cheers during the last five years. I am also thankful to my friends for their unconditional support. I also would like to thank all my teachers, administrators, office staff, and colleagues at UMKC who helped me to achieve this milestone. Special thanks go to Coretta Carter, Michelle Heiman, and Gina Campbell.

I am very thankful to the University of Rajshahi and Southern Utah University to provide me with the opportunity to complete this dissertation.

I would like to dedicate this dissertation to my parents Md Osman Ali and Morgina Khatun, my beloved wife Sinthia Islam Liza, my daughter Samaira Monali, my two sons Areeb Mamun and Umair Mamun, and my sister Omana Akhter. Words cannot express how grateful I am to them. Special thanks to my wife for her continuous understanding, patience, encouragement, and support over the years.

This dissertation is partially supported by National Science Foundation Grant # 1526299 and partially supported by a School of Graduate Studies Research Grant at UMKC.

CHAPTER 1

INTRODUCTION

1.1 Problem Statement

In commercially deployed internet-of-things (IoT), enhanced mobile broadband (eMBB) and multimedia broadcast single frequency network (MBSFN) supportable 5G new radio (NR) networks with multiple NR OFDM numerology and utilization of centimeter wave (cmWave) and millimeter wave radio frequencies (3.4 to 3.6 GHz, 24.25 to 27.5 GHz, 27.5 to 29.5 GHz, 37 GHz, 39 GHz and 57 GHz to 71 GHz), cyclic prefixed orthogonal frequency division multiplexing (OFDM) and cyclic prefixed discrete Fourier transform-spread-OFDM (DFT- s-OFDM) multiple access schemes have been implemented for downlink and uplink transmissions [1, 2]. Global mobile data traffic has been steadily increasing over the past ten years. According to the International Telecommunication Union (ITU), monthly mobile data traffic will amount to 5 zettabytes (ZB). The fifth generation (5G), the most recent effort to advance mobile communications technology, is anticipated to hit its limits by 2030. Numerous rapidly developing, highly data-intensive use cases and applications, such as multiway virtual meetings with holographic projection, virtual and augmented reality (VAR), brain communication interface, teleportation, remote surgery, etc., show that the latency, reliability, and data rate requirements of these future applications clearly exceed the capabilities of current 5G systems [3-6]. In

consideration of such a realistic scenario, significant emphasis is being given to the development of B5G-compatible enabling technology rather than implementing CP-OFDM and DFT-s-OFDM multiple access schemes. In the CP-OFDM signaling technique, different OFDM sub-channels/subcarriers are assigned to different users which in fact not indicative of showing the robustness of the system/network in terms of spectral efficiency. In addition, the excessive usage of the Cyclic Prefix (CP) degrades spectral efficiency as well as transmission latency in the CP-OFDM system.

1.2 Motivation

Orthogonal frequency division multiplexing (OFDM) is the widely accepted transmission waveform for Wi-Fi, Long-Term Evolution (LTE), 5G New Radio, and narrowband IoT. While OFDM has many advantages such as efficient use of the spectrum through the division of channels into fading subchannels, it also has issues such as high Peak-to-Average Power Ratio (PAPR), spectral leakage, strict synchronization requirements, and frequency offset sensitivity.

To overcome some of these problems, the cyclic prefix is used with OFDM, but there are also some disadvantages. For example, when the cyclic prefix (CP) is excessively used, particularly in highly dispersive channels, potential degradation of Single-Input Single-Output (SISO) performance is possible, in terms of spectral efficiency as well as transmission latency.

To circumvent these impacts, a promising CP- Less uncoded OFDM system for SISO was proposed in [7]. In such a system, it is expected that the CP-Less OFDM

waveform would be capable of fulfilling of the low latency and high spectral efficiency requirements. The authors made Out-of-Band-Emission (OOBE), PAPR, BER, Transmission efficiency, Transmission latency, and Power efficiency comparisons between CP-Less uncoded SISO OFDM and conventional CP OFDM system with FFT size of 64 and QPSK, 4-QAM and 16-QAM digital modulations. In merely transmission efficiency comparison, low to higher-order digital modulations (64-QAM, 32-QAM, 16-QAM, and 4-QAM) were used. On the basis of simulation results, the authors demonstrated that their CP-Less SISO OFDM technique would be suitable for future 5G and beyond wireless services and applications including URLLC, IoT- based mMTC, and eMBB. In their paper, the authors pointed out that the applicability of their proposed CP-Less OFDM scheme is highly desirable for MIMO and it may require some modifications to make it fully compatible with MIMO due to having multiple channels interaction that may impact the orthogonality among subcarriers when CP is not used. We note that little work has been done on the MIMO CP- Less OFDM system so far.

On the other hand, considering non-terrestrial networking, the 3^{rd} Generation Partnership Project (3GPP) has initiated studies on the role of satellites in terrestrial mobile radio communications. 3GPP 5G releases provide a promising opportunity to integrate previously independent terrestrial and satellite networks.

The overall structure of integrated terrestrial-non-terrestrial airborne networks generally incorporates Low Altitude Platforms (LAPs), High Altitude Platforms (HAPs), and satellite platforms. In $3GPP$ activity, a great emphasis is given to the role of LAPs in

addition to integrating satellites and HAPs into the terrestrial network. In LAPs sub networking, the Unmanned Aerial Vehicle (UAV) is located at a height between 0.1 km to 1 km from the ground surface [14].

UAVs are the most prominent example of LAPs. The UAVs, popularly known as drones, are expected to be an important component of near-future wireless networks. With strong Line-of-Sight (LoS) linking, high data rate transmission capability, and fast and flexible deployment, UAVs can provide non-terrestrial Communication (NTC) services in various types of natural and man-made disasters such as floods, fires, and earthquakes that have devastating impacts on the economy and human life. UAVs can facilitate fast and efficient information dissemination in various terrestrial networks that support Device-to-Device (D2D), Vehicle-to-Vehicle (V2V) as well as mobile ad hoc networks. UAVs can be used to enhance communication at high-frequency millimeter wave (mmWave) bands in $3D$ Multiple Input Multiple Output (MIMO), massive MIMO, and reconfigurable antenna array systems. The massive deployment of small, power-limited Internet of Things (IoT) devices in many key IoT application domains such as health care, emergency response, transportation, and smart cities can potentially benefit from the presence of UAVs [15], [16].

After commercial deployment of 5G New Radio (5G NR) networks, NTC can provide cost-effective and high-capacity connectivity in the future beyond 5G (B5G)/ 6^{th} generation (6G) wireless networks. The 6G research is currently focusing on the development of NTC to promote ubiquitous and high-capacity global connectivity. $6G$ is expected to envision a three-dimensional ($3D$) heterogeneous architecture in which

terrestrial infrastructures are complemented by non-terrestrial stations, including UAVs as Low Altitude Platform Stations (LAPSs), High Altitude Platform Stations (HAPSs), and satellites [17].

In the present scenario of mobile networks, 5G NR is based on the utilization of both Centimeter Wave (cmWave) and Millimeter Wave (mmWave) radio frequencies. In such networks, Cyclic Prefixed OFDM (CP-OFDM) in the downlink and Cyclic Prefixed Discrete Fourier Transform-spread-OFDM (DFT-s-OFDM) in the uplink have been adopted as radio waveforms [18], [19]. Other radio waveforms such as filtered OFDM, Universal Filtered Multicarrier (UFMC), and Filter Bank Multicarrier (FBMC) were also suggested for $5G$ NR networks.

However, an advanced windowing-based waveform called - Weighted Overlap and Add based OFDM (WOLA-OFDM) is believed to be capable of mitigating the OOB emission by providing faster side lobe decay. This WOLA-OFDM is constrained, however, in terms of a data collision problem between consecutive OFDM symbols. Cyclic postfixed windowed OFDM (CPW-OFDM) is an improved and simplified version of the WOLA-OFDM system, having only one extension on the right side. Windowing is performed on both the right extension and the left part with the cyclic prefix (CP) and thus avoids data collision without any time loss between the consecutive OFDM symbols [20], [21].

1.3 Aims, Objectives, and Improvement

Here in the first part of our research works, we provide a MIMO CP-Less OFDM approach. Several changes are necessary for the SISO system.

By considering the constraints of the proposed CP-Less OFDM scheme and its compatibility with different modes of MIMO, our work addresses the design of a new DFT spread [8] system. Our approach is compatible with the utilization of low-density parity-check (LDPC) channel coding technique [9, 10] and channel encoded MIMO CP-Less OFDM system based on implemented DFT spreading, Walsh-Hadamard coding [11], and Tukey time-domain windowing [12] techniques. The 5G frame structural information provided on the website in [13] will be incorporated into our work. Our study on a number of symbols shows that our approach is very promising.

On the other hand, in the second part of our research, a comprehensive demonstration has been made on beyond 5G compatible downlink drone-assisted non-terrestrial mmWave CPW-OFDM system. Consideration is made relative to drone transmission power (46 dBm) [22], receiver sensitivity [23], and drone height for a coverage area [24].

In Fig. 19, we present a typically assumed scenario of non-terrestrial downlink transmission in which a low altitude mmWave-drone-Base station at a height of h from the ground surface is transmitting signals towards four users located in a circular area of radius R.

We present a novel framework of such a system with the introduction of (3, 2)-Single Parity Check (SPC) and Repeat and Accumulate (RA) channel coding, a Cyclic

Postfixed Windowed Orthogonal Frequency Division Multiplexing (CPW-OFDM) signaling scheme, a Tukey windowing technique combined with Clipping and Filtering and Block Diagonalization (BD) channel precoding techniques. The impact of various signal processing algorithms/techniques incorporated in our simulated system has been analyzed properly.

In our research work, we gave emphasis to present a robust system in terms of enhancing data transmission bandwidth, reducing Out-of-Band (OOB) spectral power and Peak-to-Average Power Ratio (PAPR) with reasonably acceptable Bit Error Rate (BER) and multiuser interference (MUI) reduction. In the proposed system, all the subcarriers in the OFDM signal are utilized simultaneously by all users. Numerical results ratify that our proposed system is undoubtedly robust in terms of reasonable performance metrics.

1.4 How These Works are Related

In our research work, we gave emphasis mainly on the development of a robust 5G compatible spectrally efficient system. We proposed two advanced MIMO OFDM systems, CP-less MIMO Discrete Fourier Transform Spread OFDM system using Walsch Hadamard Code and A UAV- Assisted Multiuser Non-terrestrial Cyclic Postfixed Windowed OFDM System, to enhance data transmission bandwidth, reduce Out-of-Band spectral power and Peak-to-Average Power Ratio with reasonably acceptable Bit Error Rate and Multiuser Interference reduction.

1.5 Summary of Contributions

In this section, we briefly discuss the main contributions of this dissertation.

1.5.1 CP-less MIMO Discrete Fourier Transform Spread OFDM System

- We present a new DFT (Discrete Fourier Transform) spread B5G compatible LDPC channel encoded Multiple-Input Multiple-Output (MIMO) CP-Less OFDM system based on incorporated DFT spreading, signal discrimination with Walsh-Hadamard coding and PAPR reduction with Tukey (tapered cosine) time-domain windowing techniques.

- The performances of our proposed simulated system are analyzed and discussed in terms of Bit Error Rate (BER), PAPR, Complementary Cumulative Distribution Function (CCDF) of PAPR and OOB spectral power.

- The BER performances of our system in its simplified (SISO) form are compared with the CP-less SISO OFDM system.

- Additionally, the estimated OOB powers are also compared with various future-generation wireless communication systems such as DFT-Spread Windowing and Restructuring Orthogonal Frequency Division Multiplexing (WR-OFDM), Universal Filtered Multi-Carrier (UFMC) and Filter Bank Multi-Carrier (FBMC).

- The simulation results reveal that the proposed scheme achieves reasonably acceptable OOB spectral power attenuation of $142dB$ with PAPR of $8.56dB$ and BER

of $10^{-}4$ under a scenario of E_b/N_0 value of $15dB$ with rectangular $16-QAM$ constellation.

The above contributions are published in our paper [58].

1.5.2 UAV-Assisted Multiuser Non-terrestrial Cyclic Postfixed Windowed OFDM System

- A comprehensive demonstration has been made on the suitable utilization of our 6G compatible windowing-based waveform in the Unmanned Aerial Vehicle (UAV)-assisted Non-terrestrial downlink Millimeter Wave (mmWave) Cyclic Postfixed Windowed (CPW)- Orthogonal Frequency Division Multiplexing (OFDM) system.

- We present a novel framework of a UAV-assisted Non-terrestrial downlink system with the implementation of a windowing-based waveform, CPW-OFDM.

- The key contribution of our research work is to make proper designing of a multi-antenna configured Windowed OFDM System which incorporates additional Cyclic post fixing scheme for 6G compatible UAV-Assisted Multiuser Non-terrestrial networks.

- We assess our systems' performances in terms of Bit Error Rate (BER) improvement, Multi-User Interference (MUI) reduction, Out of Band (OOB) spectral power leakage reduction, and Peak to Average Power Ratio (PAPR) reduction.

- In our system, we have introduced the Block Diagonalization (BD) channel precoding technique for reducing MUI and the computational complexity of a precoding

technique.

- Applicability of the Tukey windowing technique combined with Clipping and Filtering techniques has made our system robust in perspective of reducing PAPR and OOB spectral power leakage.

- Simultaneous implementation of pre and post-fixing techniques compensates the effects of the multipath fading channel and prevents collision between two consecutive windowed OFDM symbols.

- Simulation results verify the significant enhancement of the achievable BER performance with the implementation of various useful channel coding and signal detection techniques.

- System performance metrics of our research work have also been compared with the works of other researchers and notable achievements have been received.

- We analyze the impact of various signal processing algorithms/ techniques incorporated in our simulated system.

  The above contributions are published in our paper [59].

1.6 Organization

The rest of this dissertation is organized as follows: Chapter 2 presents an extensive literature survey on Cyclic Prefix and Cyclic Prefix-less SISO and MIMO OFDM Systems and UAV-assisted terrestrial and non-terrestrial networking systems.

We discuss our proposed Cyclic Prefix-less MIMO DFT-Spread OFDM System in Chapter 3. First, we provide a description of our proposed system. Then we present a comprehensive treatment of the signal model. Then the numerical results including BER, PAPR, CCDFs of PAPR, and OOBE are presented in this chapter.

In Chapter 4, we present the UAV-assisted multiuser non-terrestrial CPW OFDM system. In this chapter, firstly, the signal model of our proposed mmWave non-terrestrial Downlink CPW-OFDM system is described. The system description is given. Then the simulation and numerical results are presented at the end of this chapter.

Finally, We conclude this dissertation and briefly discuss several future research directions in Chapter 5.

CHAPTER 2

LITERATURE REVIEW

In this chapter, we discuss the state-of-art researches that have been done to improve the spectral efficiency, performance, and robustness of wireless communication systems. As mentioned in Chapter 1, this dissertation is divided into two major sections such as CP-less MIMO DFT-Spread OFDM System and UAV-Assisted MUltiuser Non-terrestrial CPW OFDM System, thus, the literature review is also organized into two sections based on these issues. In each section, we present the related works and how our work has novel contributions compared to other works.

2.1 Cyclic Prefix-Less MIMO Discrete Fourier Transform Spread OFDM System

2.1.1 Literature Review

In reviewing literature for enhancing 5G/B5G system performance, various approaches to the problem of OOB power and PAPR reduction are found in addition to estimating BER. Hamamreh et al. [7] introduced an alignment signal for a CP-Less SISO OFDM system and studied its performance in terms of spectral efficiency as well as transmission latency with consideration of degradation due to the excessive usage of CP. In their work, degraded BER performances are presented for the CP-Less SISO OFDM system in comparison with a regular SISO CP-OFDM system. The transmission efficiency, transmission latency, and out-of-band emissions (OOBE) of the CP-Less SISO OFDM

system are much better in comparison with regular the SISO CP-OFDM system. PAPR is almost identical in both cases. To our knowledge, this is the only work on SISO CP-Less OFDM. Because our work builds on this work to provide MIMO capabilities by adding several additional mechanisms, we believe our work to be the first work on MIMO CP-less OFDM. Plus we demonstrate high-quality BER, PAPR, and OOB performance.

In regards to DFT spreading, there have been a number of works. Choi et al. [25] extended the idea of a DFT spreading-based low PAPR Filter Bank Multi-Carrier (FBMC) scheme to the intercarrier interference-free Alamouti-coded FBMC. Substantially lower PAPR than the previous Alamouti-coded FBMC scheme was achieved in their study. Additionally, a properly chosen sub-block size in DFT spreading was found to have produced better BER performance in comparison to the theoretical Alamouti-coded BER with a diversity order of two.

Furthermore, Nazmul et al. [26] proposed a DFT-spread Windowing and Restructuring OFDM (WR-OFDM) communication system for PAPR and OOB spectrum power reduction under consideration of a cyclic prefix length of 128 with 512 active carriers with an FFT size of 1024. In their work, the authors demonstrated 3 dB more PAPR reduction as compared to the WR-OFDM system and achievement of OOB attenuation of 110 dB at the window length of 62 (less than half of the CP length).

In [27], Wu and et al., proposed an improved joint precoding method based on two precoding schemes for simultaneous reduction of OOB emission and high PAPR under-utilization of merely 64 subcarriers and low order digital modulation (QPSK constellation mapping). The estimated OOB attenuation was found to have a value of less than 50dB.

In [28], Kim et al., suggested a WR-OFDM system and showed competitive and desirable OOB spectrum characteristics that were very important to save the frequency resources and competitively similar shape to the OOB spectra of FBMC and UFMC system. In their work, the Kaiser window was used with an FFT size of 128 and a cyclic prefix length of 16. The authors made a comparative study on the OOB power spectrum showing OOB power reduction of 26 dB, 80 dB, and 117dB in comparison to in-band spectral power for OFDM, UFMC, and FBMC systems under the scenario of linearity condition. In [21] Zayani et al., investigated the performance of a Weighted Overlap and Add based OFDM (WOLA-OFDM) system under consideration of cyclic prefix length of 72, FFT size of 1024, Window length of 32 with 16-QAM digital modulation. In their work, the authors showed that 20dB OOB power reduction was achieved in the WOLA-OFDM system in comparison with the CP-OFDM system.

In [56], Saeedi et al., focused on low-complexity channel estimation techniques for CP-less MIMO-OFDM systems. The authors proposed an efficient channel estimation algorithm based on the exploitation of pilot subcarriers and sparsity properties of the MIMO channel. The algorithm significantly reduced the computational complexity while maintaining satisfactory channel estimation accuracy.

Xu et al., investigated the performance of CP-less MIMO-OFDM systems in the presence of channel estimation errors in [57]. The authors analyzed the impact of imperfect channel estimation on system performance and proposed a technique to mitigate the performance degradation caused by channel estimation errors. The results provided insights into the robustness of CP-less MIMO-OFDM systems under practical conditions.

It is observable from numerical results presented in previous related works that no effort has not yet been done on the MIMO CP-Less OFDM system which motivated me to develop a spectrally efficient robust 5G/B5G compatible wireless communication with reasonably acceptable BER, PAPR, CCDF of PAPR, and OOB spectral power.

We note that little work has been done on the MIMO CP- Less OFDM system so far. We address this by using a new approach as described in the following section.

2.1.2 Recent Advancements

To explore the most recent advancements in CP-less MIMO OFDM systems we review and refer to a few recent and remarkable works on CP-less MIMO OFDM systems. These papers provide valuable insights into various aspects, including transceiver design, modulation and coding, channel estimation, and performance analysis.

In [52] Tang et al., presented a CP-less MIMO OFDM transceiver design specifically tailored for 5G New Radio (NR) systems. The authors proposed a novel scheme for channel estimation and equalization, considering the characteristics of CP-less OFDM. The performance of the proposed system is evaluated through simulations, and the results demonstrate its feasibility and benefits in 5G NR scenarios.

Furthermore, F. Ahmad et al., explored the advanced modulation and coding techniques for CP-less MIMO-OFDM systems [53]. The authors investigated the performance of different modulation schemes, such as Quadrature Amplitude Modulation (QAM) and

Phase Shift Keying (PSK), in combination with advanced coding techniques like Low-Density Parity-Check (LDPC) codes. Simulation results showed the achievable data rates and error performance of the proposed system.

Recently, in [54] Jiang et al., proposed a Full-Duplex MIMO System Based on Cyclic Prefix (CP)-Free orthogonal frequency division multiplexing (OFDM) in Sensor Network. Their results have shown that full-duplex (FD) system based on OFDM is potential for wireless sensor networks. They extended FD to further improve spectral efficiency by removing CP with optimal canceling self-interference (SI) remains a challenge. In this paper, they analytically studied the conventional FD OFDM system and proposed a CP-free system on this basis. The key point of the proposed scheme is the symbols are transmitted in a unit of two identical symbols without CP. To eliminate the intersymbol interference, the disturbed part was replaced by the repeated signal at the receiver, which had the same effect as CP. Finally, an SI cancellation was down to restore the transmitted symbols. As a key of analysis, a multiple-input multiple-output (MIMO) FD simulation model was carried to show that their proposed scheme is effective in terms of the bit error ratio (BER).

Another very recent work [55] has been carried out by Zhang et al., where they tackled the problem of the signal-to-noise ratio estimation for a cyclic prefix (CP)-Less orthogonal frequency division multiplexing (OFDM) system in the presence of Gaussian noise over multipath fading channels. First, they introduced the cyclic correlation of the CP-Less OFDM signal with CP, and analyze the cyclic correlations for Gaussian noise and received signal. Second, they isolated the Gaussian noise power from the signal

power. Finally, they obtained the close-form expression of SNR estimation by using cyclic correlations. Computer simulation results verified the effectiveness of the proposed method.

These papers represent a sample of recent research on CP-less MIMO OFDM systems. Further exploration of these works can offer a deeper understanding of the advancements and challenges in the field.

Other advancements in CP-less MIMO OFDM systems generally revolve around addressing challenges such as inter-carrier interference (ICI), inter-user interference (IUI), signal processing algorithms, precoding, and beamforming, while maximizing the benefits of the increased spectral efficiency. Some notable advancements include:

1. ICI and IUI mitigation techniques: Researchers have proposed various algorithms and techniques to mitigate the effects of ICI and IUI in CP-less MIMO OFDM systems. These include advanced equalization algorithms, such as minimum mean square error (MMSE) and zero-forcing (ZF) techniques, as well as interference cancellation schemes.

2. Advanced signal processing algorithms: Researchers have developed advanced signal processing algorithms to improve the performance of CP-less MIMO OFDM systems. These algorithms aim to optimize resource allocation, precoding, and beamforming techniques to maximize system capacity, minimize interference, and enhance overall system performance.

3. Channel estimation and equalization techniques: Accurate channel estimation is crucial in MIMO OFDM systems. Researchers have proposed novel channel estimation

techniques that exploit the characteristics of CP-less OFDM signals, such as pilot-based estimation, sparse channel estimation, and compressed sensing techniques. These techniques aim to improve channel estimation accuracy, reduce pilot overhead, and enhance system performance.

4. Hybrid precoding and beamforming: Hybrid precoding and beamforming techniques combine the advantages of analog and digital beamforming in MIMO OFDM systems. These techniques enable efficient use of limited RF chains in massive MIMO systems, leading to improved spectral efficiency and reduced hardware complexity.

5. Nonlinear Precoding Techniques: Researchers have explored nonlinear precoding techniques to improve the performance of CP-less MIMO OFDM systems. Nonlinear precoding algorithms, such as Tomlinson-Harashima precoding (THP) and vector perturbation (VP) precoding, can effectively mitigate inter-symbol interference (ISI) and inter-carrier interference (ICI) in CP-less systems.

6. Hybrid CP-less MIMO OFDM Systems: Hybrid systems that combine CP-less MIMO OFDM with other modulation schemes or multiple access techniques have gained attention. For example, combining CP-less MIMO OFDM with single-carrier frequency division multiple access (SC-FDMA) can provide enhanced performance in terms of spectral efficiency and power efficiency.

7. Low-Complexity Receiver Algorithms: Researchers have developed low-complexity receiver algorithms for CP-less MIMO OFDM systems, aiming to reduce computational complexity while maintaining performance. These algorithms leverage the sparsity of the channel and exploit the structure of the received signals to achieve efficient detection and

decoding.

8. Interference Mitigation and Resource Allocation: Advanced interference mitigation techniques and resource allocation algorithms have been investigated for CP-less MIMO OFDM systems. These techniques optimize subcarrier allocation, power allocation, and user scheduling to maximize the system's capacity and mitigate inter-user interference.

9. Frequency-Domain Processing: Frequency-domain processing techniques, such as frequency-domain equalization (FDE) and iterative frequency-domain decision feedback equalization (FD-DFE), have been explored to combat inter-symbol and inter-carrier interference in CP-less MIMO OFDM systems.

10. Massive MIMO Systems: CP-less MIMO OFDM systems have also been investigated in the context of massive MIMO, which involves a large number of antennas at the base station. Massive MIMO offers significant gains in terms of spectral efficiency and interference suppression, and researchers have explored its application in CP-less MIMO OFDM systems.

11. Machine Learning Approaches: Machine learning techniques have been employed to enhance CP-less MIMO OFDM systems. Researchers have investigated the use of deep learning algorithms for channel estimation, interference cancellation, and equalization tasks. These techniques aim to improve system performance and adapt to dynamic channel conditions.

2.2 UAV-Assisted Multiuser Non-terrestrial Cyclic Postfixed Windowed OFDM System

2.2.1 Literature Review

Recently, considerable literature has grown up around the theme of UAV-assisted non-terrestrial networking. The authors of [29] optimized the performance of a UAV-assisted Wireless Powered Relay Network (WPRN) to maximize the sum rate in all service sectors. In such a network, UAV was considered to be used as a radio-frequency (RF) power transmitter and as a communication relay between Energy Harvesting Users (EHUs) and a Base Station (BS). The EHUs employed a combination of Non-orthogonal Multiple Access (NOMA) and Time-division Multiple Access (TDMA).

In [30], an optimization framework for power and time resource allocation during Time Sharing Non-orthogonal Multiple Access (TS-NOMA) transmissions performed by a UAV was proposed. An analysis on the joint optimization of various UAV systems parameters including the UAVâs position, height, beam width, and the resource allocation for uplink communications between ground IoT devices and a UAV employing short Ultra-reliable and Low-latency (URLLC) data packets is provided in [31].

A comprehensive study was made in [15] on improving the secure performance of a UAV-assisted jamming wideband CRNs where a UAV transmits the jamming signal to interfere with the eavesdropper (Eve) and the SBS provides communication services for the Secondary Users (SUs) over multiple sub-carrier channels. The authors of [16] made an investigative study on the problem of lifetime maximization of a UAV-assisted network in the presence of multiple sources of interference, where the UAVs were deployed to

collect data from a set of wireless sensors. In prolonging the lifetime of the network, the key role of UAVs was demonstrated.

A UAV-assisted disaster relief network is addressed in [32] where UAVs can disseminate emergency information to those terrestrial users in a multicast manner. At [33], the authors considered a two-phase Decode-and-Forward (DF) relay network assisted by a UAV, where the UAV performed energy harvesting and information decoding simultaneously with a Power Splitting (PS) receiver structure. For the network, the PS and Time Allocation (TA) factors were optimized to minimize the outage probability in transferring the data from a source to a destination suffering from blockages in the direct link.

A general Roadside Unit (RSU)/ UAVs joint planning solution was proposed in [34] so that UAVs could complement RSU coverage by providing flexible connectivity capable of adapting coverage for traffic fluctuations, energy consumption, and budgetary constraints that all have effects on Intelligent Transportation System (ITS) operations.

In [35], the characteristics of a mobile self-organizing network composed of multiple UAVs were analyzed to improve the communication quality of the UAV network. An investigative study was made in [36] on the transmission issue of UAV communication systems using OFDM with index modulation. In such a study, the performance of the spectrum efficiency, energy efficiency, and BER were analyzed according to different conditions and simulation parameters.

The authors of [26] worked on SISO WR-OTFS System for 5G and B5G compatible

terrestrial networks with low order digital modulation (4QAM) and estimated OOB reduction power. In [37] and [38], BER performances comparisons were made by the authors for Space-Frequency Index Modulation (SFIM) systems in different cases of SFIM, SIM, and FIM with low order digital modulation (4QAM) and constant amplitude OFDM wireless communication system with low order digital modulation (QPSK), respectively. PAPR reduction performance analysis has been investigated in [39] for FFT-NOMA with W-NOMA in discrete wavelet transformation based 5G compatible non-orthogonal multiple access networks under utilization of low order modulation (BPSK and QPSK).

The numerical results presented in the work [37]-[39], [51] have been compared with the results in our proposed system. From the points of OOB energy and PAPR reduction with simultaneous mitigation of BER at the high-quality receivers, some compensation techniques with the combination of conventional Tukey windowing technique with the Clipping and Filtering (CF) technique have not been widely investigated in most literatures. In our proposed transceiver for UAV-assisted multiuser Non-terrestrial Cyclic Postfix Windowing OFDM system, utilization of useful combined techniques has presented performance advantages. We address our proposed approach in the following section.

CHAPTER 3

CYCLIC PREFIX-LESS MIMO DISCRETE FOURIER TRANSFORM SPREAD OFDM SYSTEM

In this chapter, we present our proposed Cyclic Prefix-less MIMO Discrete Fourier Transform Spread OFDM System. Firstly, we provide our system description. After that, we present a short review of the CP-less Uncoded Single Input Single Output OFDM System before discussing our signal model in detail. At the end of this chapter, we analyze the detailed results.

3.1 System Description

The key concepts underlying the transmission mechanism of our proposed DFT spread CP-Less OFDM system with a multi-path frequency selective and slowly varying fading channel-dependent alignment signal is illustrated in Fig. 1. We assume that binary data bits are channel encoded and digitally modulated using various low and higher order digital modulation (DM) [40]. The complex digitally modulated symbols are processed with a 512-point FFT operation and subsequently spatially multiplexed in spatially multiplexed encoders; here we illustrate this by producing two independent data streams. In each of the two data streams, frequency domain data symbols are packed up near the central part of a 4096-IFFT-sized block with no data symbols at its two ends and central point in the symbol mapping to avoid nearby channel interference. The symbols are first converted from serial to parallel form to introduce a 4096-IFFT for OFDM multicarrier

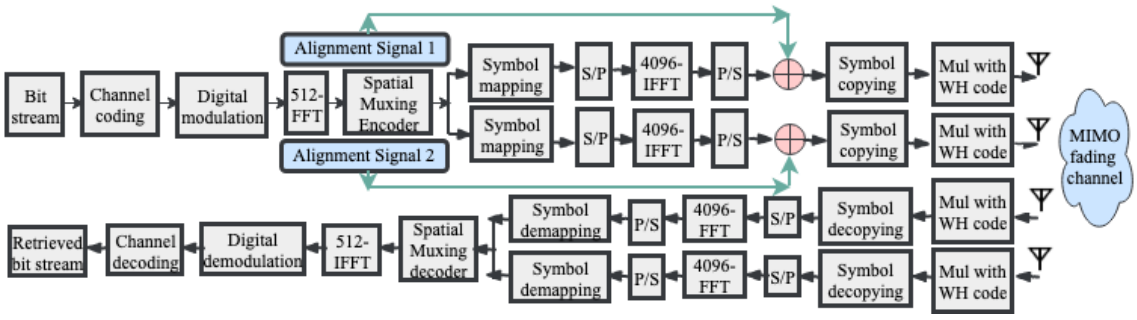

Figure 1: Block diagram of DFT Spread Windowed MIMO CP-Less OFDM System

modulation assigning each symbol to different active subcarriers.

In parallel to serial conversion, a time domain signal vector is generated whose samples are coming from the contribution of all of the frequency data symbols [41]; this is combined with an alignment signal. The resultant signal is repeated and multiplied with Walsh-Hadamard codes to produce orthogonal signals transmitted from each of the antennas (two antennas for this example).

On the receiving side, the desired transmitted signals are extracted using Walsh-Hadamard codes at each antenna. After execution of each of the reverse operations, eventually, the transmitted binary bit steam is retrieved.

3.2 Signal Model

In this section, we first review the SISO CP-Less OFDM system described in [7] to set the stage for our proposed MIMO CP-less DFT spread OFDM system. Then we present our proposed DFT Spread Windowed MIMO CP-Less OFDM System.

3.2.1 CP-Less uncoded SISO OFDM System: Review

The transceiver structure of the previously proposed CP- Less SISO OFDM system [1] is presented in Fig. 2. It is seen from Fig. 2 that the modulated frequency data symbols rearranged for each CP-Less OFDM symbol containing N number of modulated frequency data symbols are first converted from serial to parallel and then passed through an IFFT block and subsequently parallel to serial converted to produce a time domain signal vector whose samples are coming from the contribution of all the frequency data symbols.

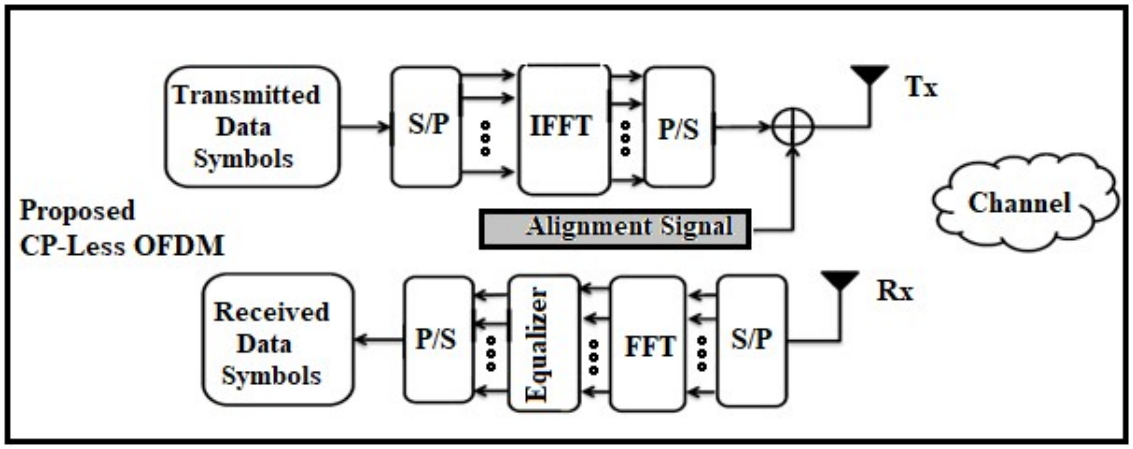

Figure 2: Transceiver structure of the proposed CP-less SISO OFDM system [7]

A time domain alignment signal ($\mathbf{c}_i$) of identical size equal to $(N \times 1)$ is added to each time domain CP-Less OFDM signal ($\mathbf{s}_i$) and i^{th} transmitted signal can be modeled as:

$$\mathbf{t}_i = \mathbf{s}_i + \mathbf{c}_i \in \mathbb{C}^{[N \times 1]}, \tag{3.1}$$

where N is the number of modulated frequency data symbols. On transmission through a

frequency selective and slowly varying fading channel, $\mathbf{h}$, of $(R+1)$ taps, the i^{th} received baseband signal vector, $\mathbf{y}_i \in \mathbb{C}^{[(N+R)\times 1]}$ can be modeled as:

$$\mathbf{y}_i = \mathbf{h} * \mathbf{t}_i + \mathbf{n}_i = \mathbf{h} * (\mathbf{s}_i + \mathbf{c}_i) + \mathbf{n}_i, \tag{3.2}$$

where, $\mathbf{n}_i \in \mathbb{C}^{[(N+R)\times 1]}$ is zero mean complex additive white Gaussian noise (AWGN) at the receiver. The convolution form of the signal model in (3.2) can be rewritten by inserting a Toeplitz matrix, $H \in \mathbb{C}^{[(N+R)\times N]}$, as:

$$\mathbf{y}_i = H\mathbf{t}_i + \mathbf{n}_i = H(\mathbf{s}_i + \mathbf{c}_i) + \mathbf{n}_i. \tag{3.3}$$

The total resulting i^{th} signal to be transmitted can be modeled under consideration of intersymbol interference (ISI) cancellation at the transmitter and circularity providing a signal at the receiver can be calculated as [7]:

$$\begin{aligned} \hat{\mathbf{t}}_i &= \mathbf{s}_i + \mathbf{u}_i + \mathbf{z}_i \\ &= \mathbf{s}_i + (H^T H)^{-1} H^T \begin{bmatrix} 0^{[N\times 1]} \\ -H_p s_1^{[R\times 1]} \end{bmatrix} \\ &\quad + (H^T H)^{-1} H^T \begin{bmatrix} H_p s_1^{[R\times 1]} \\ 0^{[N\times 1]} \end{bmatrix}, \end{aligned} \tag{3.4}$$

where $H_p \in \mathbb{C}^{[R\times N]}$ is the interference part of the Toeplitz matrix, H, while $(.)^T$ represents the Hermitian transpose operation. The i^{th} signal received at the receiver, $\hat{\mathbf{y}}_i \in \mathbb{C}^{[(N+R)\times 1]}$ with AWGN noise $\hat{\mathbf{n}}_i$ can be written as:

$$\hat{\mathbf{y}}_i = H\hat{\mathbf{t}}_i + \hat{\mathbf{n}}_i. \tag{3.5}$$

Discarding filter delay due to a time dispersive channel by eliminating the last R samples of $\hat{\mathbf{y}}_i$ from (3.5), the i^{th} received signal $\hat{\hat{\mathbf{y}}}_i$ would be of $(N \times 1)$ in size and on further

processing of $\hat{\hat{\mathbf{y}}}_i$ with frequency domain channel equalization, the time domain CP-Less i^{th} indexed OFDM signal will be detected.

3.2.2 Signal Model for DFT Spread Windowed MIMO CP-Less OFDM System

For our proposed approach for a MIMO CP-Less OFDM System, several changes are necessary from the SISO system described above in Section 3.2.1. We use 2×2 MIMO as an example to describe our approach that is depicted in the transceiver structure of the DFT Spread Windowed MIMO CP-Less OFDM System in Fig. 1.

We assume that there are four independent multi-path frequency selective and slowly varying fading channels. As two channel dependent alignment signals are to be designed, we consider that the signal transmitted from each of the two transmitting antennas reaches the two receiving antennas through identical frequency selective and slowly varying fading channels $\mathbf{g} = [g_0 g_1 \dots g_R]^T \in \mathbb{C}^{[(R+1)\times1]}$ and $\mathbf{h} = [h_0 h_1 \dots h_R]^T \in \mathbb{C}^{[(R+1)\times1]}$. The power delay profiles of the two Rayleigh multipath time dispersive channels are defined to be exponentially decaying with $(R+1)$ taps and expressed as:

$$h(DF, n) = a_1 e^{[-DF\times n]}; n = 0, 1, \dots R \tag{3.6}$$

$$g(DF, n) = a_2 e^{[-DF\times n]}; n = 0, 1, \dots R, \tag{3.7}$$

where, a_1 and a_2 are the normalization factors, n represents the tap index and DF is the decay factor of the channel.

If $G_p \in C^{[R\times N]}$ represents the interference part of the Toeplitz matrix of the channel impulse response, g with $(R+1)$ taps for a block-based transmission system, we can write:

$$G_p = \begin{bmatrix} 0 & \dots & g_R & \dots & g_0 \\ \vdots & 0 & \ddots & \ddots & \vdots \\ 0 & \dots & 0 & \dots & g_R \end{bmatrix} \tag{3.8}$$

The corresponding Toeplitz matrices, $G \in C^{[(N+R)\times N]}$

$$G = \begin{bmatrix} G_u \\ G_p \end{bmatrix} \quad = \begin{bmatrix} g_0 & 0 & \dots & \dots & 0 \\ \vdots & g_0 & 0 & \ddots & \vdots \\ \vdots & \vdots & g_0 & \ddots & \vdots \\ g_R & \vdots & \vdots & \ddots & 0 \\ 0 & g_R & \vdots & \ddots & g_0 \\ \vdots & 0 & g_R & \ddots & \vdots \\ \vdots & \vdots & 0 & \ddots & \vdots \\ 0 & 0 & \dots & \dots & g_R \end{bmatrix} \tag{3.9}$$

where G_u and G_p are the $N \times N$ interference-free channel convolution matrices. With our considered frequency selective channels, it can be expected that both of two receiving antennas would receive identical signals.

Taking the Toeplitz matrix, H, and its component, H_p, from [1] and considering preprocessed i^{th} time indexed CP-Less OFDM signals, $\mathbf{s}_{1i}$ from Layer 1 and $\mathbf{s}_{2i}$ from Layer 2, the alignment signals that will be added at Layer 1 and Layer 2 to cancel out ISI can be written as:

$$\mathbf{u}_{1i} = (H^T H)^{-1} H^T \begin{bmatrix} 0^{[N\times 1]} \\ -H_p s_{1i}^{[R\times 1]} \end{bmatrix} \tag{3.10}$$

$$\mathbf{u}_{2i} = (G^T G)^{-1} G^T \begin{bmatrix} 0^{[N\times 1]} \\ -G_p s_{2i}^{[R\times 1]} \end{bmatrix}. \tag{3.11}$$

The alignment signals that will be added at Layer 1 and Layer 2 to provide circularity can be written as:

$$\mathbf{z}_{1i} = (H^T H)^{-1} H^T \begin{bmatrix} H_p s_{1i}^{[R\times 1]} \\ 0^{[N\times 1]} \end{bmatrix} \tag{3.12}$$

$$\mathbf{z}_{2i} = (G^T G)^{-1} G^T \begin{bmatrix} G_p s_{2i}^{[R\times 1]} \\ 0^{[N\times 1]} \end{bmatrix}, \tag{3.13}$$

where $H_p \in \mathbb{C}^{[R\times N]}$ and $G_p \in \mathbb{C}^{[R\times N]}$ are the interference parts of Toeplitz matrix, H and G for transmission from Layer 1 and Layer 2, respectively.

The total resulting i^{th} signal to be transmitted prior to orthogonal signal generation from first and second transmitting antennas can be modeled and calculated as:

$$\mathbf{t}_{1i} = \mathbf{s}_{1i} + \mathbf{u}_{1i} + \mathbf{z}_{1i} \tag{3.14}$$

$$\mathbf{t}_{2i} = \mathbf{s}_{2i} + \mathbf{u}_{2i} + \mathbf{z}_{2i}. \tag{3.15}$$

The signal presented in (3.14) and (3.15) are $(N \times 1)$ matrix in size. In order to produce orthogonality between these two signals, they are multiplied block wise with two different Walsh-Hadamard codes of processing gain 8 to produce signal $\hat{\mathbf{t}}_{1i}$ and $\hat{\mathbf{t}}_{2i}$ of both $(N \times 8)$ matrix in size. The i^{th} signal received from two transmitting antennas at receiving antenna 1 and 2 with AWGN noise added can be written as:

$$\hat{\mathbf{y}}_{1i} = H\hat{\mathbf{t}}_{1i} + G\hat{\mathbf{t}}_{2i} + \hat{\mathbf{n}}_{1i} \tag{3.16}$$

$$\hat{\mathbf{y}}_{2i} = H\hat{\mathbf{t}}_{1i} + G\hat{\mathbf{t}}_{2i} + \hat{\mathbf{n}}_{2i} \tag{3.17}$$

The signal vectors $\hat{\mathbf{y}}_{1i}$ and $\hat{\mathbf{y}}_{2i}$ are $(N+R)\times 8$ matrix in size. On removing channel delay, the modified signal vectors $\hat{\hat{\mathbf{y}}}_{1i}$ and $\hat{\hat{\mathbf{y}}}_{2i}$ would be $(N \times 8)$ matrix in size. On multiplying signal $\hat{\hat{\mathbf{y}}}_{1i}$ with assigned Walsh-Hadamard codes at Layer 1 would cancel out the signal transmitted from second transmitting antenna. Similarly, on multiplying signal $\hat{\hat{\mathbf{y}}}_{2i}$ with assigned Walsh-Hadamard codes at Layer 2 would cancel out the signal transmitted from first transmitting antenna. On further processing with execution of some necessary steps as mentioned in Fig. 1, the transmitted signal is detected.

3.3 Result Analysis

In this section, we present the simulation performance results using MATLAB of the proposed DFT Spread Windowed MIMO CP-Less OFDM system. In our study, we use BER, PAPR, OOBE, and CCDFs of PAPR as main performance metrics to validate and demonstrate the performance of our simulated system as discussed in the following subsections.

In our simulated system, maximum utilization of active subcarriers is made viz. 3300 sub carriers are active and the remaining 796 subcarriers are null distributed equally at the upper and lower band edges viz. 388 null subcarriers are assigned at the band edges to reduce adjacent channel interference in a channel bandwidth of 250 MHz and FFT size of 4096. Additionally, the multipath frequency selective and slowly varying fading channel is used here to consider its coherence bandwidth smaller than the bandwidth of the signal such that the transmitted signal experiences uncorrelated fading. The proposed model is simulated to evaluate the system performance for parameter values presented in

Table 1.

In our study, we use BER, PAPR, OOBE, and CCDFs of PAPR as main performance metrics to validate and demonstrate the performance of our simulated system in various subsections as follows:

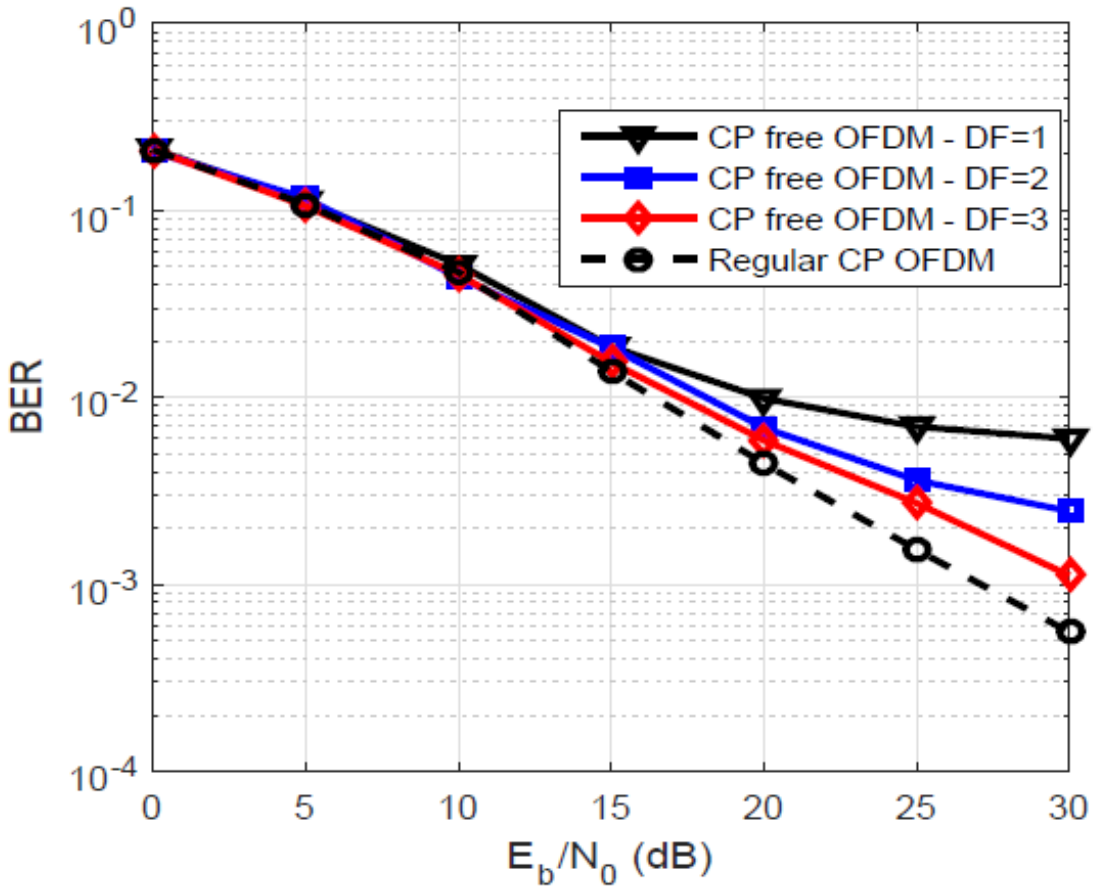

Figure 3: BER comparison between CP-less OFDM and CP OFDM with different channel decaying factors underutilization of channel spread length equal to one forth Of the OFDM symbol period, QPSK modulation and 64 subcarriers [7]

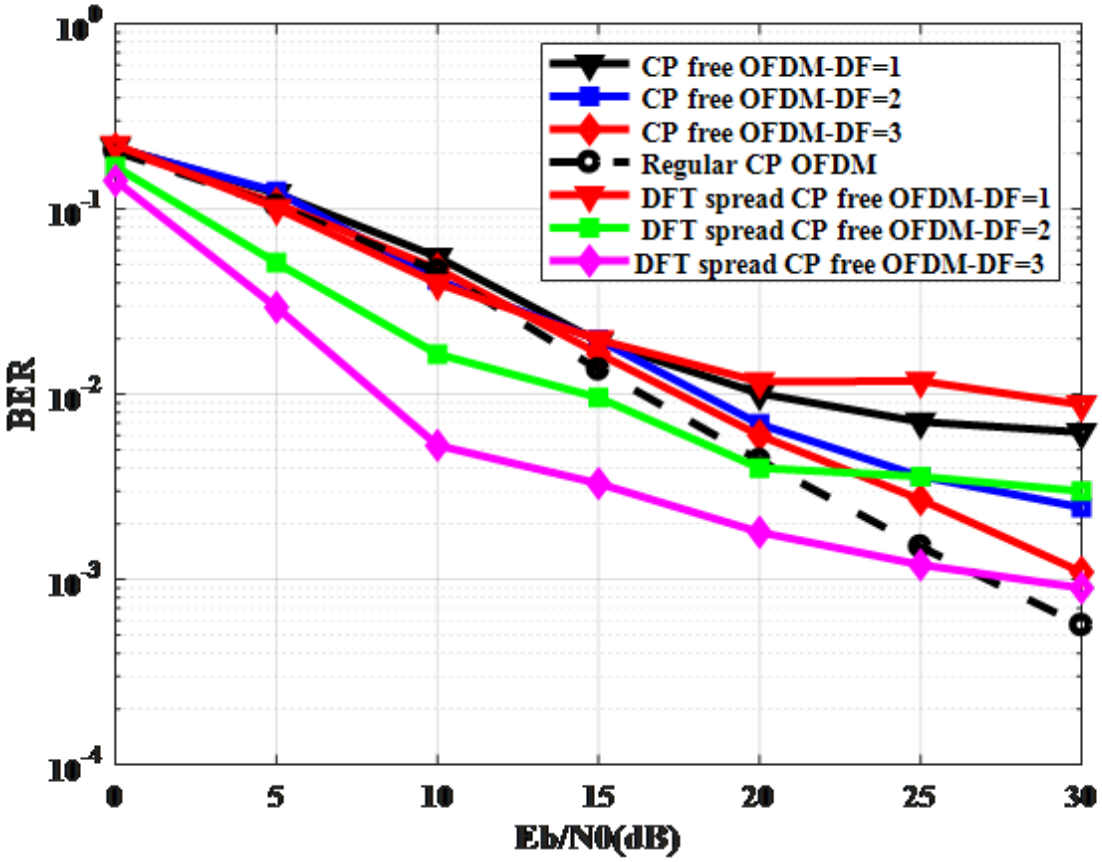

Figure 4: BER performance comparison of our DFT spread CP free uncoded OFDM system in its simplified single-input single-output (SISO) form with Regular SISO uncoded CP OFDM and SISO uncoded CP free OFDM system under scenario of utilizing identical parameters presented in Figure 3

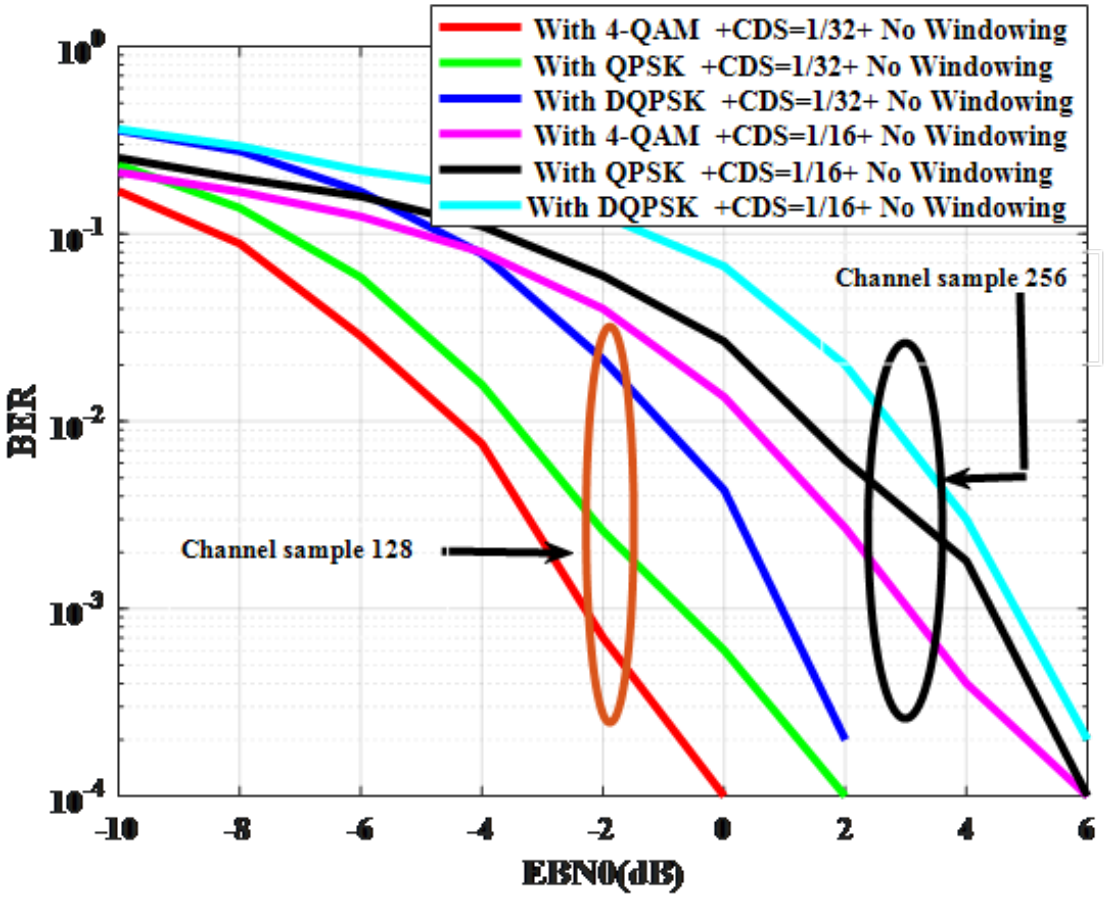

Figure 5: BER performance of CP-Less MIMO OFDM system for low order digital modulations: At various lengths of CDS

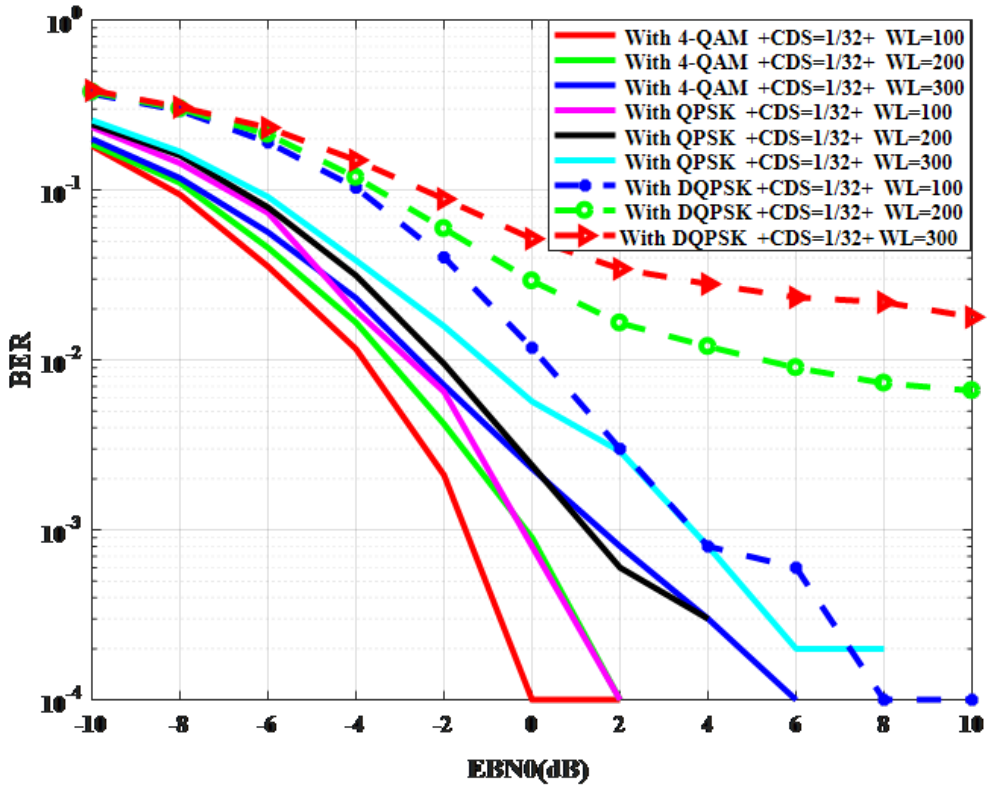

Figure 6: BER performance of CP-Less MIMO OFDM system for low order digital modulations: Windowed at CDS=$1/32$

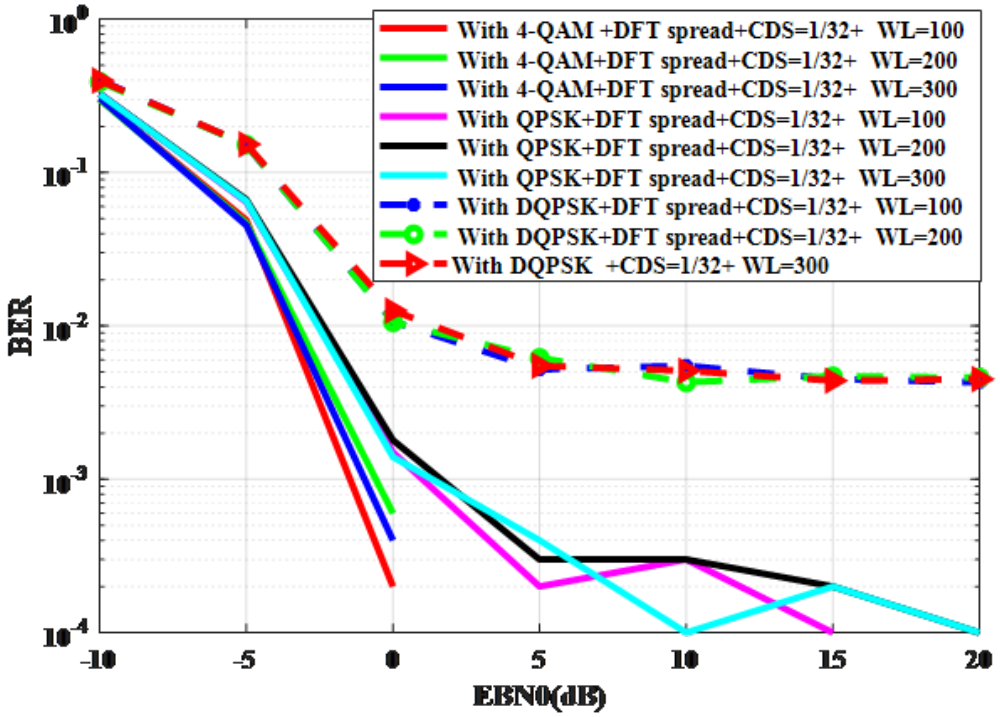

Figure 7: BER performance of CP-Less MIMO OFDM system for low order digital modulations: DFT spread and windowed at different CDS

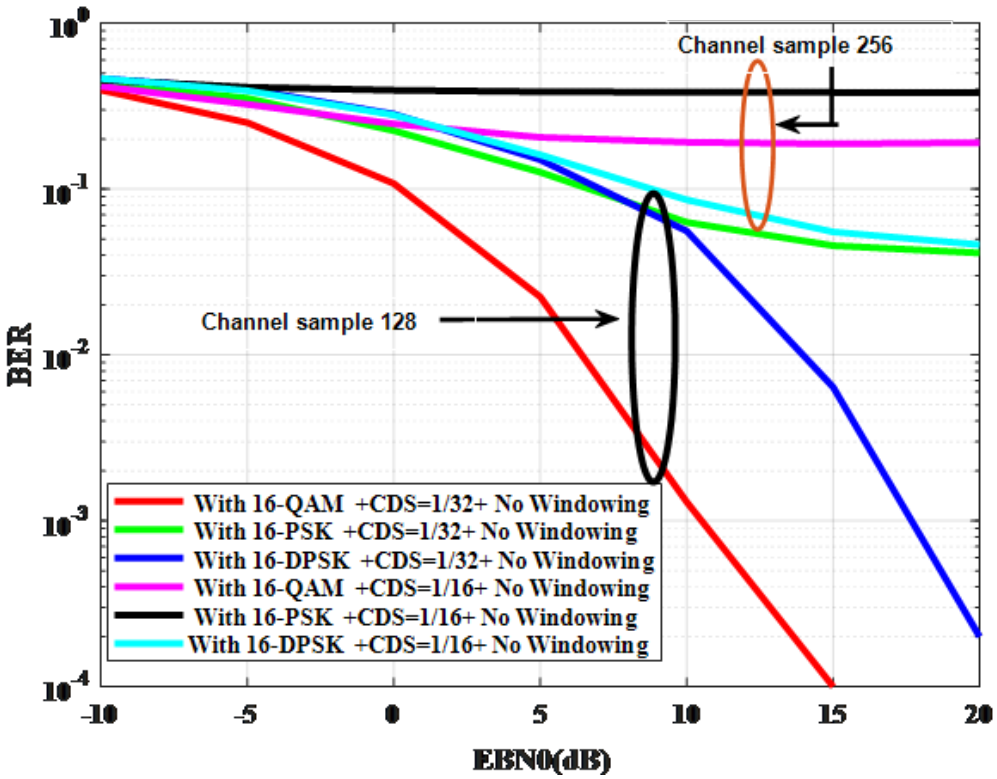

Figure 8: BER performance of CP-Less MIMO OFDM system for higher order digital modulations: At various lengths of CDS

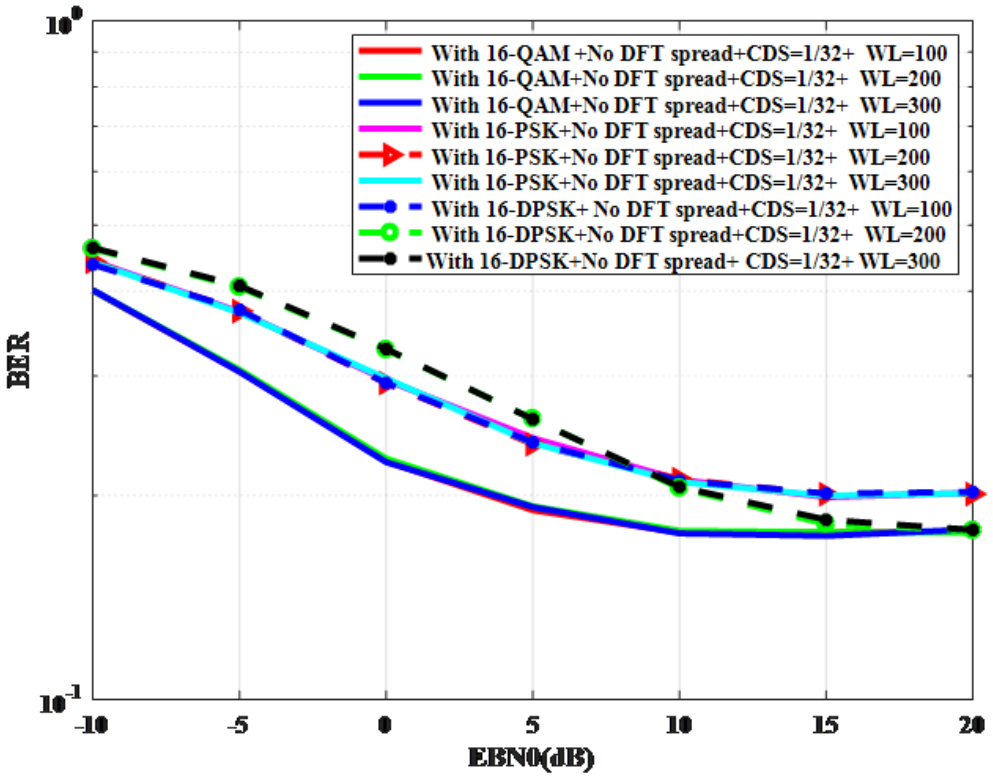

Figure 9: BER performance of CP-Less MIMO OFDM system for higher order digital modulations: Windowed at CDS=$1/32$

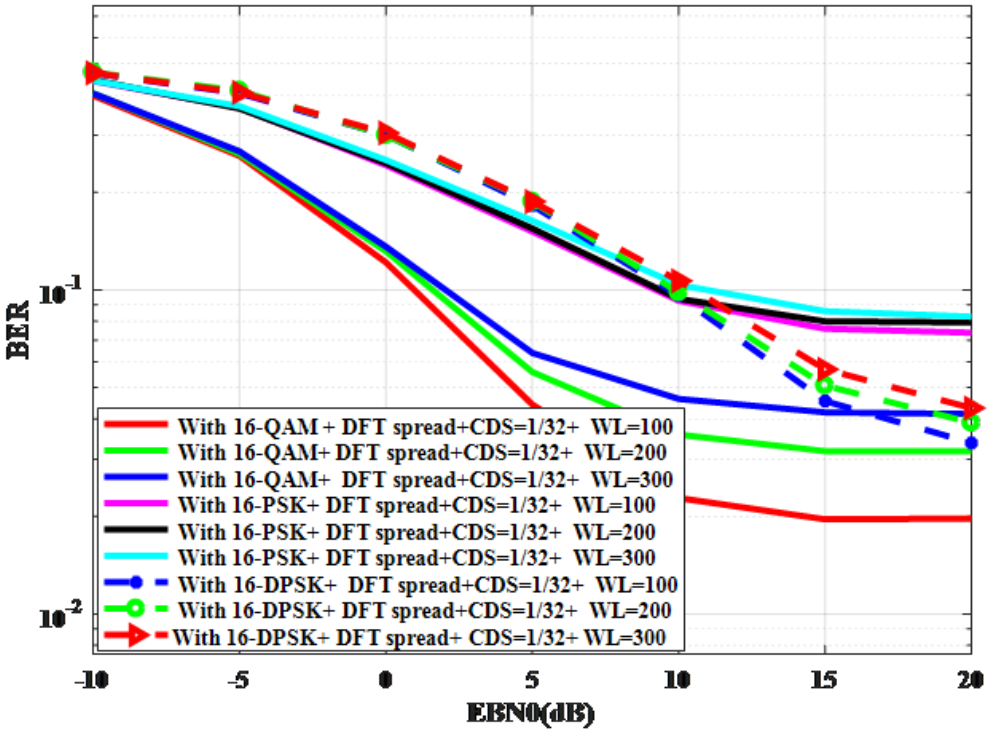

Figure 10: BER performance of CP-Less MIMO OFDM system for higher order digital modulations: DFT Spread and Windowed at different CDS

3.3.1 BER Comparison

Fig. 3 shows the BER performance comparison for previous SISO CP-Less OFDM. It is seen from graphical illustrations presented in Fig. 3 that the previous SISO CP-Less OFDM technique removes totally the redundancy of CP and exhibits BER performance close to that provided by regular OFDM as the decaying factor of the channel increases.

Fig. 4 compares SISO cases. It shows the uncoded BER performance of the our DFT spread CP-Less OFDM system in its simplified SISO form compared with Regular SISO CP OFDM and the SISO CP-Less OFDM system presented in [7] utilizing identical parameters. Various decay factors (DF) are shown, as used in (3.6) and (3.7). Notice the best case for lower E_b/N_0 is SISO compatible DFT spread scheme considering higher channel DF(=3), QPSK modulation with 64 subcarriers.

Fig. 5 - 7 show the BER curves of the proposed CP-Less MIMO OFDM system for low order modulation (4-QAM, QPSK, and DQPSK) with the utilization of $1/2$ rate LDPC forward error correction (FEC) over various Rayleigh multipath channel delay spread (CDS) with and without implementation of DFT spreading and windowing techniques. The performance improvement of the CP-Less MIMO OFDM system without implementing DFT spreading and windowing techniques is clearly observed in Fig. 5, in the case of lower CDS of the time dispersive channel. The estimated BER is 10^{-4} for E_b/N_0 value of 0dB for 4-QAM. At a typically assumed $BER = 10^{-3}$, a SNR gain of approximately 5.3 dB is obtained for 4-QAM with lower channel delay spread length in comparison with 4-QAM under consideration of comparatively higher channel delay spread length.

Fig. 6 shows BER curves of windowed CP-Less MIMO OFDM system without implementing DFT spreading and utilization of low order modulation with lower channel delay spread length. It can be seen from the figures how the system performance degrades with an increase in windowing length. Such operation affects frequency-domain complex input data symbols modulated by active subcarriers. BER performance is found to be reasonably acceptable. Here, BER is 10^{-4} for E_b/N_0 value of 0dB with 4-QAM at windowing length of 100 samples. Fig. 7 shows BER curves of DFT Spread windowed CP-Less MIMO OFDM system and utilization of low ordermodulation with lower channel delay spread length. It can be seen from the figures that the system performance is not well discriminated from each other at low SNR values. At a 0 dB value of E_b/N_0 with 4-QAM, the estimated BER is found to have a value of 2×10^{-4} at windowing length of 100 samples.

Fig. 8 - 10 show the BER curves of the proposed LDPC channel encoded CP-Less MIMO OFDM system for higher order modulation (16-QAM, 16-PSK, and 16-DPSK). For the CP-Less MIMO OFDM system in Fig. 8, the estimated BER is 10^{-4} for $E_b/N_0 = 15$ dB using 16-QAM. Fig. 9 shows BER curves of the windowed CP-Less MIMO OFDM system without implementing DFT spreading and utilization of higher order digital modulations with lower channel delay spread length. The system performance in 16-QAM is comparatively better but no discrimination is seen for different windowing lengths. Fig. 10 presents BER performance curves for DFT spread CP-Less MIMO OFDM system with implementing windowing technique and and lower channel delay spread (CDS). It can be seen from the figures that the system performance is better in

16-QAM and little discrimination is seen for lower E_b/N_0. At 15 dB value of E_b/N_0 with 16-QAM, the estimated BER is found to have an approximate value of 2×10^{-2} at windowing length of 100 samples.

3.3.2 PAPR and OOBE

Figs. 11 - 14 show graphical illustrations of the OOB spectrum of the DFT spread CP-Less OFDM system with and without implementing windowing technique and utilization of higher order digital modulations for Layer 1 and Layer 2. In every case, we observe that implementation of windowing technique improves OOB reduction performance.

In Table 2 and Table 3, numerically estimated OOB powers in comparison to in-band spectral power are presented. Note that with the higher order modulation (Table 2), the maximum OOB power reduction of approximately 134 dB is achieved in a windowed CP-Less OFDM system without the implementation of DFT spreading. On the other hand, a maximum OOB power reduction of approximately 143 dB is achieved in a windowed CP-Less OFDM system with the implementation of DFT spreading. With the lower order modulation (Table 3), we observe that the maximum OOB power reduction of approximately 143 dB is achieved in the windowed CP-Less OFDM system *without* implementation of DFT spreading. On the other hand, maximum OOB power reduction of approximately 139 dB is achieved in the windowed CP-Less OFDM system *with* implementation of DFT spreading. It is also observable that in low-order modulation, the DFT spread CP-Less OFDM system has reasonably satisfactory OOB reduction performance. From Table 4 and Table 5, we see that PAPR values confirm that implementation of the

Tukey windowing technique in the DFT spread CP-Less OFDM system reduces PAPR in comparison with non-implementation of the Tukey windowing technique. It is also observable that in low-order digital modulation, the DFT spread CP-Less OFDM system has reasonably satisfactory OOB reduction performance.

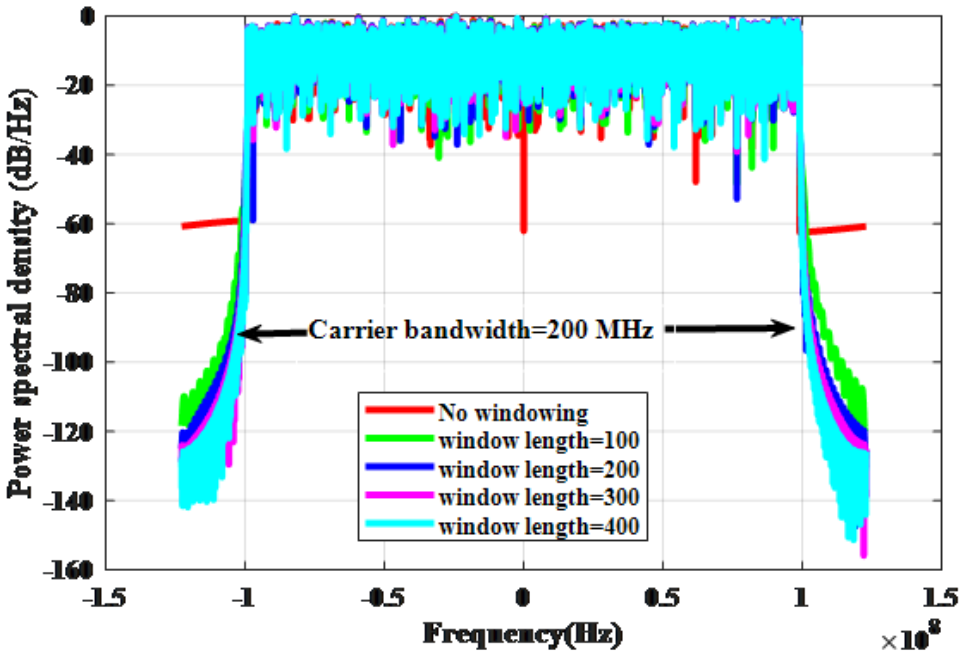

Figure 11: Power Spectral density of DFT spread CP-Less OFDM with and without implementing windowing technique and utilization of lower order digital modulation for Layer 1 (First Transmitting antenna)

3.3.3 CCDFs of PAPR

Fig. 15 plots the CCDFs of PAPR for our DFT spread CP-Less OFDM system with utilization of lower order modulation. From the figure, we can observe that a PAPR

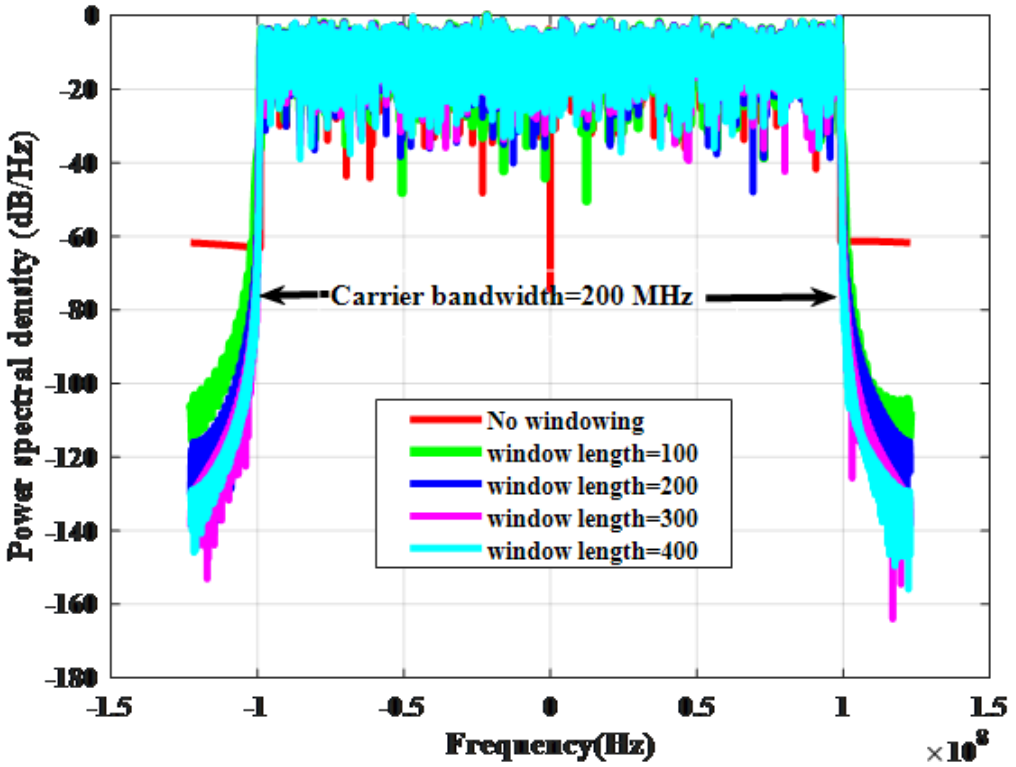

Figure 12: Power Spectral density of DFT spread CP-Less OFDM with and without implementing windowing technique and utilization of lower order digital modulation for Layer 2 (Second Transmitting antenna)

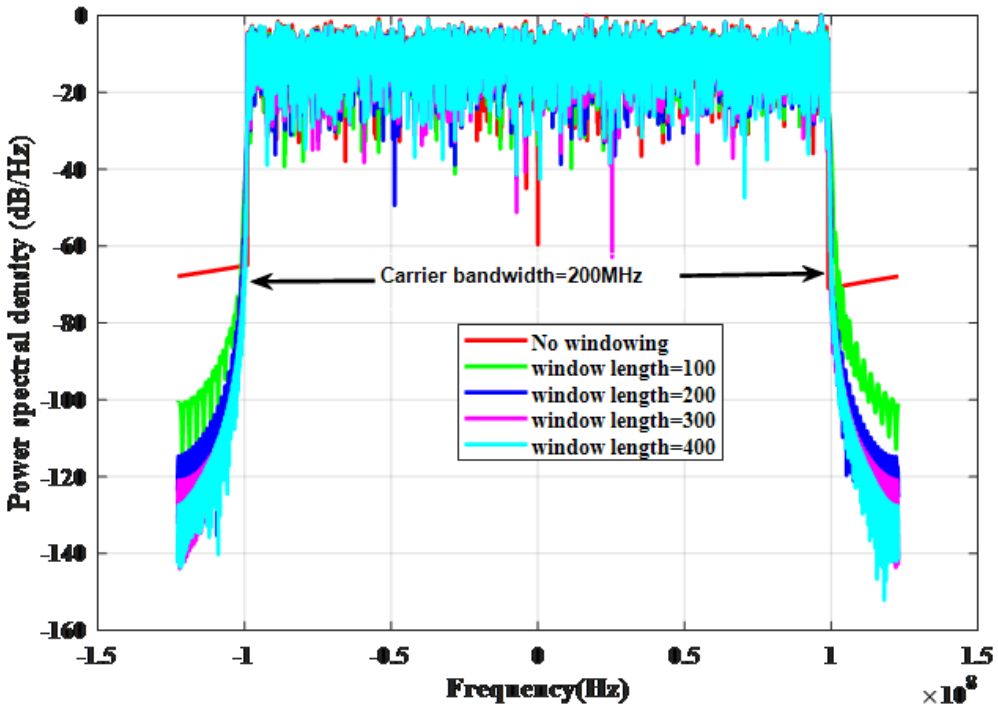

Figure 13: PSD of DFT spread CP-Less OFDM for higher order digital modulation (Layer 1)

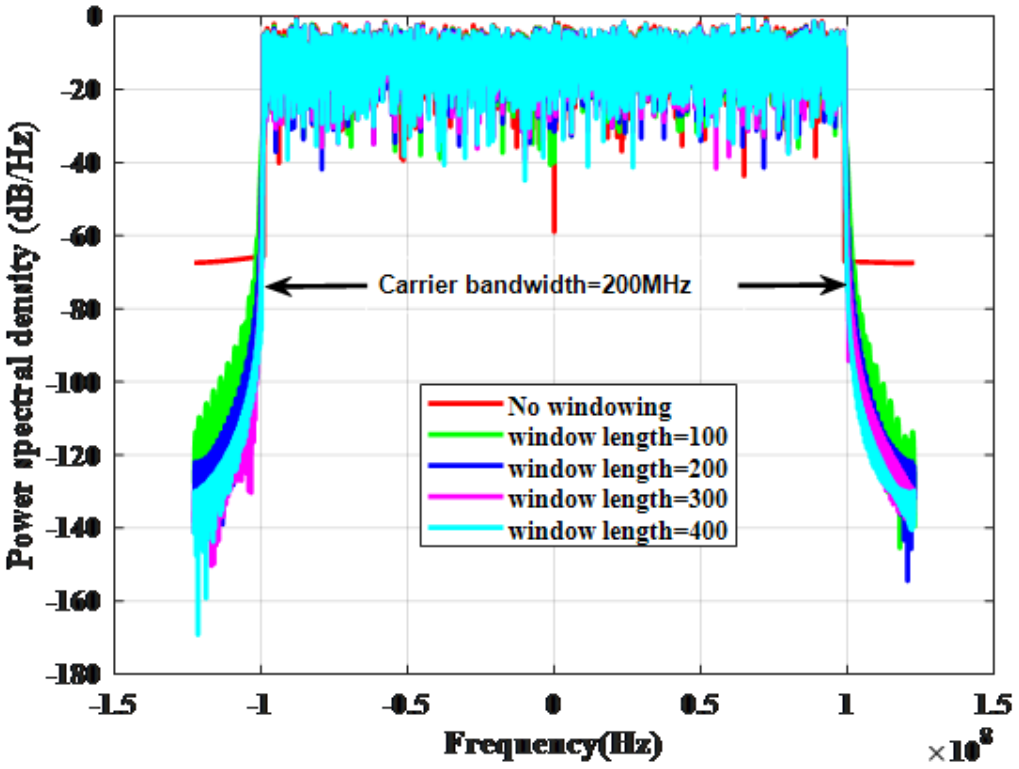

Figure 14: PSD of DFT spread CP-Less OFDM for higher order digital modulation (Layer 2)

reduction of 0.5 dB at $CCDF = 10^{-2}$ can be obtained with Layer 1 under scenario of no windowing compared with Layer 1 with windowing length of 300 samples. In case of Layer 2, a PAPR reduction of 0.4 dB is found to have achieved at $CCDF = 10^{-2}$.

Fig. 16 plots the CCDFs of PAPR for our DFT spread CP-Less OFDM system with utilization of higher order modulation. We can observe that a PAPR reduction of 0.4 dB at $CCDF = 10^{-3}$ can be obtained with Layer1 under a scenario of no windowing compared with Layer 1 with windowing length of 300 samples. In case of Layer 2, a PAPR reduction of 0.3 dB is found to have achieved at $CCDF = 10^{-3}$.

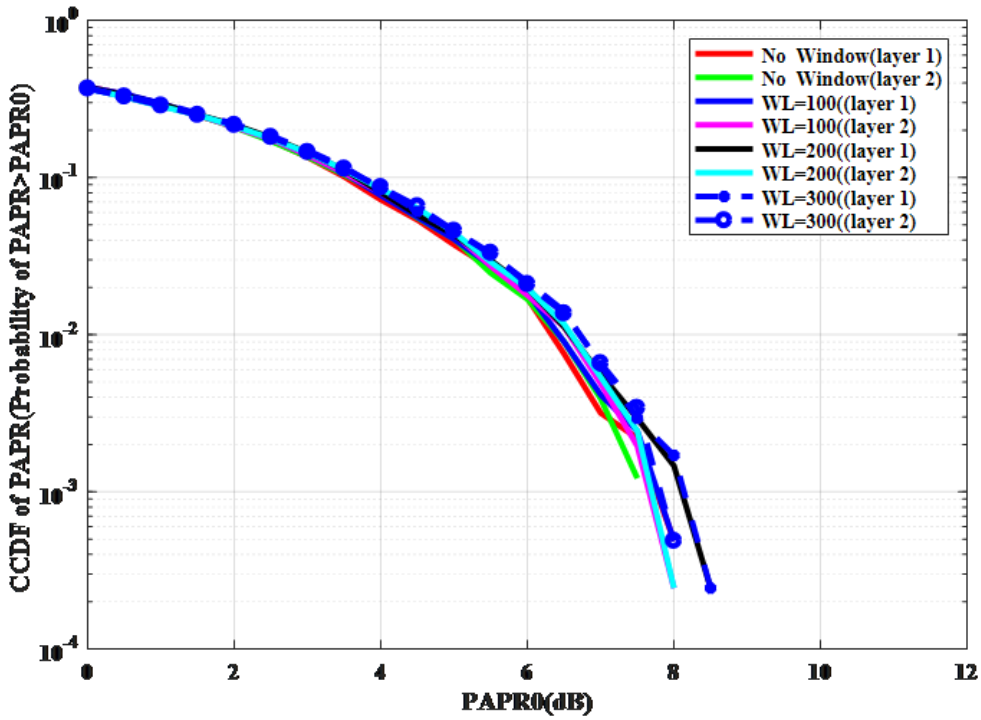

Figure 15: CCDFs of PAPR for DFT spread CP-Less OFDM system for lower order digital modulation

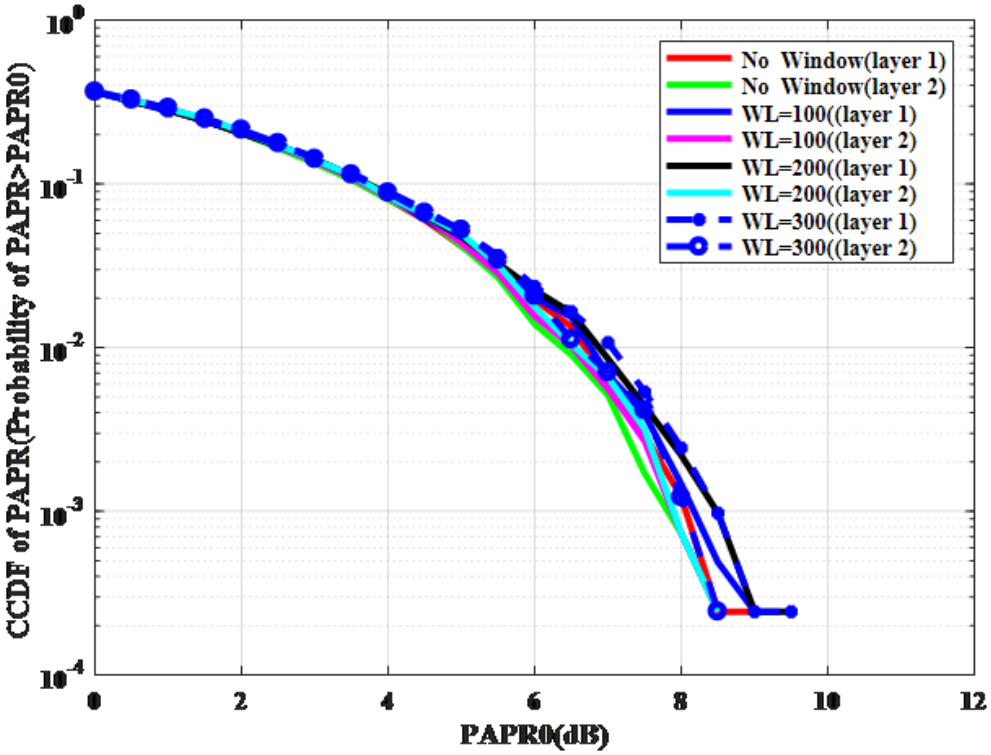

Figure 16: CCDFs of PAPR for DFT spread CP-Less OFDM system for higher order digital modulation

Table 1: Simulation Parameters for the Cyclic Prefix-Less MIMO Discrete Fourier Transform Spread OFDM System

FFT size	4096
Effective subcarriers, number of frequency-domain complex input data symbols in a single OFDM	3300
Subcarrier spacing [KHz]	60
Sampling frequency [MHz]	245.76
Carrier Bandwidth [MHz]	200
System Bandwidth [MHz]	250
No of OFDM symbol	2
Input data symbols	4-QAM, QPSK, DQPSK, 16-QAM, 16-PSK, 16-DPSK
Windowing	Tukey (Tapered cosine)
Window length (samples) at both ends of Tukey windowing function	100, 150, 200, 250, 300, 350 and 400
No of frequency domain symbols in DFT spreading	512
Length of the dispersive part of OFDM symbol (sample)	128 and 256
Normalized Signal to Noise ratio, Eb/N0 [dB]	-10 to 20
Channel	AWGN and multi-path frequency selective and slowly varying fading channels
Spreading code	Walsh-Hadamard code
Spreading factor of spreading codes	8
Normalization factor of power delay profile of Rayleigh multipath time dispersive channel	0.8 and 0.7
Decaying factor of the channel	3

Table 2: OOB Power Comparison for Higher Order Modulation (16-QAM)

Window Length	**OOB power (dB) for 16-QAM**			
	CP-Less OFDM without DFT spreading		**DFT-spread CP-Less OFDM**	
	Layer 1	***Layer 2***	***Layer 1***	***Layer 2***
0	-63.98	-53.45	-67.83	-67.44
100	-104.86	-108.73	-100.74	-127.83
150	-108.78	-112.64	-114.86	-114.88
200	-120.07	-123.35	-123.84	-141.60
250	-122.61	-122.19	-119.63	-129.78
300	-130.89	-124.30	-132.23	-135.28
350	-123.16	-134.09	-127.92	-141.46
400	-126.47	-126.74	-142.50	-138.14

Table 3: OOB Power Comparison for Lower Order Modulation (4-QAM)

Window Length	**OOB power (dB) for 4-QAM**			
	CP-Less OFDM without DFT spreading		**DFT-spread CP-Less OFDM**	
	Layer 1	***Layer 2***	***Layer 1***	***Layer 2***
0	-55.33	-62.89	-60.70	-61.76
100	-105.70	-99.57	-118.35	-106.96
150	-108.69	-111.61	-124.34	-119.98
200	-112.35	-121.36	-124.85	-130.01
250	-122.57	-123.61	-121.37	-127.81
300	-118.83	-125.59	-128.79	-139.09
350	-128.82	-134.14	-126.60	-134.33
400	-143.15	-135.50	-127.59	-130.61

Table 4: PAPR Comparison (16-QAM)

Window Length	**PAPR (dB) for 16-QAM**			
	CP-Less OFDM without DFT spreading		**DFT-spread CP-Less OFDM**	
	Layer 1	***Layer 2***	***Layer 1***	***Layer 2***
0	10.23	10.17	9.34	8.55
100	10.37	10.32	9.46	8.70
150	10.44	10.40	9.53	8.77
200	10.51	10.48	9.60	8.84
250	10.59	10.55	9.67	8.91
300	10.31	10.62	9.74	8.98
350	10.29	10.70	9.81	9.05
400	10.37	10.77	9.88	9.13

Table 5: PAPR Comparison (4-QAM)

Window Length	**PAPR (dB) for 4-QAM**			
	CP-Less OFDM without DFT spreading		**DFT-spread CP-Less OFDM**	
	Layer 1	***Layer 2***	***Layer 1***	***Layer 2***
0	9.03	8.78	8.24	7.91
100	9.15	8.95	8.36	8.05
150	9.22	9.02	8.43	8.12
200	9.28	9.09	8.50	8.19
250	9.35	8.89	8.56	8.26
300	9.42	8.70	8.63	8.33
350	9.49	8.78	8.70	8.40
400	9.56	8.87	8.77	8.48

CHAPTER 4

UAV-ASSISTED MULTIUSER NON-TERRESTRIAL CYCLIC POSTFIXED WINDOWED OFDM SYSTEM

In this chapter, we present our proposed UAV-Assisted Multiuser Non-terrestrial Cyclic Postfixed Windowed OFDM System. First, we provide the system description of our proposed system. After that, we discuss the detailed signal modeling. Finally, we conclude this chapter by providing a detailed results analysis.

4.1 System Description

In our proposed system model (presented in Fig. 17 and Fig. 18), the binary data of each user is channel encoded using (3,2)-SPC coding [42] and subsequently digitally modulated to produce complex data symbols. Such symbols are rearranged and mapped in accordance with the information of [43], [44] addressed in Section 4.2. The properly mapped symbols are serial to parallel converted and fed into the OFDM modulator. The OFDM modulated signals are operated on with the clipping and filtering technique in combination with Tukey windowing for simultaneous reduction of PAPR and OOB and subsequently processed with pre- and post-fixing for generation of CPW-OFDM modulated signals. The windowed CPW-OFDM modulated signals are D/A converted using the root-raised cosine pulse shaping filter as an interpolation filter. The D/A converted signals are parallel to serial converted and their transmission powers are scaled. Such signals are rearranged to make the signals compatible for processing in the subsequent

precoding section. All the precoded signals for individual users are summed up to transmit simultaneously from a drone-based base station. At the receiving section of each user, the received signals are processed with signal detection techniques. The detected signals are rearranged with signal power rescaled, serial to parallel converted, and fed into an A/D converter. The A/D converted signals are restructured by removing additional pre- and post-fixed data samples and sent up to the OFDM demodulator section. The OFDM demodulated signals are parallel to serial converted, symbol demapped, digitally demodulated, and channel decoded to recover the transmitted data. The required data processing techniques have been addressed in Section 4.2. We use MATLAB to simulate our proposed model.

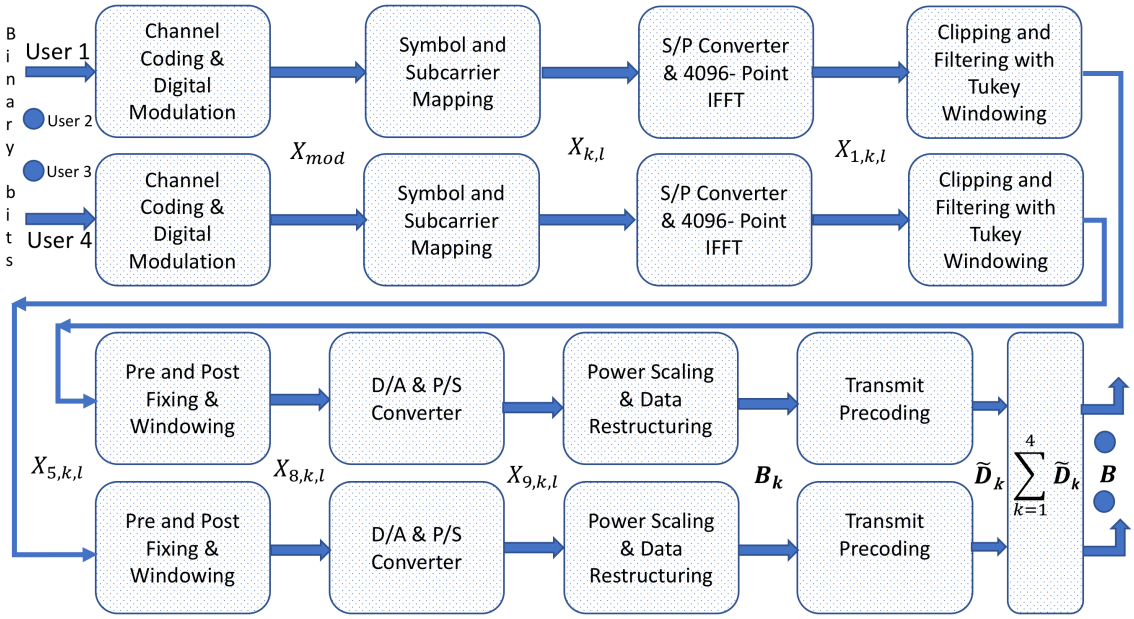

Figure 17: Block diagram of a Non-terrestrial Downlink CPW-OFDM System: Transmitting Section

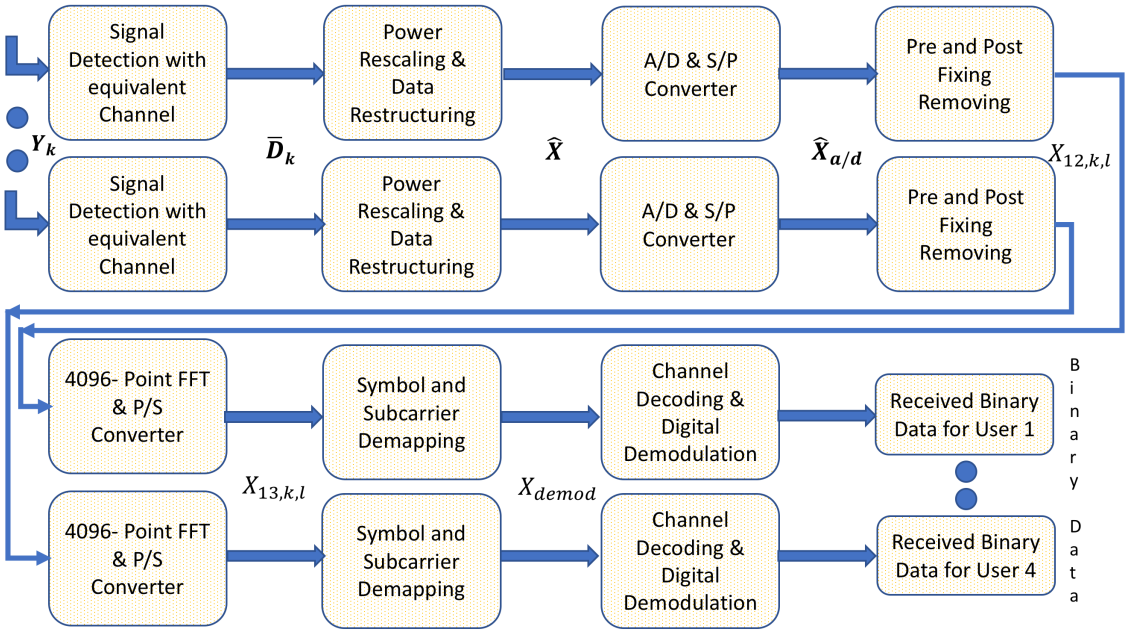

Figure 18: Block diagram of a Non-terrestrial Downlink CPW-OFDM System: Receiving Section

4.2 Signal Model

In our proposed Non-terrestrial simulated downlink CPW-OFDM system presented in Fig. 17 and Fig. 18, the drone-assisted base station comprises of N_T transmitting antennas and each of the N_S users comprises of N_R receiving antennas. All users are considered to receive identical numbers of binary data. The preprocessed digitally modulated complex symbols, x_{mod}, discussed in section 4.1 are mapped on the basis of the 5G frame structural information provided at [43] for localized subcarrier mapping [44]. In such a subcarrier mapping scheme, if the number of active subcarriers in an OFDM symbol of each user with IFFT/FFT size is of N is N_{active}, the number of null subcarriers would be $N_{null} = N - N_{active}$. In the $N-$point IFFT, the transmitter assigns zero amplitude

to the N_{null} null subcarriers. The number of null subcarriers are distributed at both ends of the input signal vector applied to the N-point IFFT modulator is $0.5N_{null}$. The l^{th} discrete-time OFDM symbol for the n^{th} time sample and k^{th} user with its input signal vector $x_{k,l}[n] = [x_{k,l}[0], x_{k,l}[1], x_{k,l}[2].....x_{k,l}[N-1]]^T$ can be written as:

$$X_{1,k,l}[m] = 1/N \sum_{n=0}^{N-1} x_{k,l}[n] e^{-j2\pi mn/N} \tag{4.1}$$

where, $k = 1, 2, \cdots, N_s$; $m = 0, 1, 2, \cdots, N-1$; and $l = 1, 2, 3, \cdots, L$; here, L is the total number of OFDM symbols.

In Equation (4.1), each discrete-time OFDM symbol is operated with the CF technique for PAPR reduction [45]. In such an operational step, the discrete-time OFDM symbol of sample size N is processed with N-point FFT and oversampled with a factor $\widetilde{L}(=4)$ by padding $N(\widetilde{L}-1))$ zeros in its middle part and is subsequently transformed into another form of discrete-time OFDM symbol $X_{2,k,l}[\overline{m}]$ by $\widetilde{L}N$-point IFFT, where, $\overline{m} = 0, 1, 2, \cdots, \widetilde{L}N-1$. The $X_{2,k,l}[\overline{m}]$ signal vector for the k^{th} user is clipped for $\overline{m} = 0, 1, 2, \ldots, \widetilde{L}N-1$ to create the clipped signal vector $X_{3,k,l}[\overline{m}]$ as follows.

$$X_{3,k,l}[\overline{m}] = \begin{cases} X_{2,k,l}[\overline{m}]; & |X_{2,k,l}[\overline{m}]| \leq A_{clip} \\ A_{clip} e^{jarg(X_{2,k,l}[\overline{m}])}; & |X_{2,k,l}[\overline{m}]| > A_{clip} \end{cases} \tag{4.2}$$

where A_{clip} is the clipping amplitude derived by the Clipping Ratio (CR) defined as:

$$CR = 20log_{10}\left(\frac{A_{clip}}{\sigma}\right)(dB) \tag{4.3}$$

where, σ is the RMS signal power of the signal vector $X_{2,k,l}[\overline{m}]$.

The clipped signal vector $X_{3,k,l}[\overline{m}]$ is processed with the $\widetilde{L}N$-point FFT and the out-band frequency components are removed with adaptation of a filter to produce the

clipped and filtered signal vector $X_{4,k,l}[m]$ of sample size N. The signal vector $X_{4,k,l}[m]$ is windowed by the Tukey tapered cosine technique for digital communication systems and such tapered cosine windowing technique can be written [46] as:

$$w(p) = \begin{cases} \frac{1}{2}[1 + cos(\frac{2\pi}{r})\frac{(p-1)}{(P-1)} - \pi]; \\ for\ p < \frac{r}{2}(P-1) + 1 \\ 1; \quad for\ \frac{r}{2}(P-1) + 1 \leq p \leq P - \frac{r}{2}(P-1) \\ \frac{1}{2}[1 + cos(\frac{2\pi}{r} - \frac{2\pi}{r}\frac{(p-1)}{(P-1)}) - \pi]; \\ for\ P - \frac{r}{2}(P-1) < p) \end{cases} \tag{4.4}$$

where $p = 1, 2, \cdots, P(= N)$, r is the ratio of taper to constant sections ($r = \frac{2WL}{N}$) and its value is in between 0 and 1. WL is the length of the samples at each of the two ends of the signal vector $X_{4,k,l}[m]$.

The Tukey (tapered cosine) windowed l^{th} discrete-time domain signal vector for the k^{th} user can be written as:

$$X_{5,k,l}[m] = X_{4,k,l}[m] \bigodot w(p) \tag{4.5}$$

where, $m = 0, 1, 2, \cdots, N-1$ and $\bigodot$ denotes the point-wise product respectively.

On applying the N-point IFFT operation to combine CF and Tukey windowing techniques implemented in the signal model of Equation (4.5), the newly formed l^{th} discrete-time OFDM symbol for the k^{th} user can be written as:

$$X_{6,k,l}[m] = \frac{1}{N}\sum_{n=0}^{N-1} X_{5,k,l}[n] e^{\frac{-j2\pi mn}{N}} \tag{4.6}$$

where, $k = 1, 2, \cdots, N_S;\ m = 0, 1, 2, \cdots, N-1$; and $l = 1, 2, 3, \cdots, L$.

In the case of a cyclic prefixed l^{th} discrete-time OFDM symbol generation with a cyclic prefixing sample length of $\widetilde{N}$, Equation (4.6) can be written in a modified form of $(N+\widetilde{N})\times 1$ matrix in size as:

$$X_{7,k,l}[\overrightarrow{m}] = \begin{bmatrix} X_{6,k,l}[\widetilde{m}] = \frac{1}{N}\sum\limits_{\widetilde{n}=N-\widetilde{N}}^{N-1} X_{5,k,l}[\widetilde{n}]e^{\frac{-j2\pi\widetilde{m}\widetilde{n}}{N}} \\ X_{6,k,l}[m] = \frac{1}{N}\sum\limits_{n=0}^{N-1} X_{5,k,l}[n]e^{\frac{-j2\pi mn}{N}} \end{bmatrix} \tag{4.7}$$

where, $\overrightarrow{m} = 0,1,2,3,\cdots,(N+\widetilde{N}-1)$; $\widetilde{m} = N-\widetilde{N},\cdots,N-1$; $k = 1,2,\cdots,N_S$; $m = 0,1,2,\cdots,N-1$; and $\widetilde{n} = N-\widetilde{N},\cdots,N-1$, respectively.

In the CPW-OFDM signaling scheme, post fixing is executed to the signal model of Equation (4.7) with an assumed sample length of $\breve{N}(=0.5\widetilde{N})$. On the basis of the fundamental idea on CPW-OFDM in [20], the CPW-OFDM signaling scheme is implemented for the l^{th} discrete-time OFDM symbol for the k^{th} user of $(N+1.5\widetilde{N})\times 1$ matrix size and can be written as:

$$X_{8,k,l}[\overline{\overline{m}}] = \begin{bmatrix} X_{6,k,l}[\widetilde{m}] = \frac{1}{N}\sum\limits_{\widetilde{n}=N-\widetilde{N}}^{N-1} X_{5,k,l}[\widetilde{n}]e^{\frac{-j2\pi\widetilde{m}\widetilde{n}}{N}} \\ X_{6,k,l}[m] = \frac{1}{N}\sum\limits_{n=0}^{N-1} X_{5,k,l}[n]e^{\frac{-j2\pi mn}{N}} \\ X_{6,k,l}[\widehat{m}] = \frac{1}{N}\sum\limits_{\widehat{n}=0}^{(0.5\tilde{N}-1)} X_{5,k,l}[\widehat{n}]e^{\frac{-j2\pi\widehat{m}\widehat{n}}{N}} \end{bmatrix} \tag{4.8}$$

where, $\overline{\overline{m}} = 0,1,2,3,\cdots,(N+1.5\widetilde{N}-1); \widetilde{m} = N-\widetilde{N},\cdots,N-1$; and $\widehat{m} = 0,\cdots,(0.5\widetilde{N}-1)$, respectively.

To perform Inter Symbol Interference (ISI) reduction and Digital-to-Analog (D/A) conversion, a root-raised cosine pulse shaping filter [47] is applied to the signal model of Equation (4.8). The response of the root-raised cosine pulse shaping filter can be written

as:

$$h_{SRC}(s) = \frac{[\frac{4\alpha}{\pi}(\frac{cos(1+\alpha)\pi s}{R})] + [(1-\alpha)(\frac{sinc(1-\alpha)\pi s}{R})]}{\sqrt{R}[1-(\frac{4\alpha s}{R})^2]} \tag{4.9}$$

where, α is the roll-off factor, and R is the number of samples of each symbol of the signal vector $X_{8,k,l}[\overline{\overline{m}}]$.

As an ideal raised cosine filter has an infinite impulse response, its response is truncated through assigning the number of symbols β_1 that the filter spans. In such consideration, β_1 is introduced in the root raised cosine filter and the length of its filter coefficient is $(\beta_1 R + 1)$ and the sample index number, s used in Equation (4.9) is $s = 0, 1, 2, \cdots, \beta_1 R$.

The signal vector $X_{8,k,l}[\overline{\overline{m}}]$ is up sampled with an up sampling factor R and filtered with a root raised cosine filter. The filtered signal vector $X_{9,k,l}[\widehat{\widehat{m}}]$ can be written as:

$$X_{9,k,l}[\widehat{\widehat{m}}] = X_{10,k,l}[\overline{\widetilde{m}}] \otimes h_{SRC}(s) \tag{4.10}$$

where, $h_{SRC}(s)$ is the response of the root raised cosine pulse shaping filter, s is the sample index number, $X_{10,k,l}[\overline{\widetilde{m}}]$ is the up sampled form of a signal vector of $X_{8,k,l}[\overline{\overline{m}}]$ with $\overline{\widetilde{m}} = 0, 1, \cdots, (N + 1.5\widetilde{N})R - R$, $\otimes$ is the discrete convolution operator and the sample length of the signal vector $X_{9,k,l}[\widehat{\widehat{m}}]$ is $Q = [(N + 1.5\widetilde{N})R - R + (\beta_1 R + 1)]$ with $\widehat{\widehat{m}} = 0, 1, 2, \cdots, Q - 1$ [48]. $(\beta_1 R + 1)$ is the length of the filter coefficient.

The power level of the signal in Equation (4.10) for k^{th} user is scaled and is written in a matrix form of size $Q \times L$ as $\mathbf{B}_k$. Then stack all the elements of the matrix $\mathbf{B}_k$ into a single column vector $\mathbf{b_k}$ with assigning desired transmission signal power, and the modified form of the signal vector is $\widetilde{\mathbf{b}}_k$ with a sample length of QL. Prior to designing the transmit precoder, a probabilistic path loss model based on the 3D geometry of

MIMO fading channels has been considered for UAV-ground communications. The LOS probability for the k^{th} user can be written as:

$$P_{LOS}^{k} = \frac{1}{1 + \psi e^{-\beta[\theta_k - \psi]}} \tag{4.11}$$

where, ψ and β are functions of the carrier frequency and environment, θ_k represents the elevation angle and $\theta_k = \frac{180}{\pi} \times sin^{-1}(\frac{h_{uav} - h_k}{d_k})$,

where $d_k = \sqrt{(x_k - x_{uav})^2 + (y_k - y_{uav})^2 + (h_{uav} - h_k)^2}$ is the 3D distance between UAV and the k^{th} user. The 3D coordinates of the k^{th} user and UAV respectively are $[x_k, y_k, h_k]$ and $[x_{UAV}, y_{UAV}, h_{UAV}]$.

The NLOS probability for the k^{th} user is simply $P_{NLOS}^{k} = 1 - P_{LOS}^{k}$. The path loss for the k^{th} user in both the LOS link and NLOS link can be written as:

$$L_k = \begin{cases} \eta_1(\frac{4\pi f_c d_k}{c})^{\alpha};\ for\ LOS\ link \\ \eta_2(\frac{4\pi f_c d_k}{c})^{\alpha};\ for\ NLOS\ link \end{cases} \tag{4.12}$$

where, α is the path loss exponent, f_c is the carrier frequency $(28\ GHz)$, η_1 and η_2 are the excessive path loss coefficients for LOS and NLOS links, and c is light speed. The average path loss between the UAV and the k^{th} user is:

$$\overline{L}_k = P_{LOS}^{k}\eta_1(\frac{4\pi f_c d_k}{c})^{\alpha} + P_{NLOS}^{k}\eta_2(\frac{4\pi f_c d_k}{c})^{\alpha} \tag{4.13}$$

$$\begin{aligned} \overline{L}_k[dB] = [\alpha log_{10}(\frac{4\pi f_c d_k}{c})][log_{10}(P_{LOS}^{k}) + \\ log_{10}\eta_1 + log_{10}(P_{NLOS}^{k}) + log_{10}\eta_2] \end{aligned} \tag{4.14}$$

where, f_c is the carrier frequency, η_1 and η_2 are the excessive path loss coefficients for

LOS and NLOS links, respectively. The average path loss model of Equation (4.14) is preferred for channel estimation.

In block diagonalization precoding, an aggregate channel matrix of N_S users is considered as:

$$\mathbf{H} = [\mathbf{H}_1^T \mathbf{H}_2^T \cdots \mathbf{H}_{N_s}^T]^T \in \mathbb{C}^{N_S N_R \times N_T} \tag{4.15}$$

For the k^{th} user, its channel matrix $\mathbf{H}_k$ is removed from $\mathbf{H}$ to create a channel matrix $\widetilde{\mathbf{H}_k} \in \mathbb{C}^{(N_S N_R - N_R) \times N_T}$ as:

$$\widetilde{\mathbf{H}_k} = [\mathbf{H}_1^T \cdots \mathbf{H}_{k-1}^T \mathbf{H}_{k+1}^T \cdots \mathbf{H}_{N_S}^T]^T \tag{4.16}$$

On singular value decomposition (SVD) of $\widetilde{\mathbf{H}_k}$, we get

$$\widetilde{\mathbf{H}_k} = \widetilde{\mathbf{U}}_k \widetilde{\mathbf{\Sigma}}_k (\widetilde{\mathbf{V}}_k^1 \widetilde{\mathbf{V}}_k^0)^H \tag{4.17}$$

From Equation (4.17), it is noticeable that the diagonal matrix $\widetilde{\mathbf{\Sigma}}_k$ has dimensions $(N_S N_R - N_R) \times (N_S N_R - N_R)$ containing non-zero singular values and the matrix $\widetilde{\mathbf{V}}_k^0$ holds $N_T - (N_S N_R - N_R)$ right singular vectors forming a basis for the null space of $\widetilde{\mathbf{H}_k}$. The precoding matrix $\mathbf{W}_k$ of $N_T \times N_R$ in matrix size is constructed with the columns of $\widetilde{\mathbf{V}}_k^0$ to satisfy the MUI condition [49]. Prior to executing the precoding operation, the signal vector $\widetilde{\mathbf{b}}_k$ is reshaped to produce a matrix $\mathbf{D}_k$ of size $N_R \times 0.5QL$. The output of the k^{th} userâs precoder $\widetilde{\mathbf{D}}_k$ matrix is of size $N_T \times 0.5QL$ and is given by

$$\widetilde{\mathbf{D}}_k = \mathbf{W}_k \mathbf{D}_k \tag{4.18}$$

Summing all the precoded signals from Equation (4.18), the transmitted signal matrix $\mathbf{B}$ is produced.

The signal received at the k^{th} user with user interference terms can be written as:

$$\begin{aligned}\mathbf{Y}_k = \mathbf{H}_k\mathbf{B} = \mathbf{H}_k(\mathbf{W}_1\mathbf{D}_1 + \mathbf{W}_2\mathbf{D}_2 + \cdots \\ +\mathbf{W}_{N_S}\mathbf{D}_{N_S}) + \mathbf{n}_k\end{aligned} \tag{4.19}$$

where, the term $\mathbf{W}_1\mathbf{D}_1$ is applicable to the first user, $\mathbf{W}_2\mathbf{D}_2$ is applicable to the second user and so on; $\mathbf{n}_k$ is the AWGN noise with variance σ_k^2 associated with the received signal. From Equation (4.19), the received average signal power, $P_{user}^{(k)}$ for the k^{th} user is estimated from the signal represented by the matrix $[\mathbf{H}_k\mathbf{W}_k\mathbf{D}_k]$ and the received average interference power $P_{interference}^{(k)}$ is estimated from the sum of $[\mathbf{H}_{k\neq j}\mathbf{W}_{k\neq j}\mathbf{D}_{k\neq j}, j = 1, 2, \cdots, N_S]$, and the $P_{noise}^{(k)}$ from $\mathbf{n}_k$. The Signal to Interference Ratio (SINR) for the k^{th} user can be written as:

$$SINR_k = \frac{P_{user}^{(k)}}{P_{interference}^{(k)} + P_{noise}^{(k)}} \tag{4.20}$$

However, Equation (4.19) can be written for the k^{th} user with interference components neglected as:

$$\mathbf{Y}_k = \mathbf{H}_k\mathbf{W}_k\mathbf{D}_k + \mathbf{n}_k = \widehat{\mathbf{H}_k}\mathbf{D}_k + \mathbf{n}_k \tag{4.21}$$

where, $\widehat{\mathbf{H}_k} = \mathbf{H}_k\mathbf{W}_k$ is the equivalent channel matrix with size $N_R \times N_R$ for the k^{th} user.

With the application of the zero forcing signal detection technique [50], the detected signal $\overline{\mathbf{D}}_k$ of size $N_T \times 0.5QL$ can be written as:

$$\overline{\mathbf{D}}_k = (\widehat{\mathbf{H}}_k^H\widehat{\mathbf{H}}_k)^{-1}\widehat{\mathbf{H}}_k^H\mathbf{Y}_k \tag{4.22}$$

Stacking all the elements of the matrix $\overline{\mathbf{D}}_k$ into a single column vector $\breve{\mathbf{b}}_k$ with rescaled signal power, it is rearranged into a matrix $\widehat{\mathbf{X}}$ of size $Q \times L$. Since the root-raised cosine

filter presented in Equation (4.9) is real, symmetric, and linear-phased, it can also be used as a matched filter. On application of such matched filter to deconvolve each column vector data of the matrix $\widehat{\mathbf{X}}$, an A/D converted signal matrix $\widehat{\mathbf{X}}_{a/d}$ is produced and with the execution of down-sampling factor R, the retrieved CPW-OFDM symbols, $X_{11,k,l}(\overline{\overline{m}})$, where $\overline{\overline{m}} = 0, 1, 2, 3, \cdots, (N + 1.5\widetilde{N} - 1)$; $k = 1, 2, \cdots, N_S$; and $l = 1, 2, \cdots, L$; is processed for cyclic prefixed and additional post-fixed data removal resulting in the production of retrieved l^{th} discrete-time OFDM symbol vector for the k^{th} user, $X_{12,k,l}[m]$. The OFDM signal vector $X_{12,k,l}[m]$ is demodulated to produce a signal vector, $X_{13,k,l}[m]$ and after symbol and subcarrier demapping, digitally modulated complex symbols x_{demod} are retrieved. The x_{demod} complex symbol is further processed for digital demodulation and channel decoded to recover binary bits.

Note: Throughout the paper, the notation $[.]^T$ and $[.]^H$ denote the non-conjugate matrix transpose and conjugate (Hermitian) transpose of operation, respectively.

4.3 Result Analysis

In this section, we present the simulated performance of the proposed UAV-assisted multiuser non-terrestrial CPW-OFDM system. The UAV with a height of 200 m from the ground would serve four ground users located within the coverage area of 50 m with the $3D$ distances from the UAV to users of 203.00 m, 198.31 m, 203.55 m and 204.32 m, respectively. We observe the user's own signal power and randomly distributed user's interference signal power over a coverage area of a radius of 50 m by varying the heights of the UAV (drone) from 50 m to 300 m and considering the height of all users is 1.5 m

above the ground surface in all cases. In all other simulations, the UAV (drone) at height of 200 m has been considered. The overall study assumes the probabilistic path loss model is based on a mmWave flat fading MIMO channel with Channel State Information (CSI) available at the receiver. Our proposed system is simulated under parameters in the Table 6.

4.3.1 Path Loss Model with Received Signals

On the basis of the signal model presented in Equation (4.14), the average path loss has been calculated with the consideration of both LOS and NLOS links. The estimated values of maximum and minimum average path loss are 111.14 dB and 110.39 dB, respectively. In such estimated average path loss values, LOS component values are found to be significant in comparison with NLOS components.

4.3.1.1 Height of UAV (drone) is 50 m

The distribution of the received user's signal power with a UAV height of 50 m in our study area is shown in Fig. 20. It is noticeable that the maximum and minimum signal power values are 5.1835×10^{-8} W and 3.3009×10^{-11} W, respectively. In Fig. 21, the user's interference signal power is presented. The maximum and minimum interference signal powers are found to have values of 1.3526×10^{-38} W and 5.3277×10^{-41} W.

4.3.1.2 Height of UAV (drone) is 100 m

In the case of considering UAV height of 100 m, it is seen that the maximum and minimum signal power values are 1.4512×10^{-8} W and 4.8335×10^{-11} W, respectively

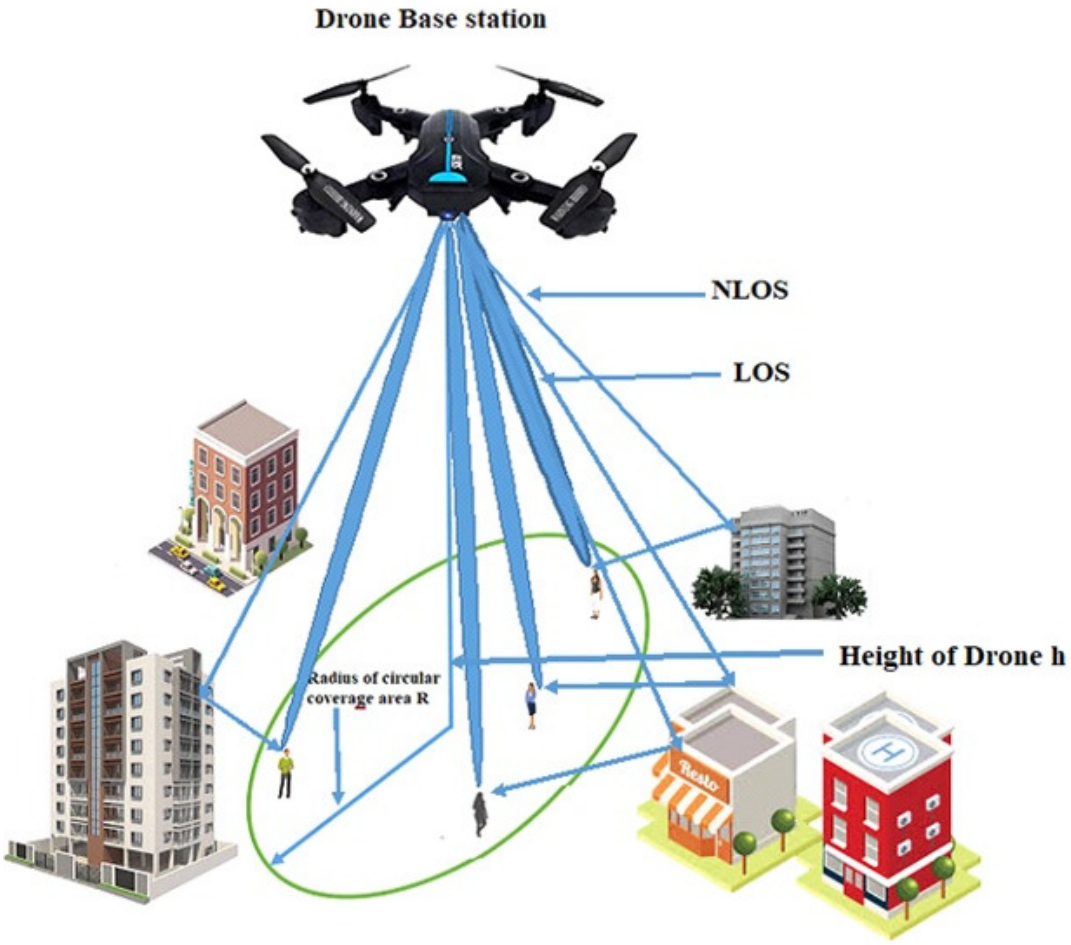

Figure 19: Scenario of a typically assumed non-terrestrial Downlink transmission showing significant LOS signal power

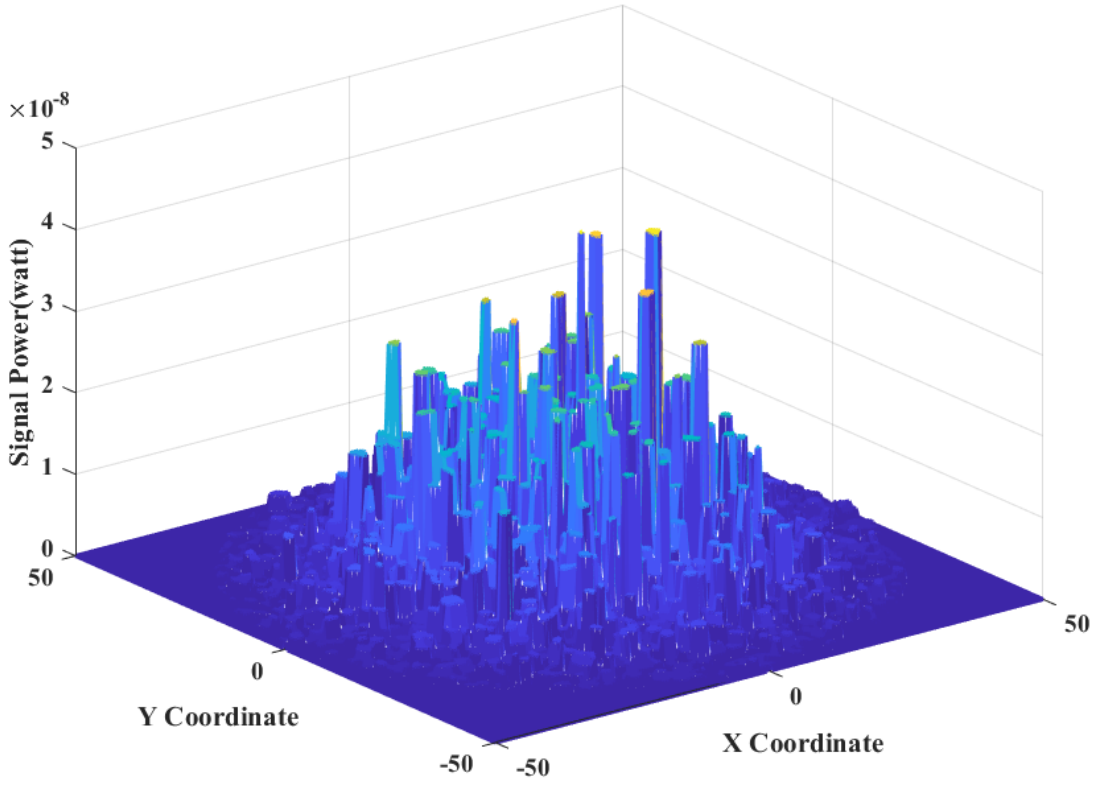

Figure 20: Received randomly distributed user's own signal power over a coverage area of radius of 50 m. Height of UAV (drone) is 50 m and height of all users is 1.5 m above ground surface

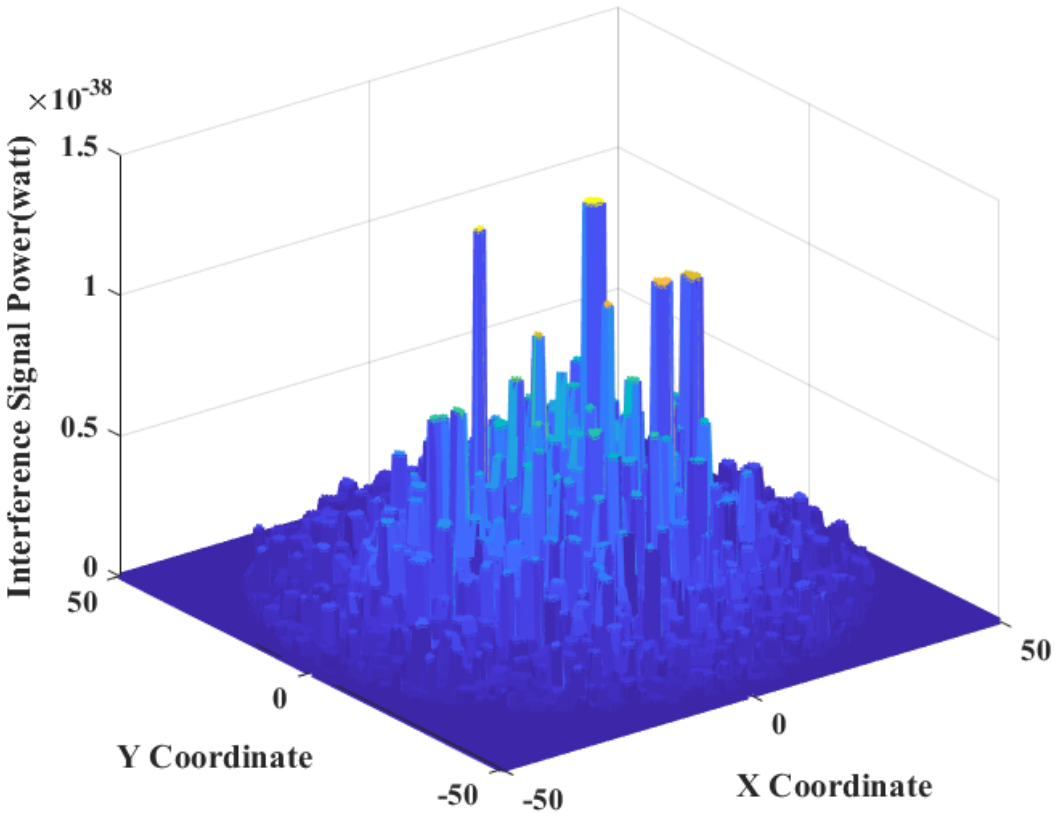

Figure 21: Received randomly distributed user's interference signal power over a coverage area of radius of 50 m. Height of UAV (drone) is 50 m and height of all users is 1.5 m above ground surface

(Fig. 22). From Fig. 23, it is also noticeable that the user's interference signal power distribution is very low as compared to the user's own signal power and the maximum and minimum interference signal power values are 3.6953×10^{-39} W and 1.2216×10^{-40} W.

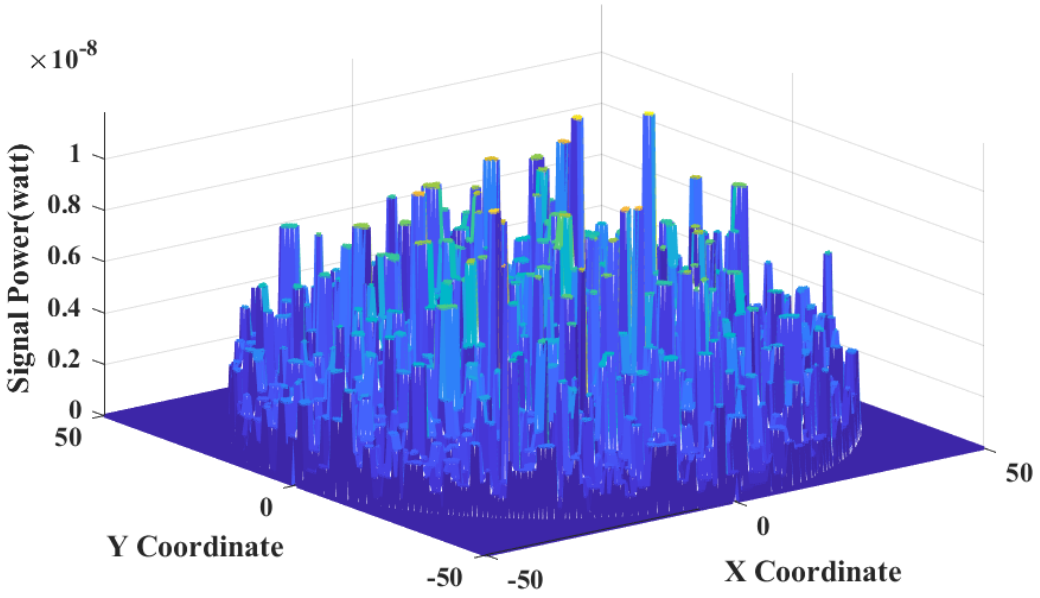

Figure 22: Received randomly distributed user's own signal power over a coverage area of radius of 50 m. Height of UAV (drone) is 100 m and height of all users is 1.5 m above ground surface

4.3.1.3 Height of UAV (drone) is 200 m

The distribution of the received user's signal power in our study area is shown in Fig. 24. We see that although the user's own signal power distribution is very low, the estimated values are above the receiver sensitivity of 1.20×10^{-13} W (-99.2 dBm).The maximum and minimum signal power values are 3.9315×10^{-9} W and 1.9442×10^{-11}

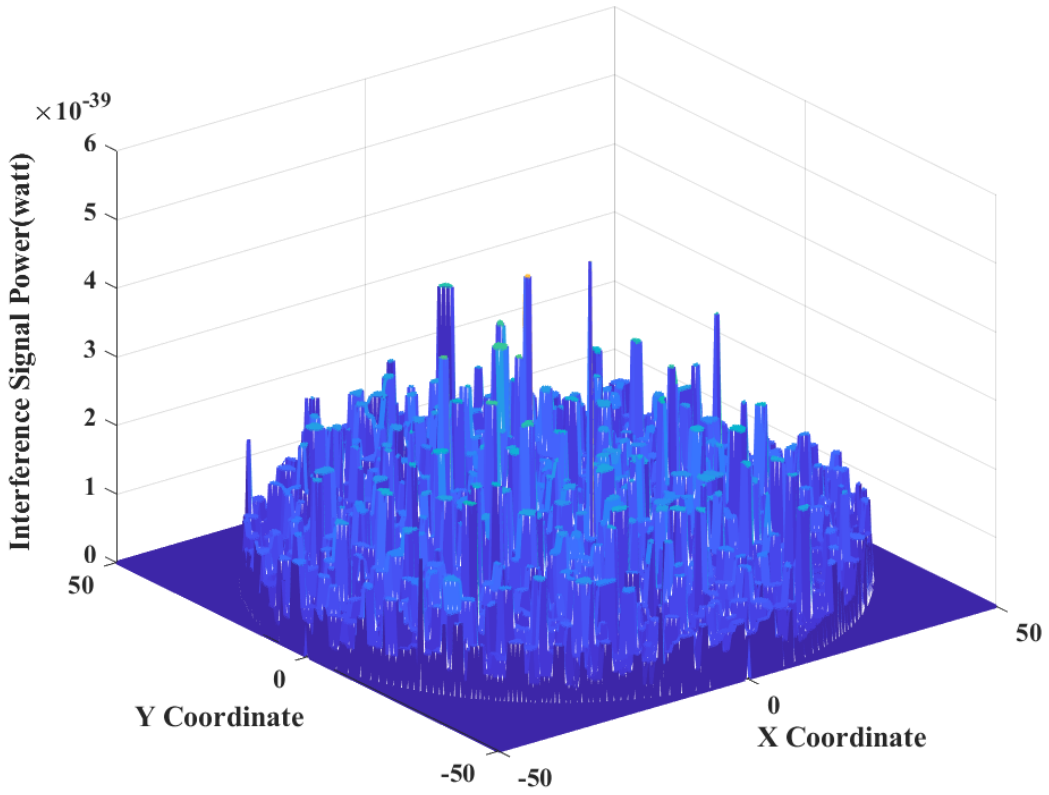

Figure 23: Received randomly distributed user's interference signal power over a coverage area of radius of 50 m. Height of UAV (drone) is 100 m and height of all users is 1.5 m above ground surface

W, respectively. The distribution of the received user's interference signal power is shown in Fig. 25. It is noticeable that the user's interference signal power distribution is very low as compared to the user's own signal power shown in Fig. 24. The maximum and minimum interference signal power values are 1.6188×10^{-39} W and 5.4698×10^{-41} W, respectively.

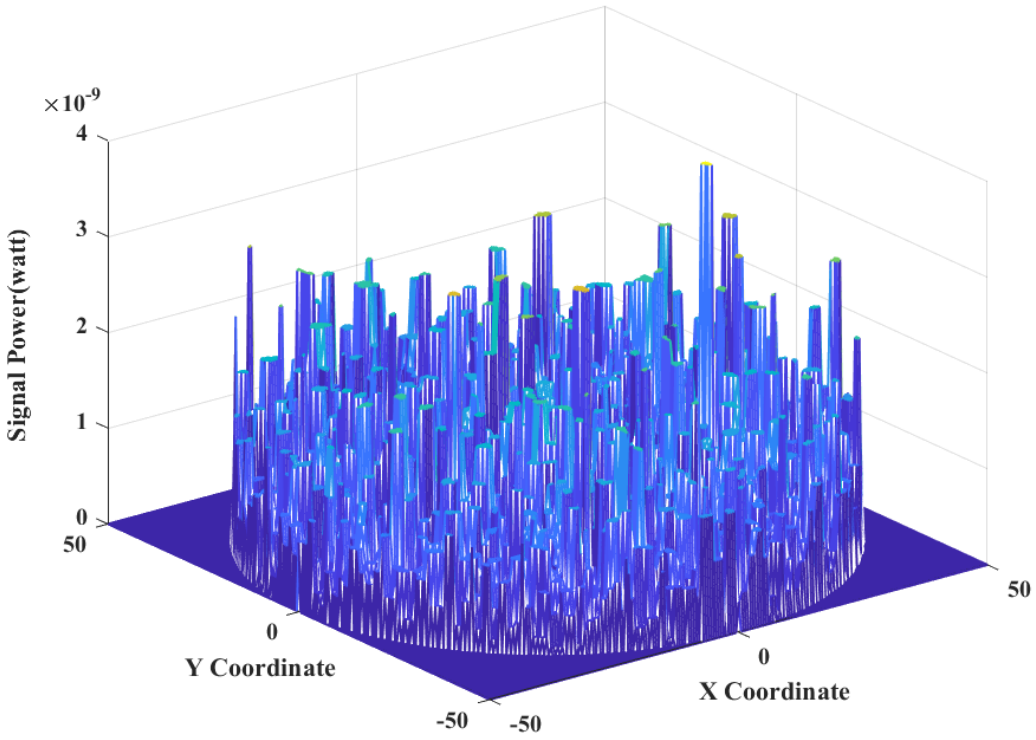

Figure 24: Received randomly distributed user's own signal power over a coverage area of radius of 50 m. Height of UAV (drone) is 200 m and height of all users is 1.5 m above ground surface

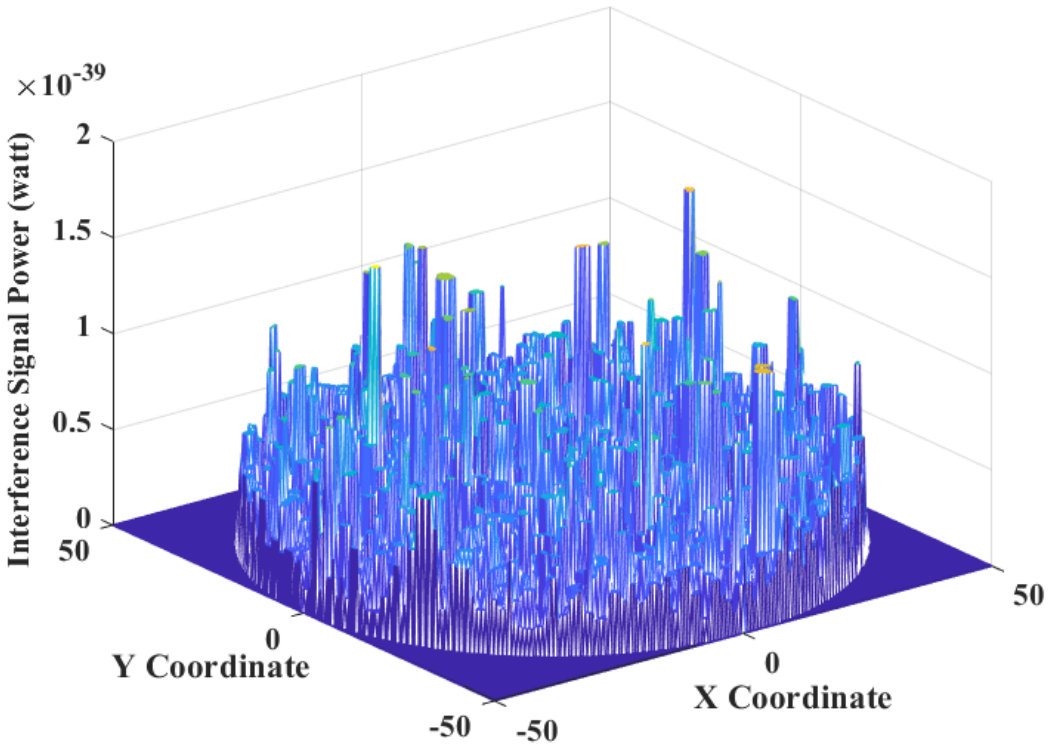

Figure 25: Received randomly distributed user's interference signal power over a coverage area of radius of 50 m. Height of UAV (drone) is 200 m and height of all users is 1.5 m above ground surface

4.3.1.4 Height of UAV (drone) is 300 m

In the case of considering UAV height of 300 m, it is seen that the maximum and minimum signal power values are 1.3755×10^{-9} W and 8.2203×10^{-12} W, respectively (Fig. 26). From Fig. 27, it is also noticeable that the user's interference signal power distribution is very low as compared to the user's own signal power and the maximum and minimum interference signal power values are 4.8110×10^{-40} W and 1.9986×10^{-41} W.

On comparing the graphical illustrations presented in Fig. 20 through Fig. 27, it is remarkable that both the user's own signal and interference power decrease with the increase in UAV heights.

4.3.1.5 Impacts of Heights on User's Own Signal Power and Interference Signal Power

Fig. 28 and Fig. 29 show the received randomly distributed user's own signal power in Watt along the profile of the length of 100 m (-50 m to $+50$ m) by taking the cross-section along the $X - axis$ and $Y - axis$, respectively for the UAV heights of 50 m, 100 m, 200 m, and 300 m.

Fig. 30 and Fig. 31 show the received randomly distributed user's interference signal power in Watt along the profile of the length of 100 m (-50 m to $+50$ m) by taking the cross-section along the $X - axis$ and $Y - axis$, respectively for the UAV heights of 50 m, 100 m, 200 m, and 300 m.

On the critical observations of the graphical illustrations shown in Fig. 28 through

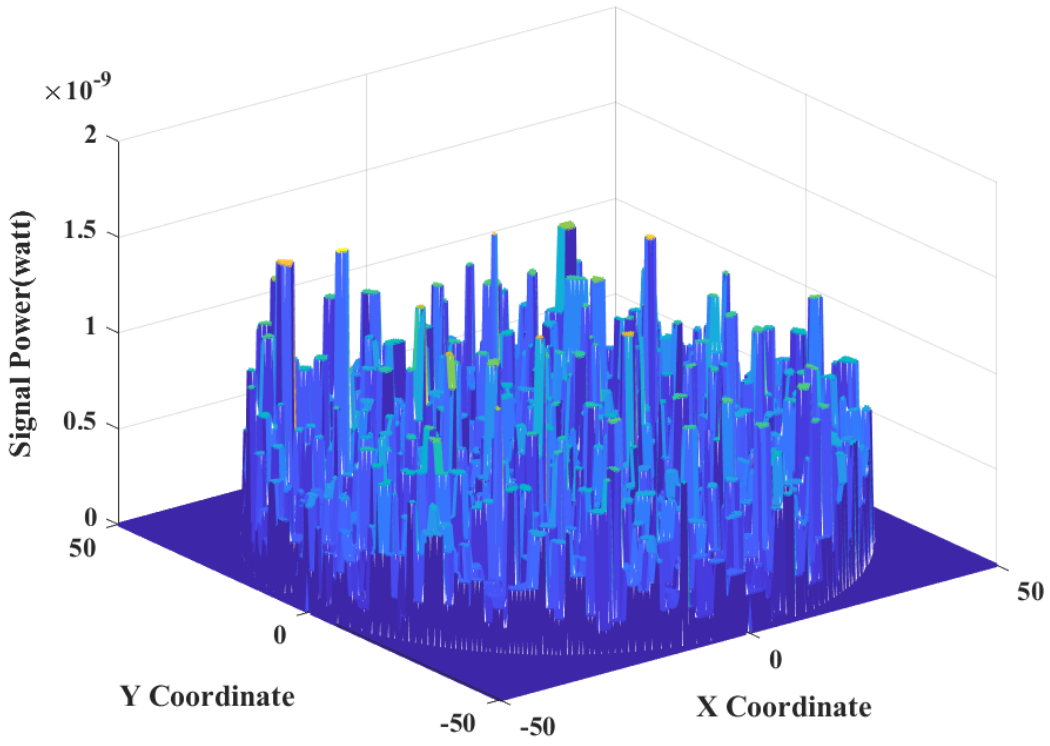

Figure 26: Received randomly distributed user's own signal power over a coverage area of radius of 50 m. Height of UAV (drone) is 300 m and height of all users is 1.5 m above ground surface

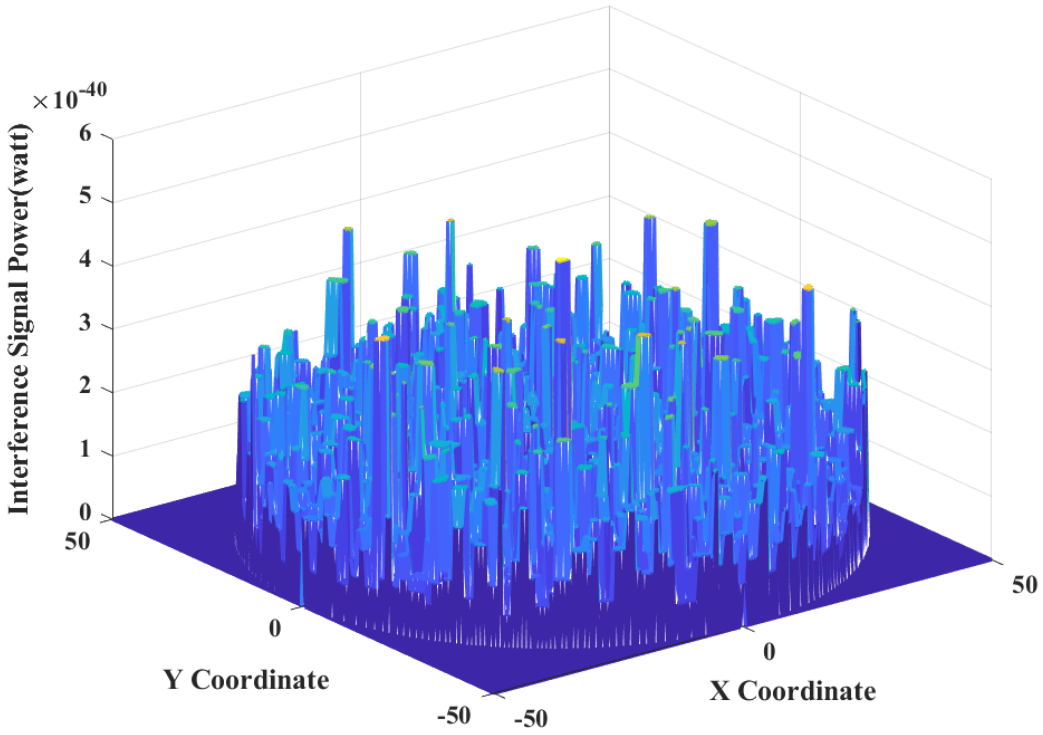

Figure 27: Received randomly distributed user's interference signal power over a coverage area of radius of 50 m. Height of UAV (drone) is 300 m and height of all users is 1.5 m above ground surface

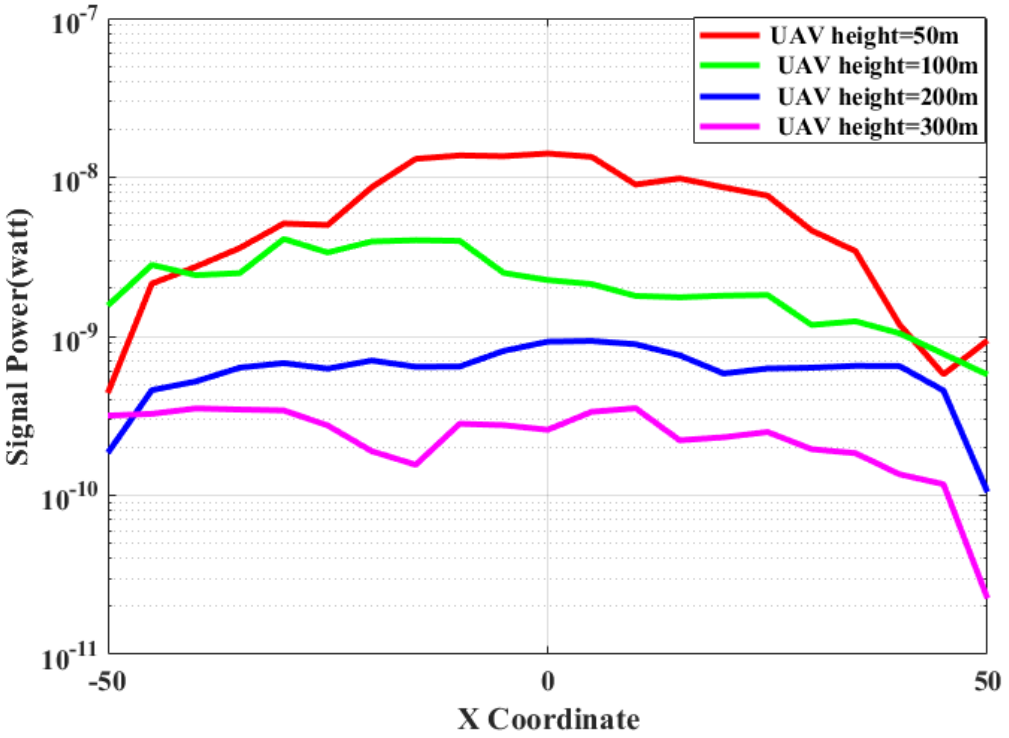

Figure 28: Signal power along the profile of the length of 100 m with taking the cross-section along the $X - axis$ for UAV heights of 50 m, 100 m, 200 m, and 300 m

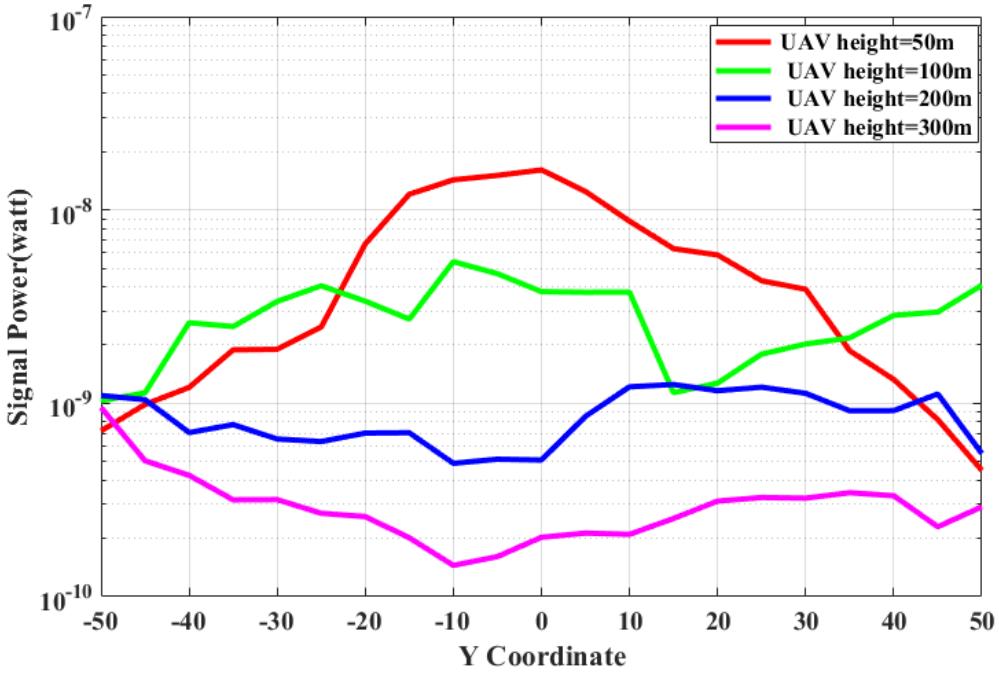

Figure 29: Signal power along the profile of the length of 100 m with taking the cross-section along the $Y - axis$ for UAV heights of 50 m, 100 m, 200 m, and 300 m

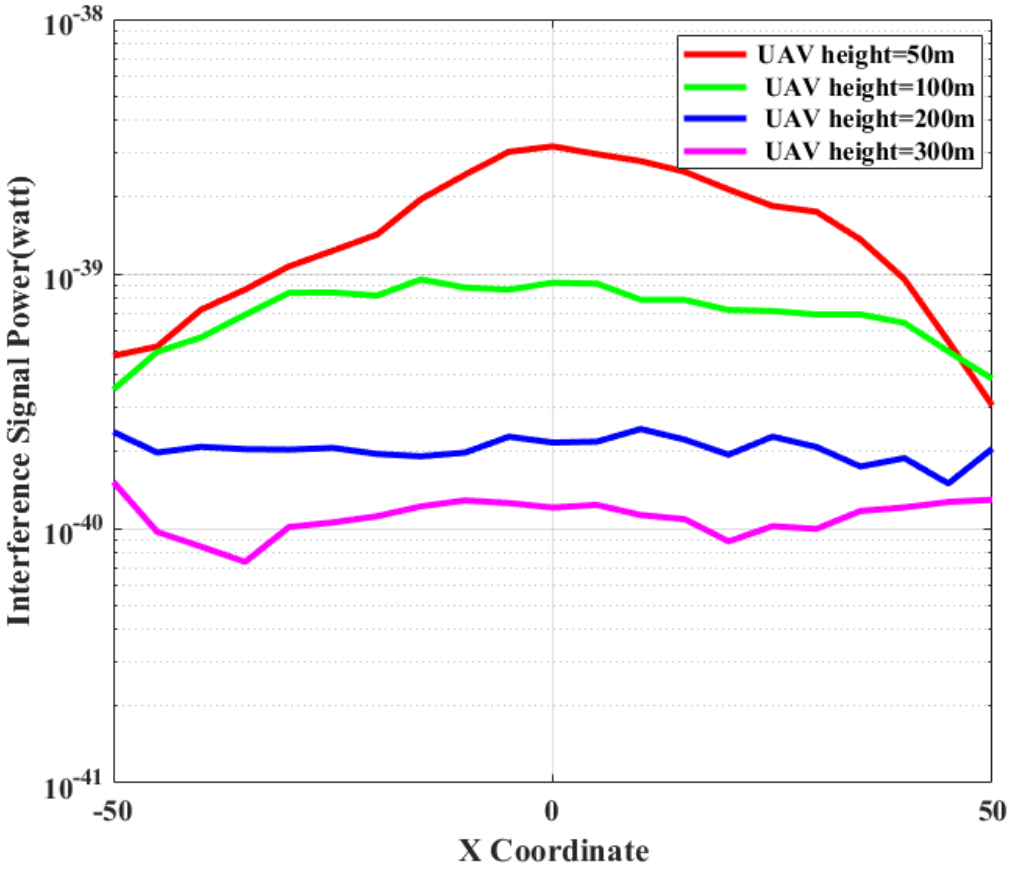

Figure 30: Interference signal power along the profile of the length of 100 m with taking the cross-section along the $X - axis$ for UAV heights of 50 m, 100 m, 200 m, and 300 m

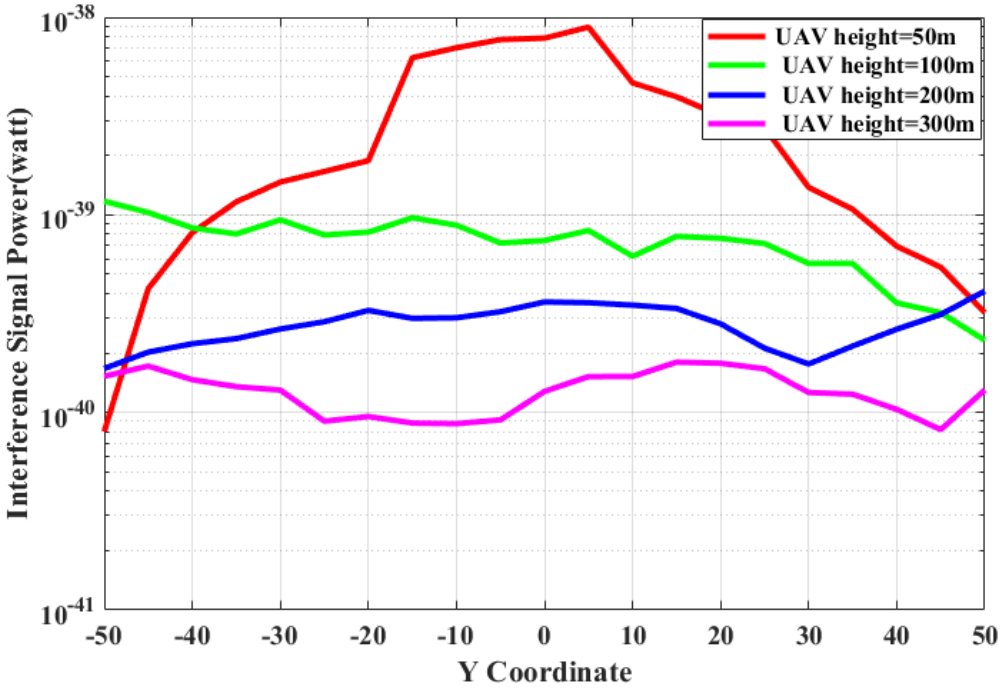

Figure 31: Interference signal power along the profile of the length of 100 m with taking the cross-section along the $Y - axis$ for UAV heights of 50 m, 100 m, 200 m, and 300 m

Fig. 31, we find that the received randomly distributed user's own signal power increases with a decrease in UAV heights. Similarly, in the case of received randomly distributed interference signal power, it is seen that such power increases with a decrease in UAV heights. In all cases, it is considered that the base station is located at the origin of the study area (X- Coordinate, Y- Coordinate) = $(0, 0)$. Away from the location of the base station user's own signal power and the received randomly distributed interference signal power gradually decreases.

4.3.2 Power Spectral Density

In Fig. 32 through Fig. 35, the simulated Power spectral density performances of the OFDM modulated signals for adaptation of the clipping and filtering technique integrated with and without Tukey windowing are presented. In our designed subcarrier mapped OFDM modulated signals from [43], the OOB reduction with merely utilization of clipping and filtering technique is low and it depends on the value of CR. The OOB reduction performance improves insignificantly with increases in the values of the clipping ratio. The average OOB power relative to in band power for CR values of 0.5 dB, 1.0 dB, and 2.0 dB are -20.34 dB, -20.95 dB, and -22.23 dB respectively. In combination of the Tukey windowing technique with the clipping and filtering technique, the average OOB power relative to in-band power for CR values of 0.5 dB, 1.0 dB, and 2.0 dB are found to have values of -116.58 dB, -117.18 dB, and -118.47 dB, respectively (Table 7, 8, and 9). It is remarkable that the highest average OOB power reduction of 117.41 dB is observed in the case of implementing the Tukey window-based clipping and

filtering technique. In the absence of utilizing the Tukey window, the average OOB power reduction reduces from 117.41 dB to 21.17 dB.

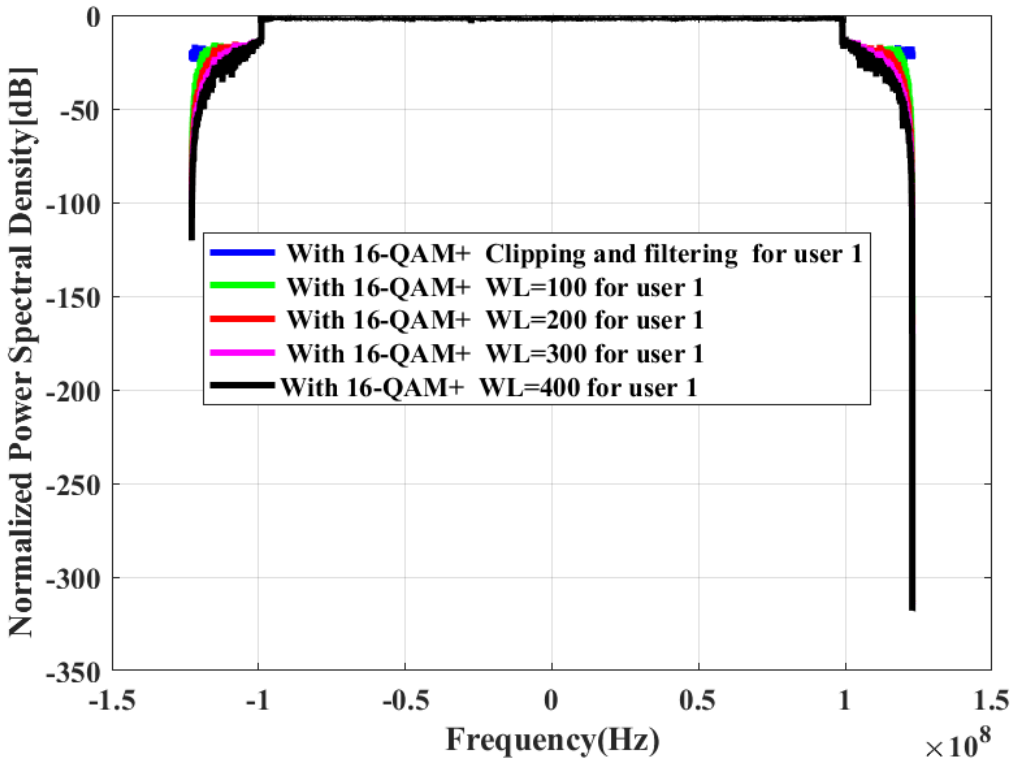

Figure 32: Power Spectral Density of OFDM modulated signals with the utilization of Clipping and Filtering technique integrated with Tukey windowing and 16-QAM digital modulation for $user\ 1$

4.3.3 Complementary Cumulative Distribution Functions and Peak-to-Average Power Ratio

In Fig. 36, simulated Complementary Cumulative Distribution Functions (CCDFs) of PAPR for our proposed schemes are presented using 16-QAM. At a CCDF of 10^{-4}, PAPR values are around 9 dB in case of combined adaptation of the clipping and filtering

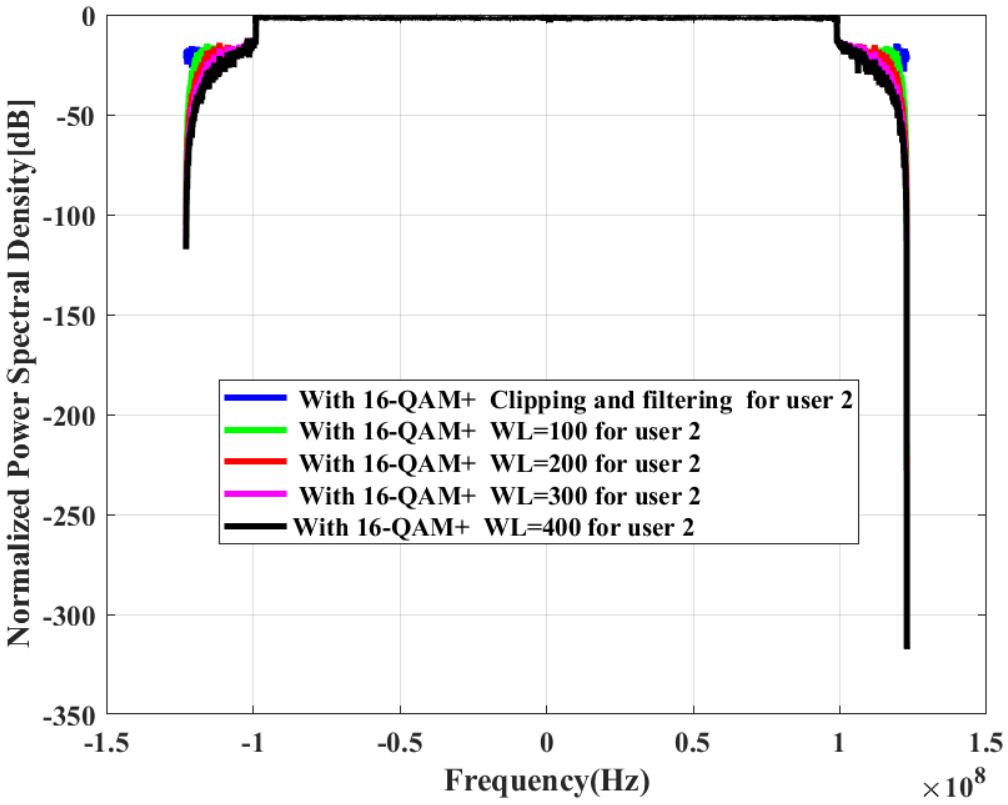

Figure 33: Power Spectral Density of OFDM modulated signals with the utilization of Clipping and Filtering technique integrated with Tukey windowing and 16-QAM digital modulation for $user\ 2$

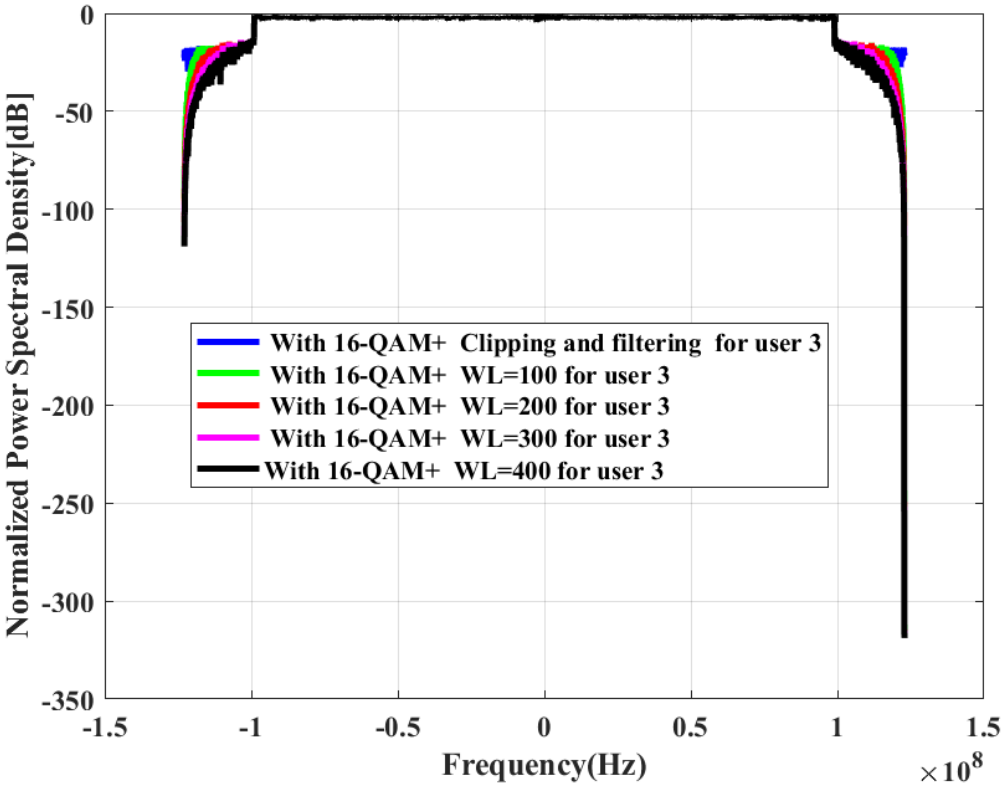

Figure 34: Power Spectral Density of OFDM modulated signals with the utilization of Clipping and Filtering technique integrated with Tukey windowing and 16-QAM digital modulation for $user$ 3

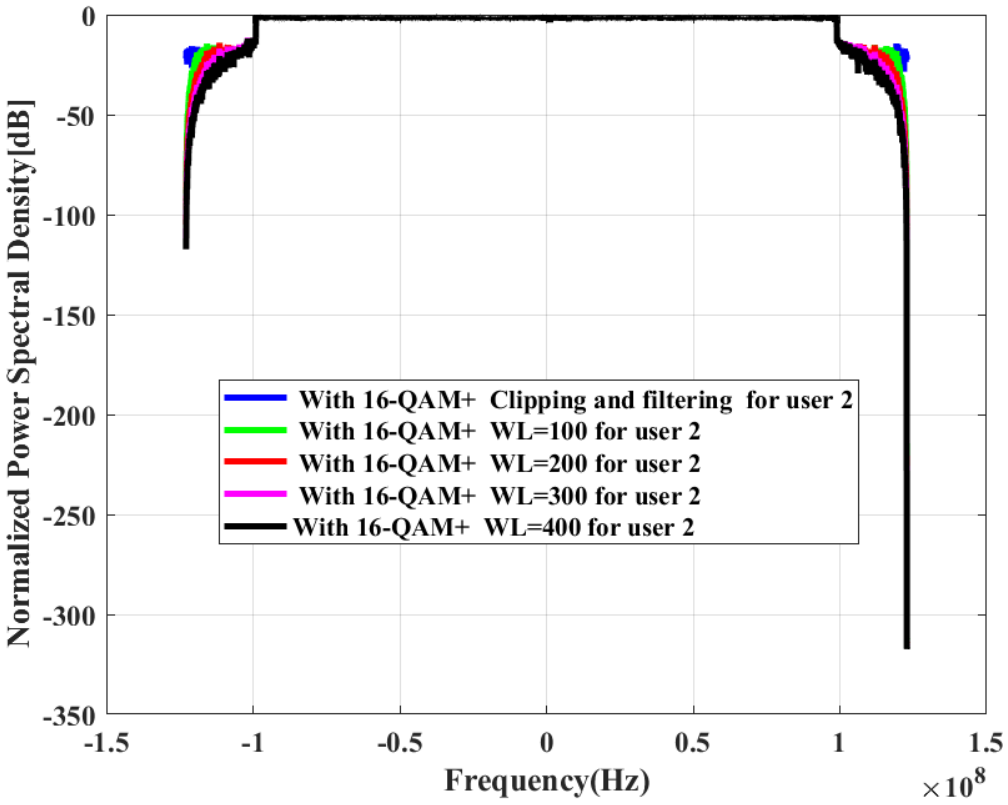

Figure 35: Power Spectral Density of OFDM modulated signals with the utilization of Clipping and Filtering technique integrated with Tukey windowing and 16-QAM digital modulation for $user\ 4$

technique and the Tukey windowing technique and the PAPR increases from 9 dB to 10 dB in a specific case of not utilizing both techniques. Numerical results clearly suggest a PAPR gain of 1 dB. In Tables 7, 8, and 9, the estimated values of PAPR with and without windowing for different clipping ratios 0.5 dB to 3.0 dB are shown. It is observable from such tables that the PAPR performance degrades insignificantly with an increase in both Tukey windowing length and clipping ratio.

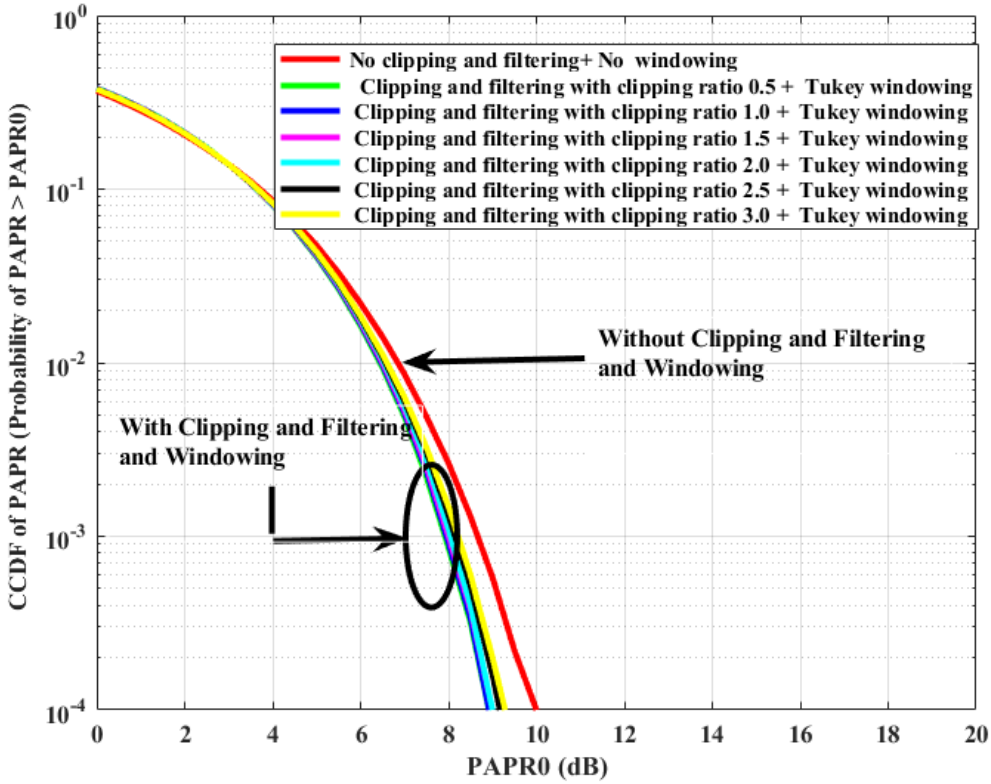

Figure 36: CCDFs of PAPR for an average transmitted signal with and without the utilization of Tukey windowing aided Clipping and Filtering technique

4.3.4 Bit Error Rate and Signal-to-Interference-plus-Noise Ratio

In all BER curves shown in Figs. 37 through Fig. 40, obvious BER performance degradation is shown and well discriminated with the implementation of $(3, 2)$- SPC channel coding compared with Repeat and Accumulate (RA) channel coding at normalized (E_b/N_0) values. In all cases, the simulated system with 16-QAM digital modulation and RA channel coding provides best performance at low E_b/N_0 values. The BER performance difference under two utilized channel coding is low and it increases with an increase in value of E_b/N_0.

To optimize the performance of our proposed system in terms of BER, PAPR, and OOB, we used a clipping ratio of 0.5 dB and a Tukey window of sample length 400. In a typically assumed $E_b/N_0 = 0$ dB, the estimated BER value in Fig. 37 decreases from 0.0919 to 0.0008 which is an improvement of 20.60 dB. The simulated system with RA channel coding achieves the BER of 10^{-1} at $E_b/N_0 = -9.50$ dB, while $(3, 2)$- SPC channel coding achieves the same BER value at a $E_b/N_0 = -1.00$ dB which is an SNR gain of 8.50 dB.

In Fig. 38, the simulated system with RA channel coding achieves the BER of 10^{-1} at $E_b/N_0 = -9.00$ dB, while $(3, 2)$- SPC channel coding achieves the same BER at a $E_b/N_0 = 0.50$ dB for an SNR gain of 9.50 dB. The estimated BER decreases from 0.0964 in $(3, 2)$- SPC channel coding to 0.0015 in RA channel coding for $E_b/N_0 = 0$ dB which indicates a system performance improvement of 18.08 dB.

Fig. 39 demonstrates that the RA channel coding achieves a BER of 10^{-1} at $E_b/N_0 = -6.00$ dB, while $(3, 2)$- SPC channel coding achieves the same BER value at

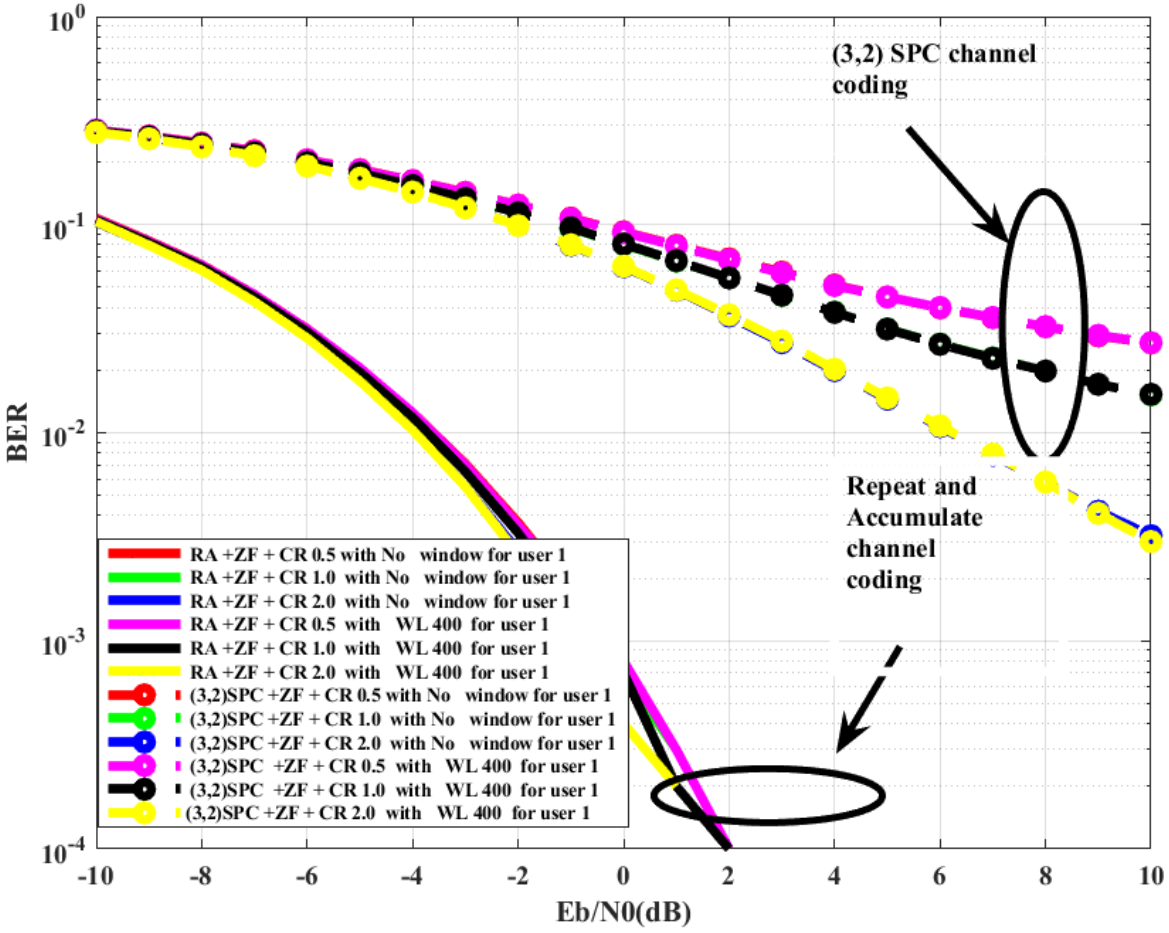

Figure 37: BER performance of Non-terrestrial Downlink CPW-OFDM with different channel coding, 16-QAM modulation, Clipping and Filtering, with and without Tukey windowing for $user$ 1

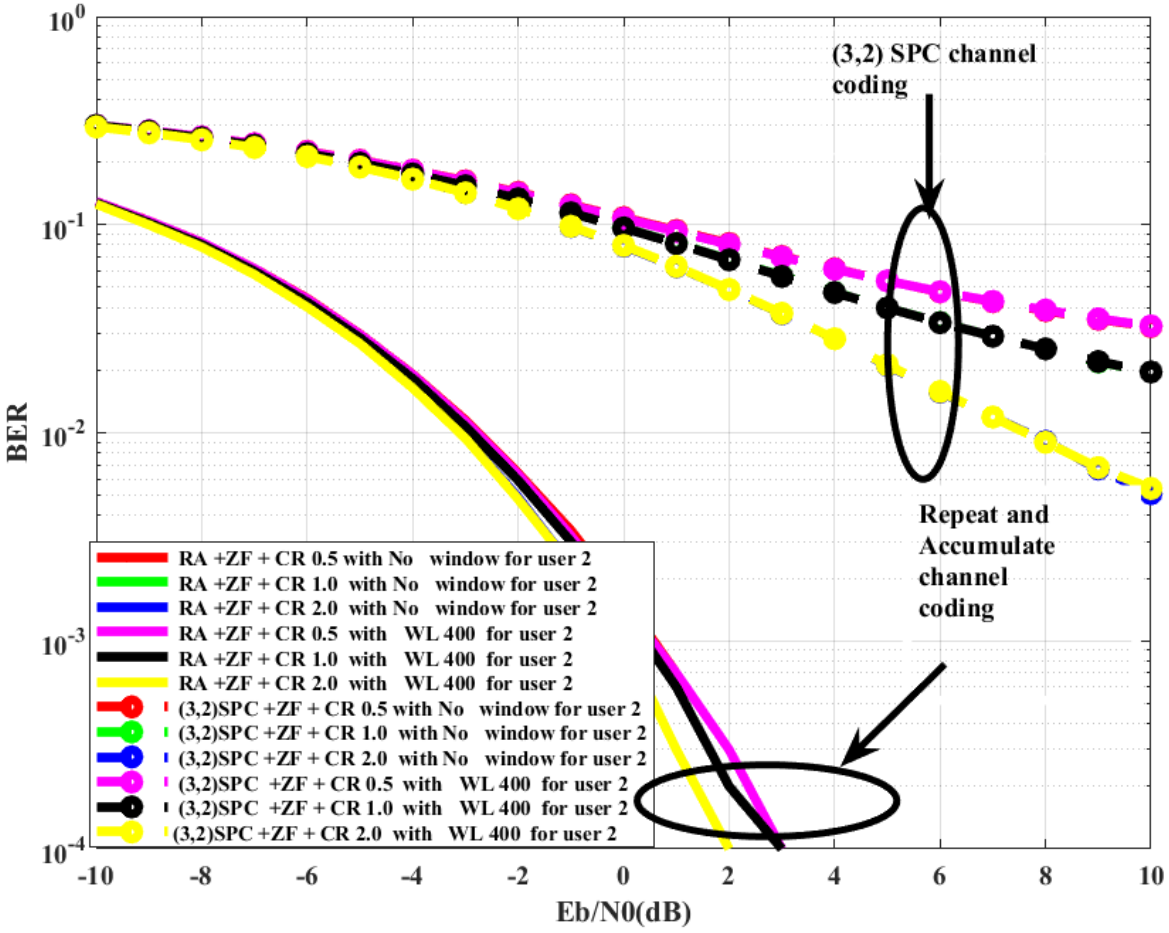

Figure 38: BER performance of Non-terrestrial Downlink CPW-OFDM with different channel coding, 16-QAM modulation, Clipping and Filtering, with and without Tukey windowing for $user$ 2

$E_b/N_0 = 3.00$ dB, which signifies an SNR gain of 9.00 dB. In identical consideration, the estimated BER decreases from 0.1517 in $(3, 2)$- SPC channel coding to 0.0122 in RA channel coding which indicates a system performance improvement of 10.95 dB.

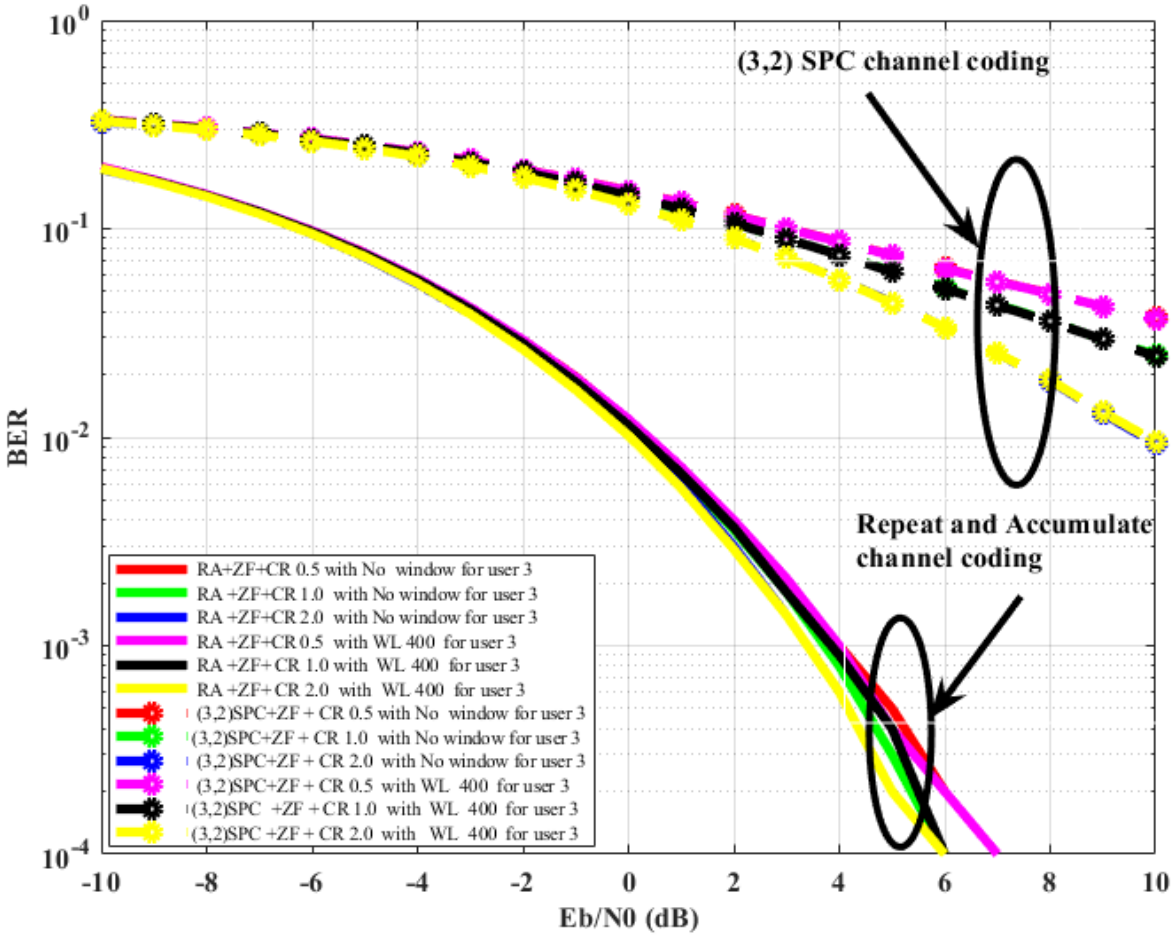

Figure 39: BER performance of Non-terrestrial Downlink CPW-OFDM with different channel coding, 16-QAM modulation, Clipping and Filtering, with and without Tukey windowing for $user$ 3

Fig. 40 shows how the RA channel coding achieves a BER of 10^{-1} at $E_b/N_0 = -5.88$ dB, while the simulated system with $(3, 2)$- SPC channel coding achieves the same

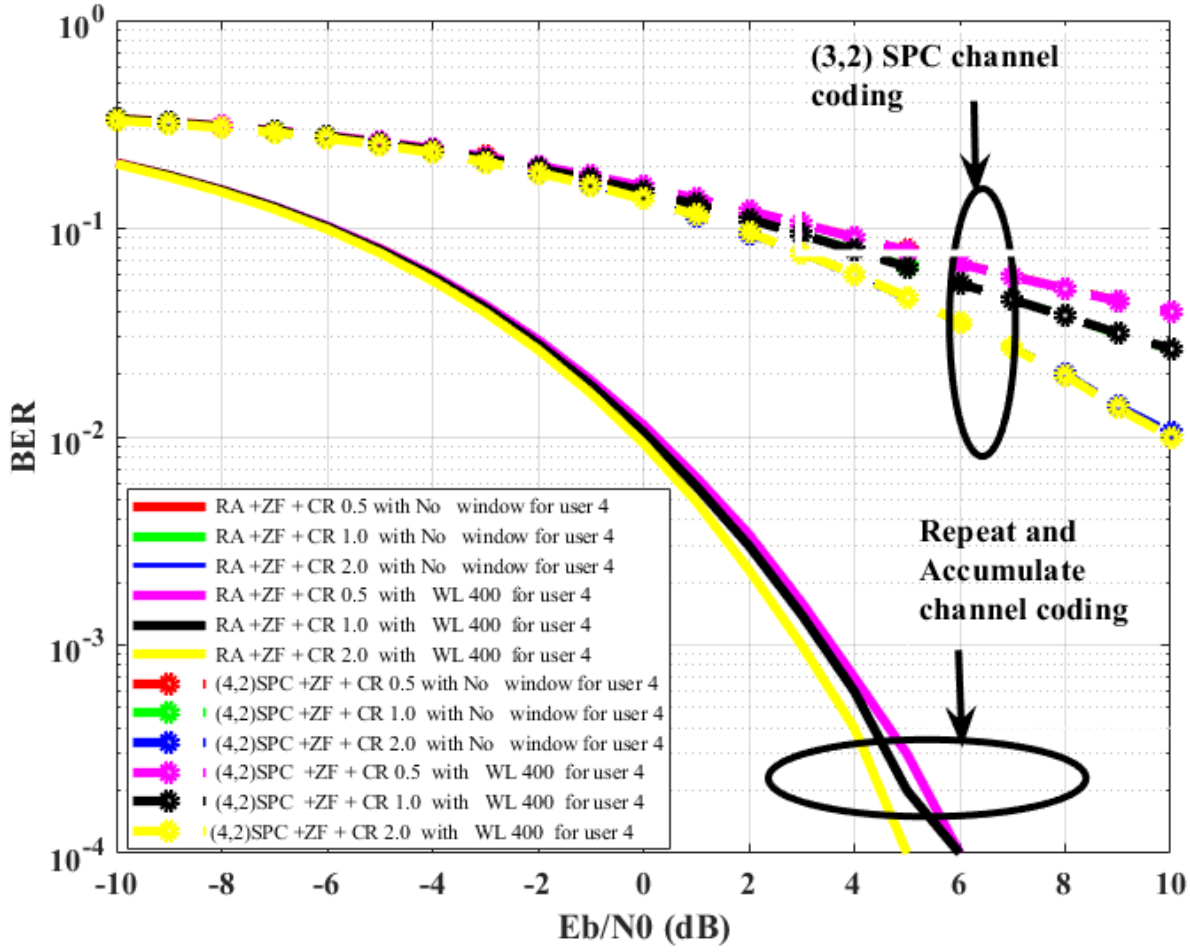

Figure 40: BER performance of Non-terrestrial Downlink CPW-OFDM with different channel coding, 16-QAM modulation, Clipping and Filtering, with and without Tukey windowing for $user\ 4$

BER value at $E_b/N_0 = 3.35$ dB. This ratifies a SNR gain of 9.23 dB. For $E_b/N_0 = 0$ dB, the estimated BER decreases from 0.1589 in $(3, 2)$- SPC channel coding to 0.0144 in RA channel coding which indicates an improvement of 11.44 dB.

In Fig. 41, BER versus SINR performance comparison curves are presented for all users. The estimated SINR values are found to have values ranges from -3.98 dB to 16.02 dB. The simulated system achieves a BER of 10^{-4} at SINR values of 8.02 dB, 9.02 dB, 13.02 dB, and 12.02 dB in case of user 1, user 2, user 3, and user 4 and subsequently BER value approaches zero at SINR values of 9.02 dB, 10.02 dB, 14.02 dB, and 13.02 dB.

In Fig. 42, the Cumulative Distribution Function (CDF) of SINR for four users is shown in a scenario of eight transmitting antennas of UAV with transmit power of 46 dBm. As the power of received signals is very low due to severe path loss encountered in mmWave frequency of 28 GHz, the estimated SINR values in the case of all four users are found to be almost identical and for readability, CDF of SINR values are presented separately. From Fig. 42, it is seen that all the users achieve a SINR value of 10 dB with probability 30%. The value of the probability would increase with the requirement of higher SINR values.

4.3.5 Performance Comparison with Existing Works

Our estimated system performance evaluation indicator values in terms of BER, OOB, and PAPR can be compared with the numerical results of many authors [37]- [39], [51]. In comparison, our estimated OOB reduction power is 117.41 dB (Tables 7, 8, and

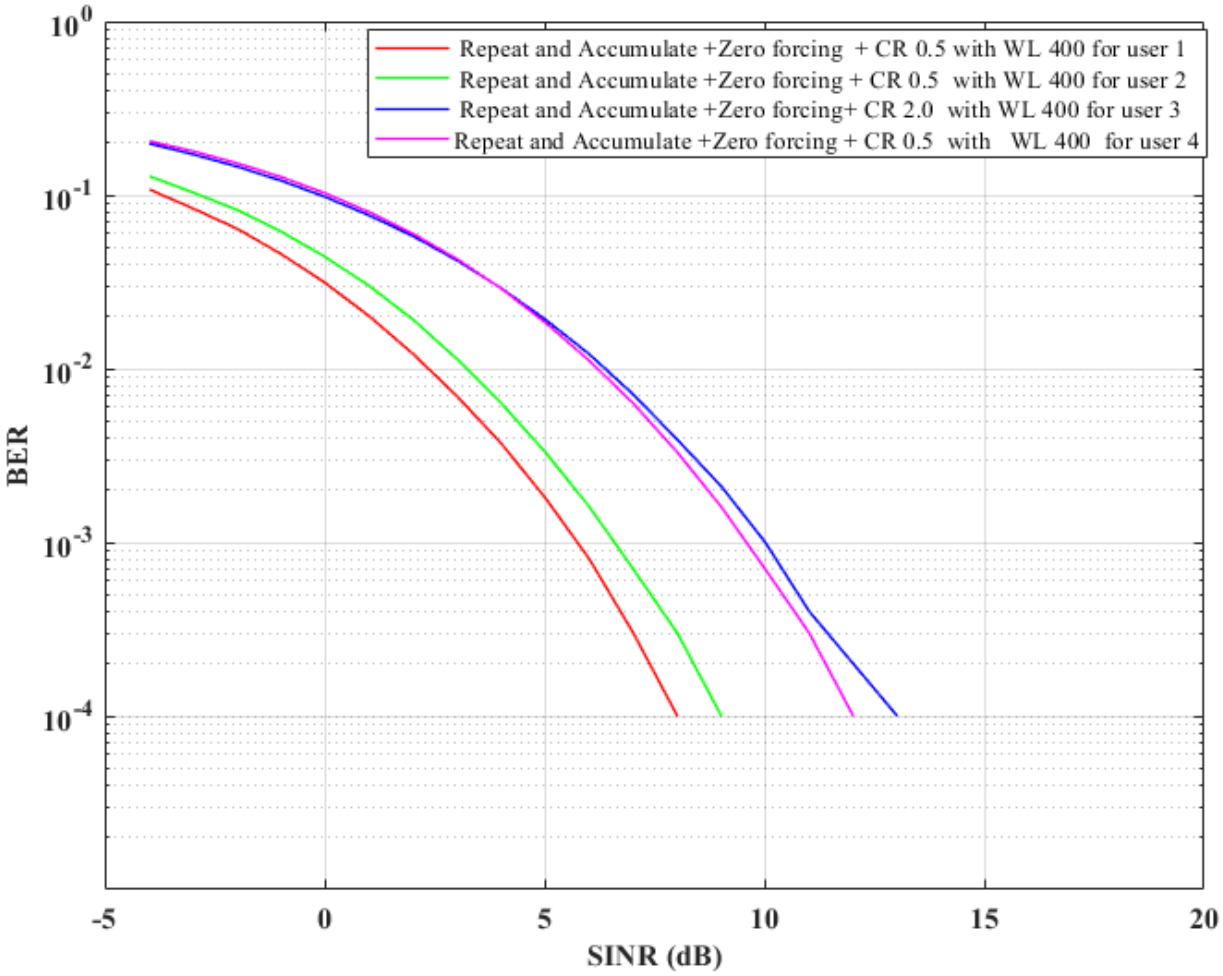

Figure 41: BER versus SINR performance comparison in Non-terrestrial Downlink CPW-OFDM system with implementation of Repeat and Accumulate channel coding, 16-QAM digital modulation, Clipping and Filtering technique with Tukey windowing for all users

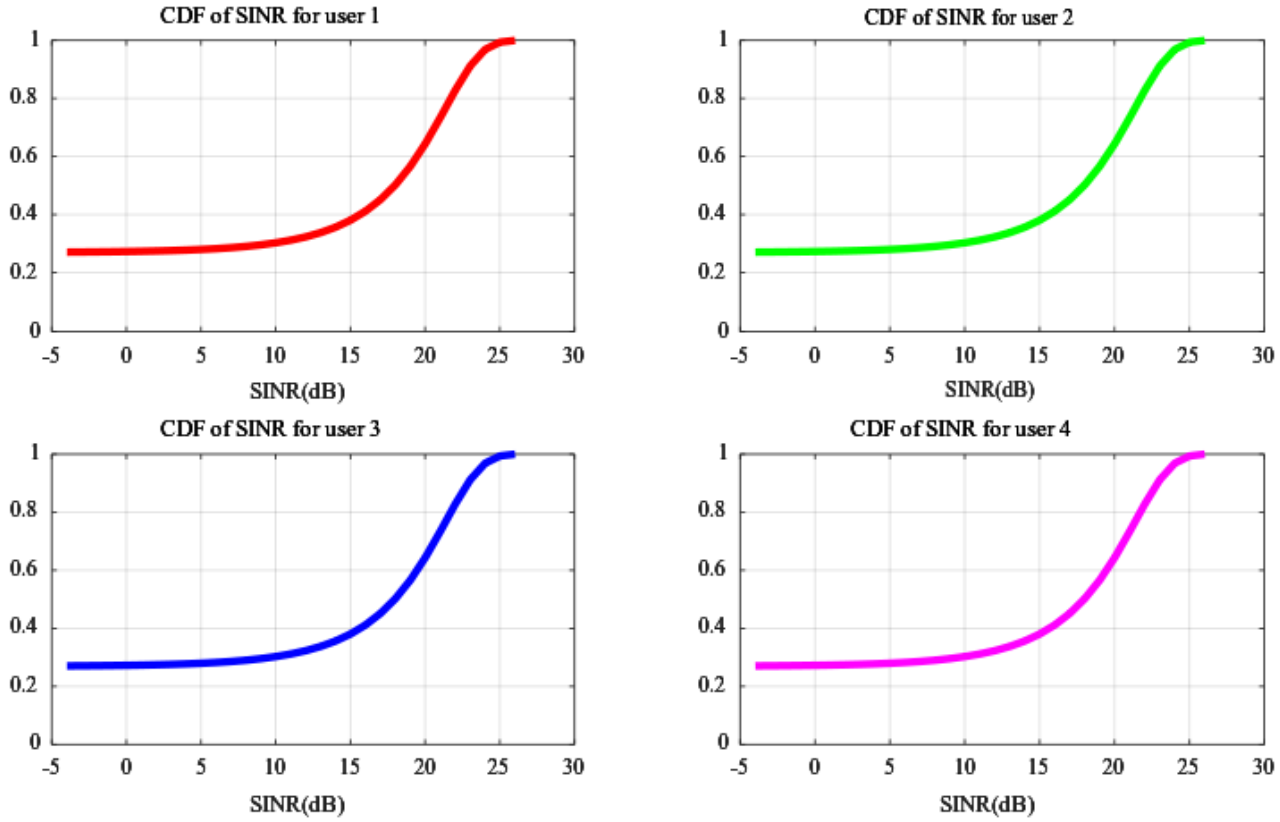

Figure 42: CDF of SINR with total number of transmitting antenna 8 and transmit power 46 dBm

9) which is higher as compared to their estimated OOB reduction power (110 dB) [51].

The estimated BER value of 1×10^{-4} was shown for SNR value ranges from 9.25 dB to 14 dB for three different cases (SFIM, SIM, and FIM) [37]. Our simulated system presents BER value of 1×10^{-4} at E_b/N_0 value ranges from 2 dB to 7 dB (Fig. 37 - Fig. 40) which corresponds to SNR value ranges from 8.02 dB to 12.02 dB.

The BER value of 2.34×10^{-2} was shown at an average E_b/N_0 value of 10 dB [38]. Our simulated system presents BER value of 2.64×10^{-2} at average E_b/N_0 value of -3.5 dB (Fig. 38).

From [39], the estimated PAPR values with the complementary cumulative distribution function (CCDF of 10^{-2}), are found to have values of 2.67 dB, 5.30 dB, 6.71 dB, 7.55 dB, and 9.20 dB under consideration of W- NOMA (Haar wavelets), W- NOMA (Cioflet 2), W- NOMA (Daubechies 6), W- NOMA (Daubechies 8), and FFT-NOMA. Our proposed system with clipping ratio 0.5 and Tukey window of sample length 400 at a CCDF of 10^{-2} has PAPR value within this range viz. 8.82 dB (Fig. 36) and such value is less than 9.20 dB estimated for FFT-NOMA.

Table 6: Simulation Parameters for the UAV-Assisted Multiuser Non-terrestrial Cyclic Postfixed Windowed OFDM System

ROM FT size	4096
Data subcarriers	3300
Length of cyclic prefixing	100 samples
Length of post fixing	50 samples
Length of samples in each CPW-OFDM symbol	4246 samples
No of CPW-OFDM symbols	4
Antenna configuration	$\{2, 2, 2, 2\} \times 8$
Subcarrier spacing (kHz)	60
Sampling frequency (MHz)	245.76
Carrier Bandwidth (MHz)	200
System Bandwidth (MHz)	250
PAPR reduction	Clipping and Filtering
Input data symbols	16-QAM
Windowing	Tukey (Tapered cosine)
Window length (samples), WL at both ends of Tukey windowing function	$100, 200, 300$, and 400
D/A transmit filter, A/D receive filter	Raised cosine pulse shaping with roll off 0.25, filtering spanning, β_1 = 6 and samples per symbol, R = 4
Signal to Noise ratio, E_b/N_0 (dB)	-10 to $+10$
Channel	frequency non selective geometrical fading channel

Table 7: Estimated PAPR at different transmitting channels with OOB for four users [Clipping Ratio (CR) = 0.5]

CR	Channel	WL=0	WL=100	WL=200	WL=300	WL=400
0.5	1	8.4592	8.5987	8.5737	8.5514	8.5655
	2	8.4689	8.4734	8.4931	8.4813	8.4763
	3	8.9293	9.0615	9.1136	9.1706	9.2176
	4	8.7582	8.7977	8.8159	8.8237	8.8378
	5	9.1858	9.1993	9.2214	9.2261	9.2215
	6	8.8503	8.8991	8.9466	8.9779	8.9987
	7	8.1403	8.1576	8.1371	8.1487	8.2009
	8	8.7073	8.7514	8.8459	8.9467	9.0384
	Average PAPR (dB)	8.6874	8.7424	8.7684	8.7908	8.8196
	OOB (dB)	-19.7996	-91.9513	-103.9919	-111.0355	-116.0330
		-21.6327	-93.7844	-105.8250	-112.8686	-117.8661
		-22.6960	-94.8477	-106.8884	-113.9319	-118.9295
		-17.2498	-89.4015	-101.4422	-108.4857	-113.4833

Table 8: Estimated PAPR at different transmitting channels with OOB for four users [Clipping Ratio (CR) = 1.0]

CR	Channel	WL=0	WL=100	WL=200	WL=300	WL=400
1.0	1	8.5415	8.6625	8.6351	8.6159	8.6294
	2	8.5472	8.5525	8.5720	8.5616	8.5566
	3	8.9714	9.1342	9.1740	9.2243	9.2661
	4	8.8338	8.8687	8.8863	8.8926	8.9047
	5	9.2165	9.2281	9.2472	9.2509	9.2479
	6	8.9645	9.0143	9.0617	9.0912	9.1115
	7	8.2592	8.2772	8.2603	8.2836	8.3294
	8	8.7969	8.8434	8.9308	9.0237	9.1070
	Average PAPR (dB)	8.7664	8.8226	8.8459	8.8680	8.8941
	OOB (dB)	-20.5328	-92.6844	-104.7251	-111.7687	-116.7662
		-22.2571	-94.4088	-106.4494	-113.4930	-118.4905
		-23.3472	-95.4989	-107.5396	-114.5831	-119.5806
		-17.6488	-89.8005	-101.8412	-108.8847	-113.8822

Table 9: Estimated PAPR at different transmitting channels with OOB for four users [Clipping Ratio (CR) = 2.0]

CR	Channel	WL=0	WL=100	WL=200	WL=300	WL=400
2.0	1	8.7734	8.8135	8.7877	8.7872	8.8071
	2	8.6817	8.6602	8.6574	8.6923	8.7608
	3	9.2024	9.2556	9.2720	9.3103	9.3424
	4	9.0059	9.0446	9.0335	9.0334	9.0426
	5	9.1574	9.1670	9.1816	9.1851	9.2193
	6	9.1235	9.1683	9.2137	9.2365	9.2517
	7	8.5578	8.5745	8.5638	8.5705	8.6025
	8	9.0432	9.0543	9.1213	9.1964	9.2636
	Average PAPR (dB)	8.9432	8.9672	8.9789	9.0015	9.0363
	OOB (dB)	-21.9638	-94.1155	-106.1561	-113.1997	-118.1972
		-23.5438	-95.6954	-107.7361	-114.7797	-119.7772
		-24.2724	-96.4241	-108.4648	-115.5083	-120.5058
		-19.1350	-91.2867	-103.3274	-110.3709	-115.3684

CHAPTER 5

CONCLUSION AND FUTURE WORKS

We have presented a new form of a beyond 5G compatible system based on research done with consideration of generating multi-path frequency selective and slowly varying fading channel dependent alignment signal for SISO CP-less OFDM system for enhancing spectral efficiency and reducing latency of 5G services. To our knowledge, this is the first work on CP-less MIMO OFDM. Our proposed DFT Spread Windowed MIMO CP-less OFDM system was observed to be spectrally efficient with reduced transmission latency due to significant adaptation of active subcarriers, non-utilization of CPs between OFDM symbols, and implementation of the Walsh-Hadamard encoding scheme. Simulation results show reasonably acceptable system performance in terms of its BER, PAPR, and OOB reduction. These all come from the combination of methods that were used. In low-order digital modulation with 4-QAM, the simulated system shows robust performance; the system performance degrades somewhat with higher-order digital modulation. All of the given equations and system design can be applied readily to higher-order MIMO systems; we have just used 2×2 MIMO as an example. As the specially designed alignment signal is frequency selective channel dependent, the work can be extended further in the future by introducing index modulation into the DFT Spread Windowed MIMO CP-less OFDM systems.

On the other hand, we have introduced a modified form of the Clipping and Filtering technique by incorporating Tukey windowing to improve the performance of our proposed UAV-assisted multiuser non-terrestrial CPW-OFDM system, in terms of simultaneous reduction of both Out of Band and Peak to Average Power Ratio. Utilization of Block Diagonalization, Channel precoding, Repeat and Accumulate channel coding, and probabilistic average path loss model on both LOS and NLOS from UAV to ground communications have made our system robust by improving BER performance and mitigating Multi-user Interference. Our presented 3D models for both received and interference signal power over the study area are clearly indicative of severe path loss in mmWave transmission.

The presented work can be extended in non-terrestrial networking using a cyclic prefix-free OFDM multicarrier signaling technique for reducing latency and increasing data rate with minimizing extra overhead due to cyclic prefixing.

Moreover, the modeling of wireless channels for UAV-to-ground/ground-to- UAV links is an active and ongoing research area. UAV-aided wireless networks demand techniques to predict channel variations introduced by their mobility, and this challenge is magnified when source and destination nodes are also mobile. To establish and maintain link connectivity, advanced air-to-ground (A2G) channel models and communication protocols that allow robust, reliable, and adaptive responses to dynamic environments can be developed.

APPENDIX A

INFORMATION

REFERENCE LIST

[1] A. A. Zaidi, R. Baldemair, V. Moles-Cases, N. He, K. Werner, and A. Cedergren, ”OFDM numerology design for 5G new radio to support IoT, eMBB, and MBSFN,” IEEE Commun. Standards Mag., vol. 2, no. 2, pp. 78-83, Jun. 2018.

[2] 5G; NR; Physical Layer; General Description, document TS 38.201, 3GPP, Version 15.0.0, Sep. 2018.

[3] Z. Zhang et al., ”6G Wireless Networks: Vision, Requirements, Architecture, and Key Technologies,” IEEE Vehicular Technology Mag., vol. 14, no. 3, Sept. 2019, pp. 28-41.

[4] E. CalvaneseStrinati et al., ”6G: The Next Frontier: From Holographic Messaging to Artificial Intelligence Using Subterahertz and Visible Light Communication,” IEEE Vehicular Technology Mag., vol. 14, no. 3, Sept. 2019, pp. 42â50.

[5] W. Saad, M. Bennis, and M. Chen, ”A Vision of 6G Wireless Systems: Applications, Trends, Technologies, and Open Research Problems,” IEEE Network, vol. 34, no. 3, May/June 2020, pp. 134â142.

[6] M. Giordani et al., ”Towards 6G Networks: Use Cases and Technologies,” arXiv preprint arXiv:1903.12216. 2019, Mar. 28.

[7] J.M.Hamamreh,Z.E.Ankarali,andH.Arslan, ”CP-lessOFDM With Alignment Signals for Enhancing Spectral Efficiency, Reducing Latency, and Improving PHY Security of 5G Services,” IEEE Access, vol. 6, pp. 63649â63663, 2018

[8] H. G. Myung, and D. J. Goodman, ”Single Carrier FDMA, A new air interface for long term evolution,” John Wiley Sons, UK, 2008.

[9] Y. Jiang, ”A Practical Guide to Error-Control Coding Using MATLAB,” Artech House, Norwood, MA, USA.

[10] https://sites.google.com/site/bsnugroho/ldpc

[11] K.G. Beauchamp, ”Applications of Walsh and Related Functions With an Introduction to Sequency Theory,” Academic Press, London, 1984.

[12] T. Sultana, M. S. A. Showkat, M. S. Alam, M. D. Hossain, and A. K. Mandal, ”Reducing Peak to Average Power Ratio of OFDM Signals using Tukey Window Technique,” International Journal of Scientific Engineering and Technology, vol. 2, issue no. 9, pp. 879â883, 2013.

[13] https://www.sharetechnote.com/html/5G_FrameStructure_Candidate.html

[14] Antti Anttonen, Pekka Ruuska, and Markku Kiviranta, ”3GPP non terrestrial networks: A concise review and look ahead,” VTT Technical Research Centre of Finland. VTT Research Report, No. VTT-R-00079-19, http://www.vtt.fi, 2019.

[15] Y. Wang, L. Chen, Y. Zhou, X. Liu, F. Zhou and N. Al-Dhahir, ”Resource Allocation and Trajectory Design in UAV-Assisted Jamming Wideband Cognitive Radio Networks,” in IEEE Transactions on Cognitive Communications and Networking, doi: 10.1109/TCCN.2020.3014208

[16] A. Rahmati, S. Hosseinalipour, I. Guvenc, H. Dai and A. Bhuyan, ”Lifetime Maximization for UAV-assisted Data Gathering Networks in the Presence of Jamming,” 2020 IEEE 21st International Workshop on Signal Processing Advances in Wireless Communications (SPAWC), Atlanta, GA, USA, 2020, pp. 1-5, doi: 10.1109/SPAWC48557.2020.9154318.

[17] Marco Giordani, Michele Zorzi, 2019: Non-Terrestrial Communication in the 6G Era: Challenges and Opportunities

[18] Technical specification on 5G NR; Physical layer; General description (3GPP TS 38.201 version 15.0.0 Release 15)

[19] 5G-NR Physical Layer Specifications Overview; https://wirelessbrew.com/5g-nr/5g-nr-physical-layer-specifications-overview/

[20] C. An and H. Ryu, ”CPW-OFDM (Cyclic Postfix Windowing OFDM) for the B5G (Beyond 5th Generation) Waveform,” 2018 IEEE 10th Latin-American Conference on Communications (LATINCOM), Guadalajara, 2018, pp. 1-4, doi: 10.1109/LATINCOM.2018.8613242

[21] R. Zayani, Y. Medjahdi, H. Shaiek and D. Roviras, "WOLA-OFDM: A Potential Candidate for Asynchronous 5G," 2016 IEEE Globecom Workshops (GC Wkshps), Washington, DC, 2016, pp. 1-5, doi: 10.1109/GLOCOMW.2016.7849087

[22] J. A. L. Calvo, G. Alirezaei and R. Mathar, "Wireless powering of drone-based MANETs for disaster zones," 2017 IEEE International Conference on Wireless for Space and Extreme Environments (WiSEE), Montreal, QC, 2017, pp. 98-103, doi: 10.1109/WiSEE.2017.8124900

[23] 5G NR mmWave outdoor and indoor deployment strategy,

[24] L. Wang, B. Hu and S. Chen, "Energy Efficient Placement of a Drone Base Station for Minimum Required Transmit Power," in IEEE Wireless Communications Letters, doi: 10.1109/LWC.2018.2808957

[25] K. Choi, 2019, "Alamouti Coding for DFT Spreading-based Low PAPR FBMC," *IEEE Trans. on Wireless Comm.*, vol. 18, pp. 926–941.

[26] M. N. Hossain, T. Shimamura, D. Kim, and H. G. Ryu, 2018, "Waveform Design of DFT-Spread WR-OFDM System for the OOB and PAPR Reduction," In *Proc. of IEEE ICTC*, pp. 792–796.

[27] F. Wu , J. Wang, J. Wang, and J. Song, 2018, "A Precoding Method for Both Out-of-Band Emission and PAPR Reduction in OFDM Systems," In Proceeding of IEEE International Symposium on Broadband Multimedia Systems and Broadcasting (BMSB), pp. 1–5.

[28] C. An, B. Kim, and H. G. Ryu, 2017, "WR-OFDMsystem and OOBspectrumcomparison," In proceeding of Ninth International Conference on Ubiquitous and Future Networks (ICUFN), pp. 373–377.

[29] 2Z. Hadzi-Velkov, S. Pejoski, N. Zlatanov and R. Schober, "UAV-assisted Wireless Powered Relay Networks with Cyclical NOMA-TDMA," in IEEE Wireless Communications Letters, doi: 10.1109/LWC.2020.3013296.

[30] A. Masaracchia, L. D. Nguyen, T. Q. Duong, C. Yin, O. A. Dobre and E. Garcia-Palacios, "Energy-Efficient and Throughput Fair Resource Allocation for TS-NOMA UAV-Assisted Communications," in IEEE Transactions on Communications, doi: 10.1109/TCOMM.2020.3014939.

[31] A. Ranjha and G. Kaddoum, "Quasi-Optimization of Uplink Power for enabling Green URLLC in Mobile UAV-assisted IoT Networks: A Perturbation-based Approach," in IEEE Internet of Things Journal, doi: 10.1109/JIOT.2020.3014039.

[32] B. Wang, Y. Sun, N. Zhao and G. Gui, "Learn to Coloring: Fast Response to Perturbation in UAV-Assisted Disaster Relief Networks," in IEEE Transactions on Vehicular Technology, vol. 69, no. 3, pp. 3505-3509, March 2020, doi: 10.1109/TVT.2020.2967124.

[33] Y. H. Kim, I. A. Chowdhury and I. Song, "Design and Analysis of UAV-Assisted Relaying With Simultaneous Wireless Information and Power Transfer," in IEEE Access, vol. 8, pp. 27874-27886, 2020, doi: 10.1109/ACCESS.2020.2971692.

[34] M. C. Lucic, H. Ghazzai and Y. Massoud, ”A Generalized Dynamic Planning Framework for Green UAV-Assisted Intelligent Transportation System Infrastructure,” in IEEE Systems Journal, doi: 10.1109/JSYST.2020.2969372.

[35] X. Tan, S. Su, X. Guo, and X. Sun, ”Application of MIMO-OFDM Technology in UAV Communication Network,” 2020 2nd World Symposium on Artificial Intelligence (WSAI), Guangzhou, China, 2020, pp. 1-4, doi: 10.1109/WSAI49636.2020.9143309

[36] Q. Wang, W. Yang, S. Xu, and X. Pei, ”OFDM with Index Modulation for UAV Communication Systems,” 2019 IEEE 5th International Conference on Computer and Communications (ICCC), Chengdu, China, 2019, pp. 1047-1052, doi: 10.1109/ICCC47050.2019.9064201

[37] Z. Zhang, F. Liu, R. Du, and X. Bai, ”SFIM Detector Based on Joint-Sparse Index Removal for MIMO-OFDM-CR System,” in IEEE Communications Letters, doi: 10.1109/LCOMM.2020.3013630

[38] Y. Chang, Y. Liu and K. Fukawa, ”Constant-Amplitude OFDM for Wireless Communication Systems,” 2020 IEEE 91st Vehicular Technology Conference (VTC2020-Spring), Antwerp, Belgium, 2020, pp. 1-5, doi: 10.1109/VTC2020-Spring48590.2020.9128630

[39] U. Ali, S. Baig, T. Umer, and Z. Ding, ”Performance analysis of discrete wavelet transform for downlink non-orthogonal multiple access in 5G networks,” in IET

Communications, vol. 14, no. 10, pp. 1666-1674, 23 6 2020, doi: 10.1049/iet-com.2019.0851

[40] T. S. Rappaport, 1996, *Wireless Communications Principles and Practice*, Second Edition, Prentice Hall, NJ.

[41] Y. S. Cho, J. Kim, W. Y. Yang, and C. G. Kang, 2010, "MIMO-OFDM Wireless Communications with MATLAB," John Wiley and Sons (Asia) Pte Ltd, United Kingdom.

[42] Giorgio M. Vitetta, Desmond P. Taylor, Giulio Colavolpe, Fabrizio Pancaldi, and Philippa A. Martin, "Wireless Communications Algorithmic Techniques," 2013 John Wiley and Sons Ltd,United Kingdom

[43] http://www.sharetechnote.com/html/5G_FrameStructure_Candidate.html

[44] Hyung G. Myung Qualcomm and David J. Goodman, "Single Carrier FDMA A New Air Interface For Long Term Evolution," 2008 John Wiley and Sons, Ltd, United Kingdom

[45] L. Cho, X. Yu, C. Chen, and C. Hsu, "Green OFDM for IoT: Minimizing IBO subject to a spectral mask," 2018 IEEE International Conference on Applied System Invention (ICASI), Chiba, 2018, pp. 5-8, doi: 10.1109/ICASI.2018.8394252

[46] Tangina Sultana, M. S. Ara Showkat , Mohammad Shah Alam, Md. Delowar Hossain and Ashis Kumar Mandal, 2013: Reducing Peak to Average Power Ratio of

OFDM Signals using Tukey Window Technique, International Journal of Scientific Engineering and Technology, Volume No.2, Issue No.9, pp. 879-883

[47] R. M. alias Isakki, C. Tharini and M. Arulvani, "Performance analysis of pulse shape filter for repetition channel coding," 2017 IEEE International Conference on Power, Control, Signals and Instrumentation Engineering (ICPCSI), Chennai, 2017, pp. 592-597, doi: 10.1109/ICPCSI.2017.8391782

[48] Tranter, William H., K. Sam Shanmugan, Theodore S. Rappaport, and Kurt L. Kosbar.Â Principles of Communication Systems Simulation with Wireless Applications.Â Upper Saddle River, NJ: Prentice Hall, 2004

[49] Elliott, R.C., Krzymien, W.A. Improved and weighted sum rate maximization for successive zero-forcing in multiuser MIMO systems. J Wireless Com Network 2011, 133 (2011). https://doi.org/10.1186/1687-1499-2011-133

[50] Yong Soo Cho, Jaekwon Kim, Won Young Yang, Chung G. Kang, MIMO-OFDM Wireless Communications with MATLAB, John Wiley and Sons (Asia) PTE Limited, Singapore, 2010

[51] M. N. Hossain, Y. Sugiura, T. Shimamura and H. Ryu, "Waveform Design of Low Complexity WR-OTFS System for the OOB Power Reduction," 2020 IEEE Wireless Communications and Networking Conference Workshops (WCNCW), Seoul, Korea (South), 2020, pp. 1-5, doi: 10.1109/WCNCW48565.2020.9124756.

[52] X. Tang, J. Yang, Y. Wang, and K. Li, ”CP-Less MIMO OFDM Transceiver Design for 5G New Radio,” IEEE Access, 2021

[53] F. Ahmad and F. A. Khan, ”Advanced Modulation and Coding for CP-less MIMO-OFDM Systems,” IEEE Transactions on Wireless Communications, 2020

[54] Hao Jiang, Hongming Chen, ”A Full-Duplex MIMO System Based on CP-Free OFDM in Sensor Network”, Journal of Sensors, vol. 2022, Article ID 6888809, 5 pages, 2022. https://doi.org/10.1155/2022/6888809

[55] Zhang, L., Li, Y., Shi, S., Qi, Q., Ye, Y. (2023). Cyclic correlation-based blind SNR estimation for cyclic prefix-Less OFDM system. Radio Science, 58, e2022RS007607. 2023
https://doi.org/10.1029/2022RS007607

[56] S. Saeedi and M. R. Nakhai, ”Low-Complexity Channel Estimation for CP-Less MIMO-OFDM Systems,” IEEE Transactions on Communications, 2019

[57] H. Xu, Z. Wang, and H. Zhang, ”Performance Analysis of CP-Less MIMO-OFDM Systems with Channel Estimation Errors,” Published: IEEE Communications Letters, 2018

[58] M. M. I. Mamun, D. Medhi, and C. Beard, ”CP-Less MIMO Discrete Fourier Transform Spread OFDM,” 2020 International Symposium on Networks, Computers and Communications (ISNCC), Montreal, QC, Canada, 2020, pp. 1-6, doi: 10.1109/ISNCC49221.2020.9297194.

[59] M. M. I. Mamun, C. Beard and D. Medhi, ”A UAV-Assisted Multiuser Non-terrestrial Cyclic Postfixed Windowed OFDM System,” 2022 International Symposium on Networks, Computers and Communications (ISNCC), Shenzhen, China, 2022, pp. 1-6, doi: 10.1109/ISNCC55209.2022.9851701.

VITA

Md Mainul Islam Mamun was born on October 8, 1982, in Bangladesh. He received his B.Sc. and M.Sc. degrees in Applied Physics and Electronic Engineering from the University of Rajshahi (RU), Bangladesh in 2006 and 2008, respectively. Then, he joined as a lecturer in the Department of Mechatronic Engineering at the World University of Bangladesh in September 2008. After that, he joined as a Lecturer of Computer Science and Telecommunication Engineering at the Noakhali Science and Technology University in July 2009. Before coming to the U.S. for his Post graduation, he served 5 years (2010 to 2015) as a faculty member in the Department of Applied Physics and Electronic Engineering at the University of Rajshahi.

Mr. Mamun achieved another M.S. degree in Computer Science from the University of Missouri-Kansas City (UMKC) in 2019. Before coming to UMKC, Mr. Mamun worked as a Research Assistant at Clemson University.

Currently, he is a Ph.D. candidate in the Department of Computer Science Electrical Engineering at UMKC. Mr. Mamun has around 15 years of teaching experience both in the undergraduate and graduate levels.

He has around three years of teaching experience at UMKC as an individual instructor. In 2021, He joined as a Lecturer/Assistant Professor in the Department of Computer Science and Information Security at Southern Utah University, Cedar City, Utah, USA. Currently, he is teaching in the Department of Computer Science at Saint Louis

University, Saint Louis, MO, USA. He is also working as an Assistant Professor of Electrical and Electronic Engineering at the University of Rajshahi.

During his studies at UMKC, Mr. Mamun received the School of Graduate Studies Research Grant and Preparing Future Faculty Award. He is serving as an Associate Editor, Technical Program Committee (TPC) member, and Reviewer in many prestigious peer-reviewed journals and conferences. He has already reviewed more than 200 research papers and has been serving as an Associate Editor and TPC member in 17 prestigious international peer-reviewed journals and conferences. Additionally, Mr. Mamun has attended more than 30 International Conferences/ Workshops/ Symposium/Training.

His research interest falls in Wireless Communications, Wireless and Computer Networking, Cybersecurity, Bioinformatics, and Data Analytics. In the future, Mr. Mamun is also interested to do research in Wireless Communications, Wireless and Computer Networking, Intelligent Cybersecurity, Bioinformatics, Data Analytics, Central Bank Digital Currency (CBDC), and Blockchain.